Studies in Quantum Chaos : Entanglement, Decoherence and All that

A THESIS

submitted for the Award of Ph.D degree of

Mohan Lal Sukhadia University

in the

Faculty of Science

BY

Jayendra Nath Bandyopadhyay

Under the Supervision of

Professor R. E. Amritkar

THEORETICAL PHYSICS & COMPLEX SYSTEM DIVISION
PHYSICAL RESEARCH LABORATORY, AHMEDABAD.

MOHANLAL SUKHADIA UNIVERSITY, UDAIPUR

Year of submission: 2004

CERTIFICATE

This is to certify that the thesis entitled "Studies in Quantum Chaos : Entanglement, Decoherence and All that" submitted for the award of the degree of Doctor of Philosophy of Mohanlal Sukhadia University in the faculty of Science is a record of bonafide investigations carried out by Shri. Jayendra Nath Bandyopadhyay under my supervision and guidance.

This is an original piece of work on which no one has been awarded a degree in this University or in any other University.

The literary presentation of the thesis is satisfactory and it is in a form suitable for publication. The work presented in the thesis has been done after registration in this University.

Further, the candidate has put in attendance of more than 200 days in my institution as required under rule 7(b) and thus completed the residential requirement.

Professor R. E. Amritkar
(SUPERVISOR)

to

Maa, Baba, Dada & Tapan

Contents

Acknowledgement

I am grateful to Dr. Arul Lakshminarayan for introducing me to the field of non-linear dynamics. I benefitted a great deal from his deep insight and excitement in the subject. I will always be indebted to him for what I have learned from him over the past few years. I am also grateful to Prof. R. E. Amritkar for his kind help and support. I thank Prof. V. B. Sheorey for his affectionate encouragement and valuable suggestions regarding this work. I benefitted academically from the comments of Prof. V. K. B. Kota and Dr. P. Panigrahi.

I would like to give a special thank to Mr. G. Bhattacharya, who motivated me to enter into this fascinating field of scientific research. I take this opportunity to express my gratitude to all my M.Sc. teachers. In particular I thank Profs. and Drs. S. Duttagupta, A. Pandey, R. Rajaraman, D. Kumar, K. B. Sinha, P. Sen, R. Ghosh and S. Ghosh, who laid the strong foundation in me. I would also like to thank all those PRL faculties who took our Ph.D. course work.

I like to thank all the staff at the Computer Center, and in particular Dholakiaji and Jigarbhai for their helpful attitude. I also thank all the library staffs for their cooperation, and especially Keyurbhai for his friendly attitude.

I like to thank all my 7th floor seniors ; to name a few Sankar, Sudheer, Sagar, Rishi, Shajesh, Pattu, Sunish and Arun. I thank all those PRLites whom I consider my friends. I have enjoyed lot of chaotic discussions (both academic and non-academic) with Sarika. Her comments and suggestions about this thesis are also invaluable.

I would also like to extend my thanks to all my affectionate juniors. All the members of the PRL Cricket team deserve a special thank. Especially I thank Ravi, Prashant Rawat, Harishji, Gohilji, Jyoti, Ratan, Dipuda, Alambhai, Santosh, Nagar, Sumit, RP and few others.

Finally, I would like to remember all of my family members who are beyond any kind of acknowledgement.

Jayendra N. Bandyopadhyay

Chapter 1

Introduction

Classical Mechanics not only is the oldest branch of physics but was and still is the basis for all of theoretical physics. Even quantum mechanics can hardly be understood (perhaps cannot even be formulated) without a good knowledge of classical mechanics. The essential physics involved in the classical mechanics of a particle is contained in Newton's celebrated laws of motion. Therefore classical mechanics is also called Newtonian mechanics.

Newtonian formulation of mechanics does not consider the presence of constraints in the systems. In presence of constraints, coordinates become function of each other and therefore they are no more a set of independent coordinates. In these cases we can define a set of independent coordinates, called *generalized coordinates*, that take presence of constraints into account. Newton's laws of motion are not valid in generalized coordinates. This is the most inconvenient part of Newton's formulation of mechanics.

1.1 Hamiltonian system

As a consequence, canonical formalism becomes a central part of the developments of classical mechanics in post-Newtonian era. In this formalism, one can study the mechanics of a particle in a general abstract space of generalized coordinates. Lagrange's formulation of mechanics and later Hamilton's formulation of mechanics are important achievements in the developments of this canonical formalism. The Hamiltonian function, simply called *Hamiltonian*, is central to the

Hamilton's formalism. Hamiltonian is defined in an abstract space called '*phase space*', which consists of generalized coordinates $\overline{\mathbf{q}}$ and its corresponding momenta $\overline{\mathbf{p}}$. In the phase space, the dynamics of the system or time evolution of $(\overline{\mathbf{p}}, \overline{\mathbf{q}})$ are determined by the following equations :

$$\frac{d\overline{\mathbf{p}}}{dt} = \frac{\partial H(\overline{\mathbf{p}}, \overline{\mathbf{q}}, t)}{\partial \overline{\mathbf{q}}} \tag{1.1a}$$

$$\frac{d\overline{\mathbf{q}}}{dt} = -\frac{\partial H(\overline{\mathbf{p}}, \overline{\mathbf{q}}, t)}{\partial \overline{\mathbf{p}}}, \tag{1.1b}$$

where $H(\overline{\mathbf{p}}, \overline{\mathbf{q}}, t)$ is the Hamiltonian of the system which describes the dynamical flow and $\overline{\mathbf{p}}, \overline{\mathbf{q}}$ are the N-component vectors $\overline{\mathbf{p}} = \{p_i\}, \overline{\mathbf{q}} = \{q_i\}$ with N being the number of degrees of freedom (DOF). The above equations are called Hamilton's *canonical equations*. If the dynamics of a system follows above set of equations, the system is called Hamiltonian system. One of the fundamental property of the Hamiltonian flow is that it preserves volume of the phase space.

1.1.1 Integrable systems

Let us consider time independent Hamiltonian system and in this case we can identify the value of the Hamiltonian with the energy E, i.e., $H(\overline{\mathbf{p}}, \overline{\mathbf{q}}) = E$. If a Hamiltonian system of N DOF, having N independent invariants $f_i(\overline{\mathbf{p}}, \overline{\mathbf{q}})$ where $i = 1, \ldots, N$ satisfying the condition $\{f_i, f_j\} = 0$ for all i and j, is called integrable system. Presence of N invariants implies that the motion of the system is in the phase space restricted to lie on the N-dimensional surface

$$f_i(\overline{\mathbf{p}}, \overline{\mathbf{q}}) = c_i, \quad i = 1, \ldots, N$$

where c_i's are N-constants. According to the *Liouville-Arnold* theorem, this surface must be an N-dimensional torus [1]. For example, in case of 2 DOF the phase space is 2-torus which has the structure of a tyre tube. These are called the invariant tori which are responsible for the regular dynamics of the integrable system.

For simplicity, let us consider 2 DOF case. In this case torus is 2-dimensional (tyre tube) and every tori can be characterized with frequencies ω_1 and ω_2. If the ratio of the frequencies $\alpha = \omega_1/\omega_2$ are rational then the tori will be called resonant

tori and if α are irrationals then the tori will be non-resonant tori. From the above definition of rational and irrational tori, it is clear that the motion will be periodic on the resonant tori and quasiperiodic on the non-resonant tori.

Note : *Chapter 2 is completely devoted to the study of the time dependent integrable Hamiltonian system. Therefore in this subsection we have restricted ourselves in the discussion of the properties of the time independent integrable Hamiltonian system.*

1.1.2 Nonintegrable systems

Integrable systems are very rare. In most of the occasions, the Hamiltonian systems will not have sufficient number of invariants and thus these systems are appropriately called nonintegrable system. In general, our understanding about nonintegrable system is based on our knowledge about integrable systems. Typically we consider that a nonintegrable system arises as a perturbation to an integrable system. Now the question is, what is the fate of an unperturbed tori under perturbation ?

Fate of the "nonresonant" tori. KAM theorem [2] :

The question of fate of the "nonresonant" tori is answered by a celebrated theorem of *Kolmogorov* (K), *Arnold* (A), and *Moser* (M), the so-called KAM theorem. Here we just state the theorem for the very simple case of two DOF system. However, this theorem holds for any arbitrary number of DOF. The theorem states that if, among other technical conditions, the Jacobian of the frequencies is nonzero, i.e.

$$\det \left| \frac{\partial \omega_i}{\partial I_i} \right| \neq 0$$

then those tori, whose frequency ratio ω_1/ω_2 is sufficiently irrational such that

$$\left| \frac{\omega_1}{\omega_2} - \frac{m_2}{m_1} \right| > \frac{K(\epsilon)}{m_1^{2.5}} \quad \text{for all } m_1,\, m_2 \tag{1.2}$$

holds, are stable under the perturbation ϵH_1 in the limit $\epsilon \ll 1$. Not much is known about $K(\epsilon)$, other than $K(\epsilon) \to 0$ as $\epsilon \to 0$. The "destroyed" tori are the complementary set satisfying

$$\left| \frac{\omega_1}{\omega_2} - \frac{m_2}{m_1} \right| < \frac{K(\epsilon)}{m_1^{2.5}}. \tag{1.3}$$

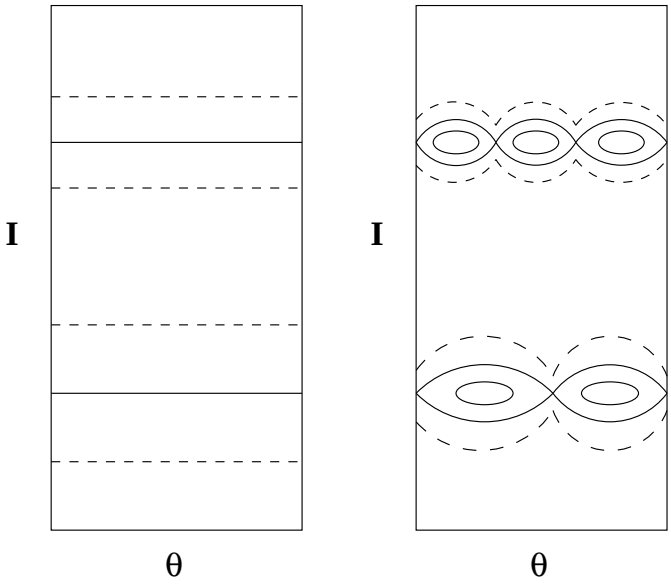

Figure 1.1: A Schematic action-angle diagram of the break-up of the rational tori, indicated by solid lines, when an integrable system (on the left) becomes slightly nonintegrable (on the right). These tori break up into elliptic points and hyperbolic points. The irrational tori, indicated by dashed curves, survive.

The above condition is more restrictive than the strict commensurability condition $m_1\,\omega_1 + m_2\,\omega_2 = 0$. However, it is important to note that the set of frequency ratios for which Eq.(1.2) holds and for which the motion is therefore regular, even after the perturbation, has a nonzero measure.

The KAM theorem also requires that the perturbation be "sufficiently small". However, there is no precise estimate of how small "sufficiently small" should be. Early estimates were of the order of 10^{-48}, whereas for most of the Hamiltonian systems studied so far the numerical evidence shows that tori are survived under much higher value of ϵ. Moreover the analyticity of the Hamiltonian is not strictly necessary. *Moser* stated that only the first 333 derivatives should exist. The underlying theme of this theorem is first to select a torus on which frequencies are sufficiently irrational and then apply perturbation theory on it.

Fate of the "resonant" tori. Poincare-Birkhoff theorem [2] :

The 'resonant' tori, which satisfy the condition given in Eq.(1.3), are destroyed under perturbation and this provides the 'seeds' of chaotic behavior observed

in nonintegrable systems. *Poincare-Birkhoff* theorem deals with the fate of the resonant tori. We know, if a system is integrable, each point on a tori corresponding to a rational frequency ratio m_2/m_1 is part of a periodic orbit. According to the Poincare-Birkhoff theorem, when the system becomes nonintegrable, the tori breaks up into an alternating sequence of m_1 elliptic points and m_1 hyperbolic points. Around each elliptic point will be a series of elliptic orbits. The event is shown schematically in Fig.1.1. This figure shows that the tori with irrational frequency ratios, indicated by dashed curves, survive, but the tori with rational frequency ratios, indicated by solid lines, break up into elliptic points and hyperbolic points.

1.2 Chaos in Hamiltonian systems

In the previous section we have seen that under a very small perturbation, unperturbed resonant tori decompose into equal number of elliptic and hyperbolic points, whereas nearby nonresonant tori survive (but may be slightly deformed). These nonresonant tori, which survive under small perturbation, are called *KAM tori*. The KAM tori are strong barriers for the development of chaos. If we increase the perturbation strength ϵ, the KAM tori destroy one by one with the last survivor being the one with frequency ratios (ω_1/ω_2) equal to the *Golden mean* $[= (\sqrt{5} - 1)/2]$, the "most irrational" of the irrational. In the absence of KAM tori, a single trajectory wanders all possible regions of the phase space and the system becomes fully 'chaotic'. For the intermediate values of ϵ, the phase space of the system consists of many stable KAM tori, and in between two KAM tori the motion is completely irregular. These kind of systems, whose phase space consists of both regular and irregular structures, are called '*mixed* system'. The 'mixed' dynamical systems are more generic than the completely integrable and completely chaotic systems.

It is now the proper time to present a formal definition of chaos. There are several versions of definitions for chaos, but we will follow the definition given in a popular textbook by *Devaney* [3]. This definition has three components and they are formulated for a continuous map $f : X \to X$ on some metric space X.

The three components of the definition are following :
(1) f is topologically transitive ; that is, for all non-empty open subsets U and V of X there exists a natural number k such that $f^k(U) \cap V$ is non-empty. This means that the points under iteration $\left[f^k(U)\right]$ move from any arbitrary small neighborhood to another.
(2) The periodic points of f form a dense subset of X. This means that if we choose a closed interval I arbitrarily close to any point, we can always find a periodic point in that interval I. Devaney refers to this condition as an *element of regularity*.
(3) The last component of the definition speaks about *sensitive dependence on initial condition*. f satisfies this property if there is a positive real number δ (a sensitivity constant) such that for every point x in X and every neighborhood N of x there exists a point y in N and a nonnegative integer n such that the nth iterates $f^n(x)$ and $f^n(y)$ of x and y respectively, are more than distance δ apart. In the mathematical notation this condition can be expressed as $|\, f^n(x) - f^n(y)\,| > \delta$.

Later it has been shown that first two components of the above definition are sufficient to show the sensitive to initial condition [4]. Moreover this is the only redundancy in Devaney's definition : (1) and (3) do not imply (2), and (2) and (3) do not imply (1). See Ref. [5]. More later, it has been shown that, on an interval, even transitivity is sufficient to imply sensitive to initial condition [6].

Sensitive dependence on initial conditions is the central idea of chaos and moreover, it provides the practical definition of chaos. However, chaos requires more stronger form of the condition (3) and according to that, two trajectories whose initial condition differs only infinitesimally diverge exponentially. According to *Chirikov* [7], this is a necessary condition. However, for any physical system, the exponential divergence cannot go on forever. Therefore, the bounded phase space is another requirement for chaos. The exponential sensitivity to initial conditions together with the condition of the bounded phase space gives a working definition of chaos.

Now we are going to present a popular measure of chaos, called *Lyapunov exponent*. The Lyapunov exponent measures the mean rate of exponential separation of neighboring trajectories. To define this quantity in proper mathematical

way, let us consider a system governed by the differential equations

$$\frac{d\,x_i}{dt} \;=\; F_i\,(\overline{\mathbf{x}}),\;\;\; i \;=\; 1,\ldots\ldots\,,N.$$

For Hamiltonian systems, the above equations are just the Hamilton's canonical equations, where the components of the vector $\overline{\mathbf{x}}$ are the phase space variables. Let us consider a trajectory in the above N dimensional phase space and a nearby trajectory with initial conditions $\overline{\mathbf{x}}_{\mathbf{0}}$ and $\Delta\overline{\mathbf{x}}_{\mathbf{0}}$, respectively. These two trajectories evolve with time yielding the tangent vector $\Delta\overline{\mathbf{x}}(\,\overline{\mathbf{x}}_{\mathbf{0}},\,t\,)$ with its norm $d(\,\overline{\mathbf{x}}_{\mathbf{0}},\,t\,)$. The time evolution for tangent vector $\Delta\overline{\mathbf{x}}$ is found by linearizing above equation, and we get

$$\frac{d\Delta\overline{\mathbf{x}}}{dt} \;=\; \mathbf{M}(\,\Delta\overline{\mathbf{x}}(t)\,)\,.\,\Delta\overline{\mathbf{x}}$$

where $\mathbf{M} \;\equiv\; \partial\mathbf{F}/\partial\overline{\mathbf{x}}$ is the Jacobian matrix of $\mathbf{F}$. Let us now introduce the mean exponential rate of divergence of two initially closed trajectories

$$\boldsymbol{\sigma}(\,\overline{\mathbf{x}}_{\mathbf{0}},\Delta\overline{\mathbf{x}}\,) \;=\; \lim_{\substack{t\,\to\,\infty\\ d(0)\,\to\,0}} \left(\frac{1}{t}\right)\,\ln\,\frac{d(\,\overline{\mathbf{x}}_{\mathbf{0}},\,t\,)}{d(\,\overline{\mathbf{x}}_{\mathbf{0}},\,0\,)},$$

where it can be shown that $\boldsymbol{\sigma}$ exists and is finite. Moreover, there is an N dimensional basis $\{\hat{\boldsymbol{e}}_{\boldsymbol{i}}\}$ of $\Delta\overline{\mathbf{x}}$ such that for any $\Delta\overline{\mathbf{x}}$, $\boldsymbol{\sigma}$ takes on one of the N values $\sigma_i(\,\overline{\mathbf{x}}_{\mathbf{0}}\,) \;=\; \sigma_i(\,\overline{\mathbf{x}}_{\mathbf{0}},\,\hat{\boldsymbol{e}}_{\boldsymbol{i}}\,)$. These σ_i's are called *Lyapunov exponents*. Due to the phase space volume preservation property of Hamiltonian flow sum of the Lyapunov exponents will be zero, i.e., $\sum_i\,\sigma_i \;=\; 0$.

1.3 Chaos in Higher-dimensional systems : Arnold Diffusion

So far we have only discussed about the dynamics of the Hamiltonian systems having two degrees of freedom, i.e. $N = 2$. There exists an important topological distinction between the systems having $N = 2$ degrees of freedom and the systems having $N > 2$ degrees of freedom. For a time independent Hamiltonian system, the energy is a constant of motion and therefore the dynamics effectively takes place in the $(2N-1)$-dimensional energy surface $H(\overline{p},\overline{q}) = E$. We know, in order for a closed surface to divide a $(2N-1)$-dimensional space into *two* disjoint parts, one inside the closed surface and another outside, the closed surface must have

a dimension one less than the dimension of the space, i.e. the dimension of this surface should be $(2N-2)$. Since the KAM surfaces are N-dimensional tori, hence they can satisfy the above condition for $N = 2$ case only. Because, for $N = 2$, the energy surface has a dimension 3 and a 2-dimensional toroidal KAM surface in a 3-dimensional space has an inside and an outside. For $N = 3$, the dimension of the energy surface is 5, and therefore a surface of dimension $5 - 1 = 4$ can divide the energy surface of dimension 5 into two disjoint parts. However, we know that the dimension of the toroidal KAM surface for $N = 3$ case is 3 and therefore this 3-dimensional toroidal KAM surface can not divide the energy surface into two disjoint parts. Consequently one single connected region forms.

Let us consider a perturbed integrable system of $N = 2$ degrees of freedom, whose tori begin to break up and are replaced by chaotic orbits. In this case the chaotic regions are trapped between surviving KAM tori. More precisely, if a chaotic orbit is outside (inside) a particular KAM torus, it remains outside (inside) that torus forever. Therefore, the chaotic orbit of a slightly perturbed integrable 2-degrees of freedom system must lie close to the orbit on a torus of the unperturbed integrable system for all time.

The situation is completely different for $N > 2$ cases. In these cases chaotic orbits are not trapped by KAM tori and hence their motions are not restricted like $N = 2$ case. Now the natural assumption is that, all the chaos created by destroyed tori can form a single connected chaotic region which is dense in the phase space. This assumption implies that if we wait for a long enough time then a chaotic orbit can come arbitrarily close to *any* point in phase space. Arnold first demonstrated this phenomenon for a particular example and therefore it is known as *Arnold's diffusion* [8].

1.4 Quantum manifestations of classical chaos : Quantum chaos

Inadequacy of classical mechanics to describe the behaviors of microscopic particles was realized at the dawn of the last century. Quantum Mechanics is the theory which not only replaced classical mechanics, but it also brought a rev-

olutionary change in our understandings of different physical processes. The concept of the 'trajectory of a particle' is completely absent in quantum mechanical framework. Therefore we can not use the notion of exponential divergence of trajectories to define chaos in quantum mechanical system. More precisely, quantum systems are not chaotic in the sense that classical systems are. So the natural question is "*Can there be Quantum Chaos* ?" If yes, then "*What is the definition of Quantum Chaos* ?" or "*What way classical chaos is reflected in the characteristics of corresponding quantum systems* ?" There is no satisfactory quantum mechanical definition of Quantum Chaos. However we can give a semiclassical definition of quantum chaos following Berry [9]. But before going into that we want to discuss some experiments related to quantum chaos. Here experiments mean traditional laboratory experiment and also numerical experiment.

1.4.1 Ionization of Rydberg states of the Hydrogen atom inside microwave cavity : Dynamical localization

According to Bohr's correspondence principle classical mechanics is contained within quantum mechanics in appropriate limit. The limit of large quantum numbers is one such appropriate limit. The states with large principal quantum numbers are called Rydberg states. In 1974, *Bayfield and Koch* [10] performed an experiment to measure the ionization of H-atoms of principal quantum number $n_p \simeq 66$ placed inside a microwave cavity as a function of microwave field strength. This experiment showed a sharp increase in the ionization signal at a certain threshold value F of the microwave field strength. Later in 1979, *Leopold and Percival* [11] provided a surprising explanation for the above experimental results by simply treating Rydberg states classically. This classical calculation showed that when the microwave field strength is less than F, the electrons move under the joint influence of the Coulomb attraction of the nucleus and the external microwave radiation field with periodic absorption of energy in captured orbits around the nucleus ; in contrary, when the field strength cross that threshold value F, chaotic orbits appear that quickly remove the electron from the influence of the nucleus, which leads to premature ionization of the electron. The absorption of energy in these orbits occur in a diffusion like manner.

Systematic comparisons between the classical prediction for the onset of chaotic ionization with the quantum ionization thresholds has shown remarkable agreement for many different Rydberg states as long as the microwave frequency is less than the *orbital frequency* of the electrons [12]. These results are actually pointing out that, even though quantum mechanics cannot satisfy the strict definitions of classical chaos, but still the quantum dynamics may mimic the classical chaotic ionization at least on these limited experimental timescales. Now a natural question is that "*Are these experiments really illustrating Quantum Chaos* ?" The answer is "*They do not*". Because chaos is unpredictability that *persists*, and in these experiments the atoms traverse only a short distance of microwave field and so diffuse for only short time.

Surprising results came with quantum mechanical calculations for microwave frequencies greater than the orbital frequency [13, 14]. These results show that, for short times, the electrons in Rydberg states indeed absorb the energy in the classical way (diffusively), after a certain '*break-time*' there is a new regime in which the electrons absorb energy more slowly.

Similar kind of behavior was also observed earlier in the study of a model system in which a particle on a ring (a rotator) is kicked periodically with an impulse that depends on the angular position of the particle [15], i.e. the Hamiltonian of this system is given by

$$H(t) = \frac{1}{2}I^2 + k\,F(\phi)\sum_n \delta\,(t - nT)).$$

For strong kicks (large k), the angular momentum I of the classical rotator shows diffusion like behavior, and consequently the energy grows linearly with time. On the other hand, in quantum mechanical treatment within the range of large quantum numbers shows that the energy increases only for a certain period of time and eventually it stops growing. This property has been experimentally verified by atom-optics realization of the kicked rotator [16].

The above results are important because these illustrate a general phenomenon : *quantum suppression of classical chaos*, which is also popularly called '*dynamical localization*'. It has been shown that the dynamical localization can be related to the mechanism of *Anderson localization* in solid state physics [17]. This

suppression of chaos is quite expected, because classical chaos can be considered as the appearance of increasingly complicated structures on infinitely fine scales in classical phase space. But quantum mechanically it is not possible to go down to such infinitely fine scales, because in the phase-space, cells smaller than Planck's constant h, every structure is smoothed away.

In the above studies we have not found any chaotic temporal evolution of quantum systems. However we have observed a new quantum phenomenon, dynamical localization, that emerges in the semiclassical limit of the systems whose classical dynamics are chaotic. Motivated with this fact, Berry defined quantum chaos (*quantum chaology*, in Berry's terminology) as [9]:

"*Quantum chaos is the study of semiclassical, but non-classical, behavior characteristic of systems whose classical dynamics exhibits chaos*".

Dynamical localization is a temporal property of a quantum chaotic system. For the time being we are leaving the temporal evolution, and will discuss some stationary properties of quantum chaotic systems. We again come back to discuss another temporal property of a quantum chaotic system, i.e. the entanglement production by the time-evolution operator corresponding to coupled chaotic system and this study is one of the major goal of this thesis.

1.4.2 Semiclassical Quantization

According to above definition of quantum chaos, in the semiclassical limit, we expect some signature of chaos can be seen in the eigenvalues and the eigenvectors of the system. In quantum mechanics, following Heisenberg's uncertainty principle, a general assumption is that any structure below the phase space cell of size $\hbar$ (Planck cell) do not exist or at least they do not matter. Therefore, $\hbar \to 0$ is a semiclassical limit. However, very recently it has been claimed that this common assumption of quantum mechanics is false. The structure associated with sub-Planck scale has some relevance for quantum decoherence [18]. In Sec.1.6, we discuss about quantum decoherence.

The most popular semiclassical technique for the determination of the eigenvalues of 1 DOF quantum system is the Wentzel-Krammer-Brillouin (WKB)

method which has been discussed in almost all textbooks of quantum mechanics. Einstein-Brillouin-Keller (EBK) quantization is the semiclassical quantization method for the systems having more than one DOF [19]. In this quantization procedure, for the N DOF case, classical action along N independent circuits of the tori are expressed as integral multiples of $\hbar$.

WKB and its extended version EBK are the quantization procedures for the integrable systems. However, if the underlying classical system is chaotic, the WKB or EBK will not work. So a new type of quantization scheme would be required . Nearly half a century later, *Gutzwiller* found a way to quantize chaotic systems, and it is popularly known as Gutzwiller's trace formula [20].

1.4.3 Statistical properties of the quantum chaotic spectra

In the preceding section we have discussed semiclassical $(h \to 0)$ quantization procedure for classically regular as well as for classically chaotic systems. Here we are now interested in to reveal the differences between the eigenvalues spectra of regular and chaotic systems. In order to do that, according to Berry, we have to examine the energy spectra on different scales of $\hbar$. On the fines scales, one can identify individual eigenvalues. This is the regime in which we can use EBK rule for regular states and Gutzwiller trace formula for the state having underlying chaotic classical dynamics. In contrary, on the largest scales, we can only get the average density of states $\overline{\rho}(E)$ given by Thomas-Fermi formula

$$\overline{\rho}(E) \;=\; \frac{1}{(2\pi\hbar)^N} \int\int \delta\left(E - H(\overline{\mathbf{p}}, \overline{\mathbf{q}})\right) d\overline{\mathbf{p}}\, d\overline{\mathbf{q}}.$$

The above expression is the Liouville measure of classical phase-space at energy E divided by the statistical volume $(2\pi\hbar)^N$ "occupied" by a quantum state. At this scale we can not expect to distinguish the effects of regular and chaotic classical motion. So two extreme scales of $\hbar$ are not suitable for our purpose, and hence we should look at the spectrum on the intermediate scales of resolution. In this scale, the various clustering and distributions of the energy levels may reveal much about the underlying motion.

The remarkable result is that, in this intermediate scale, the distribution of energy eigenvalues shows *universality*. In order to produce comparable condi-

tions, however, the spectra must be transformed in such a way that the density of states becomes uniform. This method is called 'unfolding' of spectra. This is accomplished as follows : the average level density $\overline{\rho}(E)$ is determined, average number of levels upto energy E is calculated from it,

$$\overline{N}(E) \;=\; \int_{-\infty}^{E} \overline{\rho}(E')\, dE',$$

and then we consider the spectrum $x_j \;=\; \overline{N}(E_j)$, which, by construction, has a constant average level spacing that is chosen as the energy unit. The cumulative level density $n(x)$ [number of levels upto x] then is a staircase function that fluctuates around a straight line with slope unity.

Universality is found in the statistics of the level sequences. One such statistic, a short range one, is the probability distribution $P(S)$ of the spacing between neighboring energy levels, i.e. the distribution of $S_j \;=\; x_{j+1} \,-\, x_j$. Bohigas et al [21] showed that the distribution $P(S)$ calculated from the several hundred levels of the stadium billiard and the Sinai billiard are the same, and they follow *Wigner* distribution

$$P(S) \;=\; \frac{\pi}{2}\, S\, \exp\left(-\,\frac{\pi S^2}{4}\right). \tag{1.4}$$

The above expression is pointing out that the probability of finding the levels in the same location tends to zero linearly with S. This distribution is satisfied by all the chaotic systems having time reversal like any anti-unitary symmetry. This linear repulsion is also the property of Gaussian distributed real symmetric random matrices. The probability distribution for the matrix elements of such random matrices are invariant under orthogonal transformations and therefore the ensemble of these random matrices is called Gaussian orthogonal ensemble (GOE). If a chaotic system has no anti-unitary symmetry, then their nearest neighbor levels will repel quadratically each other and their nearest neighbor spacing distribution (NNSD) will be

$$P(S) \;=\; \frac{32}{\pi^2}\, S^2\, \exp\left(-\,\frac{4S^2}{\pi}\right).$$

Quadratic level repulsion is the property of the Gaussian distributed complex Hermitian matrices and the probability distribution for the matrix elements of such

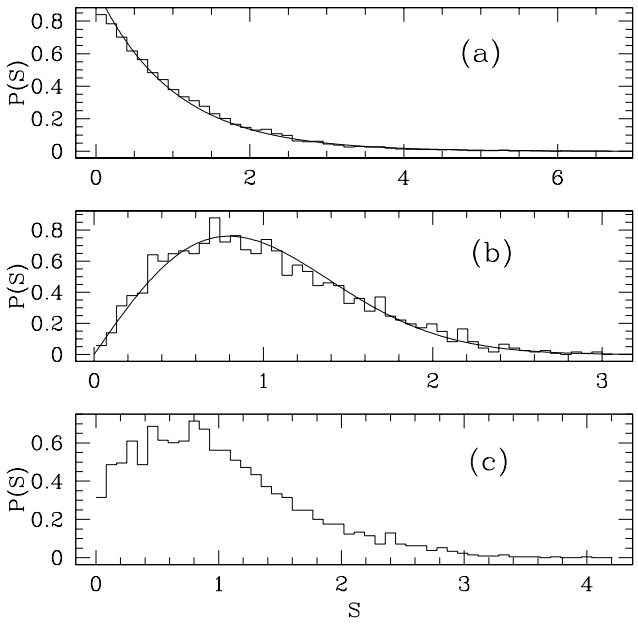

Figure 1.2: NNSD of the kicked top. (a) Nearly integrable case. NNSD satisfies Poisson distribution. (b) Chaotic case. NNSD satisfies Wigner (GOE) distribution. See Eq.(1.4). (c) Mixed case. NNSD is intermediate of Poisson and Wigner.

random matrices are invariant under unitary transformations and therefore the ensemble of these random matrices is called Gaussian unitary ensemble (GUE). On the other hand, if a given system is integrable, then the spacing distribution of the nearest level will be *Poisson* type, i.e. $P(S) = \mathrm{e}^{-S}$. In Fig.1.2 we have presented the NNSD of kicked top, a well studied model of chaotic system, for both (nearly) regular, chaotic and mixed cases. For (nearly) regular cases, shown in Fig.1.2(a), its NNSD satisfies Poisson distribution. Since the kicked top, which we have discussed in Chapter 3, has an antiunitary symmetry and hence its NNSD follows Eq.(1.4) for completely chaotic cases. See Fig.1.2(b). In Fig.1.2(c), we have shown NNSD for the mixed cases. In these cases, NNSD follow the statistics which is intermediate of Poisson and Wigner distribution. The major difference between the first two kind of spectrum is that quantum chaotic systems show level repulsion and as a consequence of this, a maximum probable level spacing comes different from zero, whereas the level distribution of regular systems show level accumulation.

1.4.4 Semiclassical properties of the eigenstates

Berry-Voros hypothesis :

In the preceding section we have discussed about the effect of underlying classical dynamics on the eigenvalues spectra. So it is very natural to expect some signature of classical dynamics also on the eigenstates. Berry suggested that, in semiclassical limit, the Wigner function of the eigenstates may show some distinct behaviors corresponding to underlying classical dynamics [22]. The Wigner function is a quantum analogue of classical phase-space density, and it is defined for a normalized state $|\psi\rangle$ as

$$W(\overline{\mathbf{p}},\overline{\mathbf{q}}) \;=\; \frac{1}{(\pi\hbar)^N}\int d\overline{\mathbf{x}}\,\langle\overline{\mathbf{q}}\,+\,\overline{\mathbf{x}}|\psi\rangle\,\langle\psi|\overline{\mathbf{q}}\,-\,\overline{\mathbf{x}}\rangle\,\exp\left(-\frac{2i\overline{\mathbf{q}}\,.\,\overline{\mathbf{x}}}{\hbar}\right).$$

Here is some important properties of the Wigner function :

$$(1)\;\int W(\overline{\mathbf{p}},\,\overline{\mathbf{q}})\,d\overline{\mathbf{p}} \;=\; |\psi(\overline{\mathbf{q}})|^2\;;\quad (2)\;\int W(\overline{\mathbf{p}},\,\overline{\mathbf{q}})\,d\overline{\mathbf{q}} \;=\; |\tilde{\psi}(\overline{\mathbf{p}})|^2\;;$$

$$(3)\;\int\int W(\overline{\mathbf{p}},\,\overline{\mathbf{q}})\,d\overline{\mathbf{p}}\,d\overline{\mathbf{q}} \;=\; 1.$$

The Wigner function is not positive definite, and therefore it is also referred as "pseudo phase-space density".

The semiclassical form of the eigenstates with quantum number $\overline{\mathbf{n}}$ corresponding to regular system is given by

$$\psi_n(\overline{\mathbf{q}}) \;=\; \sum_r \det\left|\frac{\partial^2 S_r(\overline{\mathbf{q}},\,\overline{\mathbf{I}}_{\overline{\mathbf{n}}})}{\partial q_j\,\partial I_k}\right|^{1/2}\;\exp\left[\frac{iS_r(\overline{\mathbf{q}},\,\overline{\mathbf{I}}_{\overline{\mathbf{n}}})}{\hbar}\right]$$

where $\overline{\mathbf{I}}_{\overline{\mathbf{n}}}$ represents the phase-space torus with actions $\overline{\mathbf{I}}_{\overline{\mathbf{n}}} \;=\; (\overline{\mathbf{n}}\,+\,\overline{\boldsymbol{\alpha}}/4)\,\hbar$. This form of the eigenstates can be used to evaluate corresponding Wigner function $W_{\overline{\mathbf{n}}}(\overline{\mathbf{p}},\overline{\mathbf{q}})$. Berry has shown that, in the limit $\hbar \;\to\; 0$, the above Wigner function $W_{\overline{\mathbf{n}}}(\overline{\mathbf{p}},\overline{\mathbf{q}})$ reduces to [22]

$$\overline{W}_{\overline{\mathbf{n}}}(\overline{\mathbf{p}},\overline{\mathbf{q}}) \;=\; \frac{1}{(2\pi)^N}\;\delta\,(\overline{\mathbf{I}}(\overline{\mathbf{p}},\overline{\mathbf{q}})\;-\;\overline{\mathbf{I}}_{\overline{\mathbf{n}}}).$$

The above expression shows that the Wigner function collapses onto the classical N-dimensional torus associated with the $\overline{\mathbf{m}}$th state.

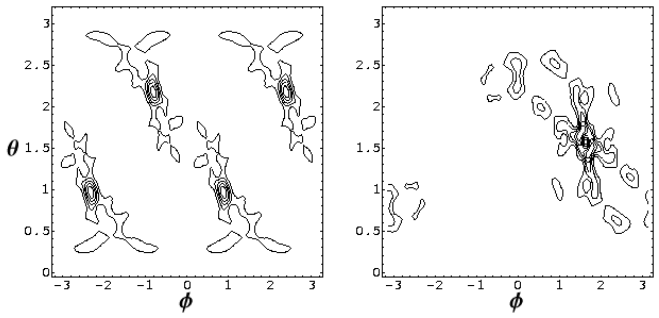

Figure 1.3: (a) A scarred eigenstate of the kicked top corresponding to an unstable period-4 orbit. (b) Another scarred eigenstate corresponding to an unstable fixed point.

Semiclassical form of the eigenstates corresponding to chaotic systems is not known. However, we have observed that the Wigner function of the eigenstates corresponding to regular systems is the phase-space manifold (torus) of the underlying classical systems specified by the energy and/or the values of the constants of motion. Now in the chaotic case, phase-space trajectories wander freely on the energy surface or some parts of this surface. Observing this, Berry and Voros [22, 23] suggested the microcanonical distribution as an approximation for the Wigner function of the chaotic eigenstates, i.e. in this case

$$\overline{W}(\overline{\mathbf{p}}, \overline{\mathbf{q}}) \;=\; \frac{\delta(\, E \;-\; H(\overline{\mathbf{p}}, \overline{\mathbf{q}})\,)}{\int\int d\overline{\mathbf{p}}\, d\overline{\mathbf{q}}\; \delta(\, E \;-\; H(\overline{\mathbf{p}}, \overline{\mathbf{q}})} . \tag{1.5}$$

The exact form of $\overline{W}$ is not known for finite $\hbar$, but one can expect that a surface of section of $\overline{W}$ would display a random splatter of phase-space density. This is somewhat similar to the Poincare surface of section observed for chaotic trajectories. The Berry-Voros hypothesis on the behavior of eigenvectors has been verified numerically for different model of chaotic systems like Henon-Heiles [24, 25], stadium billiard [26], etc.

Violation of Berry-Voros hypothesis. Scarred eigenstates :

The above approximation to chaotic eigenstates is slightly crude. There at least exists a semiclassical form for the eigenstates of regular systems, but the behavior of the eigenstates of chaotic systems was suggested somewhat in ad hoc manner. So it is not surprising to find that there exists some interesting structures which are superimposed. Eventually, Heller's extensive numerical studies on chaotic

stadium billiard have shown strikingly different behaviors of the eigenstates [27]. His study has shown that, in addition to typical eigenstates with highly complex structure as predicted by Berry-Voros hypothesis, there are also eigenstates with very regular structure. These kind of states are called '*scarred states*'. A formal definition of the scarred states is : "*A quantum eigenstate of a classically chaotic system has a scar of a periodic orbit if its density on the classical invariant manifolds near the (unstable) periodic orbit is enhanced over the statistically expected density*" [28]. Scars have been seen in a number of systems other than chaotic stadium billiard. Most popular among these systems are quantum baker's map [28], coupled quartic oscillators [29], Hydrogen atom in strong magnetic field [30], etc. But the important thing is that the scarring phenomena have been realized experimentally in microwave cavities [31], and recently in electron motion in semiconductor quantum well [32]. In Fig.1.3, we have shown two eigenstates of the kicked top which are scarred respectively by an unstable period-4 orbit and an unstable fixed point.

1.5 Chaos and Entanglement

In the last few sections we have discussed extensively about different properties of quantum chaotic systems. We are now going to discuss a very new topic "chaos and entanglement". We have taken a crucial part in the study of this particular topic. Therefore a major portion of this thesis is devoted to the study of chaos and entanglement.

We know from our previous study on quantum chaos that, except some observations of quantum signature of classical chaos, there is no existence of exact quantum analogue of classical chaos. So, for the time being, we can safely consider chaos as the phenomenon which can only be observed in classical domain. On the other hand, entanglement is an unique property of a composite quantum system which consists of more than one interacting subsystems. Entanglement is a nonclassical correlation among the subsystems which exists even between spatially well separated subsystems [33, 34]. There is no classical analogue of entanglement. Therefore it is interesting to study the connection between chaos

and entanglement, two phenomena that are prima facie uniquely classical and quantum respectively. This is one important reason to study the connection between chaos and entanglement. However, most of the recent works on this topic are motivated due to the characterization of entanglement as quantum resource for quantum information theory and quantum computation.

Since a quantum computer is a many particle system, entanglement is inevitable. In realistic situation, due to the presence of some imperfections, quantum signatures of classical chaos or simply quantum chaos can be seen in the quantum computers [35]. Therefore the study to enquire whether quantum chaos will help or hinder in the operation of a quantum computer is important. At a more basic level, it is very important to explore the connections between chaos and quantum entanglement.

In the present section, first we will discuss about some basic facts related to entanglement, e.g. definition, properties, its usefulness in quantum information processing, example of entangled state, measure of entanglement, etc. Then we will give a brief idea of the present status of this topic of research.

1.5.1 Entanglement

Once a paradox, now a useful resource :

We have already mentioned that entanglement is the property of a composite quantum system which consists of more that one interacting subsystems. Let us assume that a system consists of two subsystems A and B, and their associated Hilbert spaces are $\mathcal{H}_A$ and $\mathcal{H}_B$ respectively. A composite system which consists of two subsystems is called *bipartite* system. Naturally the tensor product space $\mathcal{H}_A \otimes \mathcal{H}_B$ will be the Hilbert space for the bipartite system $A+B$. If a pure quantum state $|\psi\rangle$ of the bipartite system $A+B$ can be decomposed into a tensor product of two pure quantum states like $|\psi\rangle = |\phi_A\rangle \otimes |\phi_B\rangle$, where $|\phi_A\rangle$ describing the state of the subsystem A and $|\phi_B\rangle$ describing the subsystem B, then the state $|\psi\rangle$ is unentangled or product state. That means, the states $|\phi_A\rangle$ and $|\phi_B\rangle$ have no quantum correlation. But this is not the generic case. In general, if the two subsystems were not prepared independently in total isolation from each other,

the above decomposition is impossible. Let us assume a state $|\psi\rangle$ of the bipartite system as

$$|\psi\rangle = c_1 |\phi_A^{(1)}\rangle \otimes |\phi_B^{(1)}\rangle + c_2 |\phi_A^{(2)}\rangle \otimes |\phi_B^{(2)}\rangle,$$

where $|c_1|^2 + |c_2|^2 = 1$. In this case, it is not possible to assign any pure state to any of the subsystems A or B. We call this state of the bipartite system as an entangled state. The most celebrated example of an entangled state of two particles is the *Einstein-Podolsky-Rosen-Bohm* state of two spin-$\frac{1}{2}$ particles,

$$|\psi\rangle = \frac{1}{\sqrt{2}}\big(|\uparrow\rangle \otimes |\downarrow\rangle - |\downarrow\rangle \otimes |\uparrow\rangle\big),$$

where $\{|\uparrow\rangle, |\downarrow\rangle\}$ are the eigenstates of the angular momentum component σ_z (Pauli matrix). $|\uparrow\rangle \otimes |\downarrow\rangle \Big(|\downarrow\rangle \otimes |\uparrow\rangle\Big)$ means that particle 1 is in the spin-up (spin-down) state and particle 2 is in the spin-down (spin-up) state. Let us now assume that the particle 1 is with an observer A and the particle 2 is with another observer B. Now if A measures σ_z of particle 1 and find spin-up (spin-down), then A can immediately predict, even before B makes any measurement, the outcome of B's measurement with certainty : B must find σ_z to be down (up) for particle 2. On the other hand, if A makes no measurement, B has a 50-50 chance of getting σ_z up or down. These correlations between the outcomes of A and B are not so unusual. This can be compared with a box containing one black ball and one white ball. If we blindly pick one ball from the box, then there is a 50-50 chance of getting black or white ball. But if the first ball we pick is black (white), then we can predict with certainty that the second ball will be white (black).

Until now everything is fine, nothing against our intuition. But in actual quantum mechanical situation, the observers are also allowed to measure σ_x. That means, quantum mechanics allows to analyze the same pair of *balls* either in terms of black and white or even in terms of say blue and red ! In terms of the eigenstates of σ_x, $\{|\Uparrow\rangle, |\Downarrow\rangle\}$, the Einstein-Podolsky-Rosen-Bohm state is written as

$$|\psi\rangle = \frac{1}{\sqrt{2}}\big(|\Downarrow\rangle \otimes |\Uparrow\rangle - |\Uparrow\rangle \otimes |\Downarrow\rangle\big).$$

Let us now assume that the observer A is allowed to measure σ_z or σ_x of particle

1 by changing the orientation of his or her apparatus, while B is only restricted to measure σ_x of particle 2. There are three possible outcomes :

(1) If A measures σ_z and B measures σ_x, there is completely random correlation between the two measurements.

(2) If A measures σ_x and B also measures σ_x, there is an exact correlation between the two measurements.

(3) If A makes no measurement, B's measurement shows random results.

The above considerations show that the outcomes of B's measurement appear to depend on what kind of measurement A decides to perform.

The above *nonlocality* was not acceptable to many physicists. Even Einstein remarked, which we called Einstein's locality principle : "*The real factual situation of the system S_2 is independent of what is done with the system S_1, which is spatially separated from the former*" [34]. This locality principle, according to our *common sense*, is quite *reasonable*. However, in 1964, J. S. Bell pointed out that Einstein's locality principle actually predicts a *testable inequality relation* among the observables of spin-correlation experiments that disagrees with the prediction of quantum mechanics [36]. Later, many experiments have conclusively established the violation of Bell's inequality. These experiments provided decisive evidence in favor of quantum mechanics [37]. These results also show that nature does not always follow our common sense.

Entanglement, once a paradox, appears today to be a potentially useful resource. The predicted capabilities of a quantum computer and also of quantum information theory rely crucially on entanglement. As an example, if A and B are sharing a pair of entangled state, then A can teleport an arbitrary quantum state to B [38] and their shared entanglement can also be converted into a shared secret key [39]. By quantum teleportation, it is also possible for A to send 2 bits of classical information to B by just sending a single qubit. This is the process called quantum superdense coding [40]. The efficiency of most of the proposed quantum algorithms is based on the entanglement [41, 42].

Density matrix :

As we have mentioned, it is not possible to assign any pure state to a subsystem which has formed an entangled pair with another subsystem. Therefore the quantum state of any of the subsystems has to be a mixed state. A mixed state can be described only by a density matrix. So before going into further discussion on the entanglement, let us first discuss some properties of density matrices. The density matrix, in general denoted by ρ, is a linear operator in $\mathcal{H}$ such that

(a) ρ is Hermitian,

(b) ρ is positive semi-definite, that is $\langle\phi|\,\rho\,|\phi\rangle \geq 0$ for any $|\phi\rangle \in \mathcal{H}$,

(c) $\mathrm{Tr}\,\rho = 1$.

A mixed state can only be expressed in terms of density matrices, but a pure state can also be represented by a density matrix as well. For a pure state, the density matrix is the projection operator corresponding to the state $|\psi\rangle$, i.e. $\rho = |\psi\rangle\langle\psi|$. Therefore, for the pure state $\rho^2 = (|\psi\rangle\langle\psi|)(|\psi\rangle\langle\psi|) = |\psi\rangle\langle\psi| = \rho$. So this property of the density matrices can be used to check whether a given density matrix is reportedly a mixed state or a pure state.

Let us now back to our discussion on the bipartite system $A+B$. Suppose $\{|a_i\rangle\}$ and $\{|b_j\}$ form an orthonormal basis for subsystems A and B respectively. Any state $|\psi\rangle \in \mathcal{H}$, which is a state of the bipartite system $A+B$, can be written in terms of the above basis as

$$|\psi\rangle = \sum_{i,j} c_{ij}|a_i\rangle \otimes |b_j\rangle.$$

Therefore the density matrix corresponding to this pure state $|\psi\rangle$ is

$$\rho = |\psi\rangle\langle\psi| = \sum_{i,j,k,l} c_{ij}\, c^*_{kl}\,(|a_i\rangle\langle a_k|) \otimes (|b_j\rangle\langle b_l|).$$

Suppose we are only permitted to observe one of the subsystem and we want to describe the properties of that subsystem regardless of the state of the other unobserved subsystem. Then we can assign reduced density matrices (RDMs) $\rho_A\,(\rho_B)$ to the subsystem $A\,(B)$ by taking partial trace over $B\,(A)$ subsystem of the density matrix ρ corresponding to $A+B$. Therefore

$$\rho_A = \mathrm{Tr}_B\,\rho = \sum_j \langle b_j|\,\rho\,|b_j\rangle = \sum_{i,j,k} c_{ij}\, c^*_{kj}|a_i\rangle\langle a_k| = CC^\dagger$$

and

$$\rho_B \;=\; \mathrm{Tr}_A\,\rho \;=\; \sum_{i,j,l} c_{ij}\, c_{il}^{*} |b_j\rangle\, \langle b_l| \;=\; C^{\dagger} C,$$

where $c_{ij} \;=\; [C]_{ij}$. The RDMs permit us to calculate all the physical prediction about the subsystem under consideration. For example, the expectation value of any observable O_A pertaining to the subsystem A being in the state specified by the RDM ρ_A is given by

$$\langle O_A \rangle \;=\; \mathrm{Tr}_A(\rho_A O_A).$$

Therefore the RDMs ρ_A and ρ_B are the effective density matrices corresponding to the subsystems A and B respectively. This can be easily shown by proving

$$\langle\, O_A \,\rangle \;=\; \mathrm{Tr}_A\,(\rho_A\, O_A) \;=\; \mathrm{Tr}_{A+B}\,[\rho\,(O_A \,\otimes\, I_B)],$$

where ρ is the density matrix of the total bipartite system $A+B$ and I_B is the unit matrix corresponding to B subsystem. The above expression shows that it is not necessary to use full density matrix ρ to calculate the expectation value of any observable which solely belongs to a particular subsystem.

Schmidt decomposition :

Let us consider a pure state corresponding to the bipartite system $A+B$ as

$$|\psi\,\rangle \;=\; \sum_{i,j} c_{ij}\, |a_i\,\rangle |b_j\,\rangle, \tag{1.6}$$

where $\{|a_i\,\rangle\}$ and $\{|b_j\,\rangle\}$ are arbitrary orthonormal bases for the subsystems A and B respectively. We will now prove that for any pure state of a bipartite system can be represented by a sum of *bi-orthonormal* bases called *Schmidt bases* and this method is called Schmidt decomposition.

Proof : We know, c_{ij}'s can be considered as the elements of a matrix C. If the dimension of two subsystems A and B are different, say N and M respectively, then C will be a $N \times M$ rectangular complex (in general) matrix. Without loss of any generality we can assume $N < M$. According to singular value decomposition,

the matrix C can be written as $C = U\Lambda V$ where U and V are unitary matrices and Λ is a rectangular matrix of the form $[\Lambda]_{mn} = \sqrt{\lambda_m}\,\delta_{mn}$. Therefore we can write

$$c_{ij} = \sum_{k=l}^{N}\sum_{l=1}^{M}[U]_{ik}\,[\Lambda]_{kl}\,[V]_{lj}.$$

Substituting this in Eq.(1.6), we get

$$|\psi\rangle = \sum_{i,k=1}^{N}\sum_{j,l=1}^{M}[U]_{ik}[\Lambda]_{kl}\,[V]_{lj}\,|a_i\rangle \otimes |b_j\rangle.$$

Let us now define

$$|\overline{a}_k\rangle \equiv \sum_{i=1}^{N}[U]_{ik}\,|a_i\rangle, \quad |\overline{b}_l\rangle \equiv \sum_{j=1}^{M}[V]_{lj}\,|b_j\rangle. \tag{1.7}$$

Hence we get

$$\begin{aligned} |\psi\rangle &= \sum_{k=1}^{N}\sum_{l=1}^{M}[\Lambda]_{kl}\,|\overline{a}_k\rangle \otimes |\overline{b}_l\rangle \\ \text{i.e., } |\psi\rangle &= \sum_{k=1}^{N}\sqrt{\lambda_k}\,|\overline{a}_k\rangle \otimes |\overline{b}_k\rangle, \quad \text{since } [\Lambda]_{kl} = \sqrt{\lambda_k}\,\delta_{kl}, \end{aligned} \tag{1.8}$$

where $\sum_{k=1}^{N}\lambda_k = 1$, which is coming from the normalization condition of $|\psi\rangle$. From Eq.(1.7), it can be easily shown that $\{|\overline{a}_k\rangle\}$ and $\{|\overline{b}_k\rangle\}$ are the orthonormal bases, i.e.

$$\langle\,\overline{a}_k|\overline{a}_l\,\rangle = \delta_{kl} = \langle\,\overline{b}_k|\overline{b}_l\,\rangle.$$

If only one λ is nonzero in Eq.(1.8), then that λ will be definitely unity and therefore

$$|\psi\rangle = |\overline{a}_k\rangle \otimes |\overline{b}_k\rangle. \tag{1.9}$$

The above state is clearly a product (unentangled) state. And if more than one λ's are nonzero in Eq.(1.8), then the state $|\psi\rangle$ is an entangled state. Therefore, by expanding a pure state in Schmidt bases, we can very easily tell whether that given state is entangled or product state.

The Schmidt decomposition pertains to a specific bipartite pure state. For every bipartite pure state there exists Schmidt decomposition. But for two different

pure states there will be two different Schmidt decompositions. Now the question is how can one determine the Schmidt decomposed form or Schmidt bases for a given pure state.

In the Schmidt bases, the density matrix ρ corresponding to the state $|\psi\rangle$ is

$$\rho = |\psi\rangle\langle\psi| = \sum_{k,l=1}^{N} \sqrt{\lambda_k \lambda_l}\,(\,|\overline{a}_k\rangle\langle\overline{a}_l|\,) \otimes (\,|\overline{b}_k\rangle\langle\overline{b}_l|\,).$$

If we now construct RDMs ρ_A and ρ_B, we will get

$$\begin{aligned} \rho_A &= \sum_{k=1}^{N} \lambda_k\, |\overline{a}_k\rangle\langle\overline{a}_k| \\ \text{and } \rho_B &= \sum_{k=1}^{N} \lambda_k\, |\overline{b}_k\rangle\langle\overline{b}_k| \end{aligned} \tag{1.10}$$

The above expressions show that the RDMs are diagonal in Schmidt basis. Therefore the Schmidt bases $\{\,|\overline{a}_k\rangle\,\}$ and $\{\,|\overline{b}_k\rangle\,\}$ are the eigenstates of the RDMs ρ_A and ρ_B respectively and $\{\,\lambda_k\,\}$'s are the nonzero eigenvalues of RDMs. So one can determine the Schmidt bases of a given bipartite pure state $|\psi\rangle$ in following steps:

- Construct the density matrix $\rho = |\psi\rangle\langle\psi|$ corresponding to the state $|\psi\rangle$. Here $|\psi\rangle$ is represented in any arbitrary basis, i.e. $|\psi\rangle = \sum_{i,j} c_{ij}\,|a_i\rangle \otimes |b_j\rangle$.
- Determine the RDMs $\rho_A = C\,C^\dagger$ and $\rho_B = C^\dagger\,C$.
- Diagonalize ρ_A and ρ_B to determine their nonzero eigenvalues $\{\,\lambda_k\,\}$ and the corresponding eigenstates $\{\,|\overline{a}_k\rangle\,\}$ and $\{\,|\overline{b}_k\,\}$. Using these, we can write the Schmidt decomposed form of $|\psi\rangle$ as given in Eq.(1.8).

Few important points about Schmidt decomposition

(a) Two interacting quantum subsystems usually lose their individual identities and form a correlated system which is represented by an entangled state. The Schmidt bases illustrate the nature of this entangled state.
(b) The summation over the single index in the Schmidt decomposed form of $|\psi\rangle$ goes to the smaller of the dimensionalities of the two Hilbert spaces $\mathcal{H}_A$ and $\mathcal{H}_B$. Like here, we have assumed $\dim \mathcal{H}_A = N < \dim \mathcal{H}_B = M$ and therefore the summation index in the Schmidt decomposed form of the state $|\psi\rangle$ varies from

1 to N. That means, the smaller subsystem forces the bigger one to behave like smaller one.

(c) Except in some special cases [43], the Schmidt decomposition cannot be extended to more than two subsystems. Presence of third subsystem breaks the tight pairwise correlation of the states. And this happens because the presence of third subsystem destroys the purity of the bipartite system and also the one-to-one correspondence which makes the Schmidt bases so useful.

Measures of entanglement :

In the present thesis, we are mainly interested in the entanglement of the pure states of bipartite systems. The von Neumann entropy of the RDM is a natural measure of quantum entanglement. We have already assumed that the state space of the bipartite system is $\mathcal{H} = \mathcal{H}_A \otimes \mathcal{H}_B$, where $\dim \mathcal{H}_A = N \leq \dim \mathcal{H}_B = M$, and therefore $\dim \mathcal{H} = d = NM$. If $\rho = \sum_i p_i \, |\phi_i\rangle \langle \phi_i|$ is an ensemble representation of an arbitrary state in $\mathcal{H}$, the entanglement of formation is found by minimizing $\sum_i p_i \, E(|\phi_i\rangle)$ over all possible ensemble realizations. Here E is the von Neumann entropy of the RDM of the state $|\phi_i\rangle$ belonging to the ensemble. It has been shown that the von Neumann entropy is a good measure of entanglement [44]. Moreover, from thermodynamical arguments, it has also been shown that the von Neumann entropy is the unique measure of entanglement [45]. For a pure state $|\psi\rangle$ there is only one unique term in the ensemble representation and the entanglement of formation is simply the von Neumann entropy of the RDM.

The two RDMs of the bipartite state $|\psi\rangle$ are ρ_A and ρ_B. In Eq.(1.10), we have already presented these RDMs in the Schmidt bases. The von Neumann entropy S_V is the entanglement $E(|\psi\rangle)$ given by

$$S_V = -\,\mathrm{Tr}_l \, (\rho_l \, \ln \, \rho_l) = -\sum_{i=1}^{N} \lambda_i \, \ln \, (\lambda_i) \, ; \quad l = 1, 2, \tag{1.11}$$

where λ_i's are the eigenvalues of the RDMs. Due to the presence of *logarithmic* function in the von Neumann entropy, it can only be calculated in the eigenbasis of the RDMs. Therefore this measure is analytically not easily tractable, unless one has some information about the eigenvalues of the RDMs. Hence another

measure of the entanglement Linear entropy of the RDMs, denoted by S_R, has been studied in different publications. This measure of entanglement is defined as

$$S_R = 1 - \mathrm{Tr}_l\, \rho_l^2 = 1 - \sum_{i=1}^{N} \lambda_i^2 ; \quad l = 1, 2. \tag{1.12}$$

The above measure can also be determined without any knowledge of the eigenvalues of the RDMs. Because, $\mathrm{Tr}_l\, \rho_l^2$ can be expressed as the summation of the square of the absolute values of all elements of the RDMs, i.e.,

$$\mathrm{Tr}_l\, \rho_l^2 = \sum_{i,j} \left| (\rho_l)_{ij} \right|^2. \tag{1.13}$$

Here we want to mention that S_R is not a true measure of entanglement, it is rather a measure of the *mixedness* of the RDMs. Since the mixedness of the RDMs increases with entanglement, hence S_R can be considered as an approximate measure of entanglement.

In case of product or unentangled state, only one eigenvalue of RDMs will be nonzero with unit value. For this case $S_V = -1 \ln 1 = 0$, where $0 \ln 0 = 0$ has been assumed. Similarly, for product state, $S_R = 1 - 1^2 = 0$. Therefore for product state, both the measures of entanglement are equal to zero. This is actually minimum value of these two measures. For the maximally entangled $|\psi\rangle$, all the eigenvalues of the RDMs are equal to $1/N$, and therefore

$$S_V^{\max} = \ln N ; \quad S_R^{\max} = 1 - (1/N).$$

1.5.2 Chaos-Entanglement : Present scenario

First paper on 'chaos and entanglement' was published in 1998. In this paper, the entanglement production in an N-atom Jaynes-Cummings model was studied [46]. Their motivation was to establish the entanglement as one of the indicator of the presence of chaos in the system. They found that the entanglement rate was considerably enhanced if the initial wavepacket was placed in a chaotic region. They also argued that their results support an earlier conjecture which predicted that the entanglement production rate would be higher for a chaotic system coupled to an environment [47]. For the N-atom Jaynes-Cummings model, each

atomic subsystem plays the role of an environment for the other. Later, it has been shown that large entanglement production rate is not the hallmark of a chaotic system [48]. Even in the integrable N-atom Jaynes-Cummings model some special initial coherent states exhibit strikingly similar entanglement production as corresponding to the chaotic case [49]. In another paper, the entanglement production rate has been related to the classical Lyapunov exponents with the help of a coupled kicked tops model [50]. They also justified their findings on the basis of the above mentioned conjecture [47]. However, the classical limit of the coupled kicked tops derived in this rather well-quoted paper is incorrect, in fact it is not even canonical. Even though this coupled map is not correct, but they consider very weakly coupled tops and therefore their conclusions turn out to be qualitatively valid. Later we derived correct classical map corresponding to coupled kicked tops. This derivation is presented in Chapter 3 of this thesis.

A major motivation of all the above mentioned works were to establish entanglement as one indicator of chaos. However, it has been shown that quantum chaos can also emerge in the quantum computer and the presence of chaos can spoil the operation of the quantum computer [35]. The authors consider a standard generic quantum computer (SGQC) model which describes a system of n qubits. A qubit is a quantum two level system. Imperfections are very common in any physical systems. These imperfections in n qubit system generate a residual interqubit coupling J and the spacing between the two levels of each qubit fluctuates in some finite detuning interval δ. Quantum chaos and ergodicity can emerge in SGQC model when the interaction strength between the qubits crosses a critical limit $J = J_c$ determined by the detuning parameter δ and the total number of qubits n in the system. In this regime, qubits of a quantum computer loose their ideal structure and that can spoil the operation of a quantum computer. To prevent this spoiling one needs to introduce an efficient error correcting codes. Later, it has been shown that the error due to the presence of chaos in a quantum computer can really be corrected by proper error correcting codes, but the presence of chaos enhances the complexity of the errors and hence much more error correction is needed [51]. Therefore, the knowledge of the presence and effects of chaos in a quantum computer is necessary to implement proper error correcting

codes.

In another work, entanglement in coupled standard maps has been studied [52]. One important observation of this work is that the entanglement increases with coupling strength, but after a certain magnitude of coupling strength corresponding to the emergence of complete chaos the entanglement saturates. This saturation value depends on the Hilbert space dimension of the participating subsystems and it is less than the maximum possible value. We derived this saturation value of entanglement using random matrix theory. Moreover we presented a universal distribution of the eigenvalues of the reduced density matrices, and demonstrated that this distribution is realized in quantized chaotic systems by using the model of coupled kicked tops. In Chapter 4, we have discussed this piece of work in a more elaborate way.

Later, an analytical explanation for the entanglement production, based on perturbation theory, has been given for two weakly coupled strongly chaotic systems [53]. The authors also found that increase in the strength of chaos does not enhance the entanglement production rate for the case of weakly coupled, strongly chaotic subsystems. In a recent work, entropy production in subsystem has been examined as a dynamical criterion for quantum chaos [54]. It has been observed that the power spectrum of the entropy production gets progressively broad banded with a progressive transition from regular to chaotic dynamics. A recent study on entanglement production in a class of baker's map has shown that in general quantum baker's map is a good dynamical system to generate entanglement [55].

We have derived the saturation value of entanglement using RMT, but this entanglement saturation is a property of the strongly chaotic interacting subsystems which are coupled very strongly. Very recently, we have studied extensively the entanglement production in coupled kicked tops corresponding to different underlying classical dynamics and different coupling strengths. We have presented this work in Chapter 5 of this thesis.

In another line of investigations, due to the possibilities of using the spin systems as quantum computers, the entanglement has been studied in the well known spin models, like the Heisenberg model [56], Ising model in a transverse

field [57], Hubbard and lattice fermionic model [58], etc. Recently, entanglement has been studied in a chain of particles whose classical limit is kicked Harper Hamiltonian (a well studied model of nonintegrable system) [59]. It has been observed that, when the underlying classical Hamiltonian is (nearly) regular, the pairwise entanglement between two particles falls as a function of the distance between them. That means, the entanglement between two *nearest neighbor* particles is larger than the two *next nearest neighbor* particles, again the entanglement between two next nearest neighbor particles is larger than the two *next to next nearest neighbor* particles, and so on. But when the underlying classical dynamics is chaotic, an equal share of entanglement between any pair of particles has been observed. More explicitly, the entanglement between a particle and its r-th neighbor is now independent of r. This equal share of entanglement has been modeled by RMT. Another important observation of this work is that, in contrast to the pure state entanglement in the coupled chaotic systems, the presence and the absence of time-reversal (TR) symmetry affect significantly the pairwise entanglement. The absence of TR symmetry leads to significantly larger entanglement sharing. Similar pairwise entanglement has also been studied in Refs.[60, 61].

1.6 Decoherence : A consequence of entanglement

In the previous section we have extensively discussed the entanglement and also the role of the chaos in the production of the entanglement. Decoherence, a consequence of entanglement, is an irreversible process in which a quantum system looses its phase coherence due to the entanglement with its surrounding or environment. More precisely, decoherence is the mechanism by which a quantum system looses its *quantumness* and behave like a classical system. For a detail discussion on decoherence and its different aspects, see Refs. [62, 63] and references there in. As a concrete example, let us again consider a spin$-\frac{1}{2}$ particle as our system which is interacting with environment. Since we are interested in to compare the state of the spin$-\frac{1}{2}$ particle with and without any interaction with environment, hence density matrix formalism of the quantum states is useful. Let

us assume the spin$-\frac{1}{2}$ particle is in a most general superposition state

$$|\psi_S\rangle = \alpha|\uparrow\rangle + \beta|\downarrow\rangle.$$

The density matrix corresponding to this state is

$$\rho_S = |\psi_S\rangle\langle\psi_S| = |\alpha|^2|\uparrow\rangle\langle\uparrow| + |\beta|^2|\downarrow\rangle\langle\downarrow| + \alpha\beta^*|\uparrow\rangle\langle\downarrow| + \alpha^*\beta|\downarrow\rangle\langle\uparrow|.$$

In the above expression, the last two terms are called quantum interference terms which have no classical analogue.

Let us now consider the case when the spin$-\frac{1}{2}$ particle is not an isolated system, rather it is interacting with the environment. We assume that the initial joint state of the system and the environment is a product state,

$$|\psi_{S+E}\rangle = |\psi_S\rangle|E_0\rangle = (\alpha|\uparrow\rangle + \beta|\downarrow\rangle)|E_0\rangle \tag{1.14}$$

where $|E_0\rangle$ is the initial state of the environment. After the interaction, following Ref.[18], the state $|\psi_{S+E}\rangle$ will evolve into an entangled state,

$$|\psi^e_{S+E}\rangle = \alpha|\uparrow\rangle|E_\uparrow\rangle + \beta|\downarrow\rangle|E_\downarrow\rangle. \tag{1.15}$$

The two conditional states of the environment $\{|E_\uparrow\rangle, |E_\downarrow\rangle\}$ evolve under the unitary operator induced by the system in a state $\{|\uparrow\rangle, |\downarrow\rangle\}$. Now the effective density matrix corresponding to the spin$-\frac{1}{2}$ particle will be the RDM which can be obtained from the above state by tracing over the environment subspace and that is given by

$$\begin{aligned}\rho^e_S &= \mathrm{Tr}_E|\psi^e_{S+E}\rangle\langle\psi^e_{S+E}| \\ &= |\alpha|^2|\uparrow\rangle\langle\uparrow| + |\beta|^2|\downarrow\rangle\langle\downarrow| + z\,\alpha\beta^*|\uparrow\rangle\langle\downarrow| + z^*\alpha\beta|\downarrow\rangle\langle\uparrow|,\end{aligned} \tag{1.16}$$

where $z \equiv \langle E_\uparrow|E_\downarrow\rangle$ determines the degree of suppression of the off-diagonal terms in ρ^e_S. If the environment contains many degrees of freedom, these two conditional states of the environment will almost be orthogonal, $\langle E_\uparrow|E_\downarrow\rangle \simeq 0$ and therefore the RDM of the system will be

$$\rho^e_S \simeq |\alpha|^2|\uparrow\rangle\langle\uparrow| + |\beta|^2|\downarrow\rangle\langle\downarrow|. \tag{1.17}$$

If we now compare the above state with ρ_S, we can clearly observe that the spin$-\frac{1}{2}$ particle has lost quantum interference terms due to its interaction with environment. Now the correlation between the states $|\uparrow\rangle$ and $|\downarrow\rangle$ of the spin$-\frac{1}{2}$ particle is like classical correlation which can be compared with the correlation between *'head'* and *'tail'* of a classical coin. A quantum correlations, like $|\uparrow\rangle\langle\downarrow|$ or $|\downarrow\rangle\langle\uparrow|$, cannot be related with any state of a classical coin. Hence decoherence can also be considered as a process by which a quantum system looses its quantum correlations.

1.6.1 Decoherence in chaotic systems

We have observed that decoherence induces a transition from quantum to classical and therefore, decoherent approach can be utilized in a more straightforward way to restore quantum-classical correspondence. We all know that there is no consensus about the quantum analogue of classical chaos, therefore Zurek, one of the proponents of decoherent approach, and some others have extensively studied decoherence of chaotic systems that are coupled to an environment [64, 65, 66, 67, 68, 69, 70, 71]. Irreversibility is the price of the decoherent model for the restoration of quantum-classical correspondence in a quantum system. This irreversibility causes entropy production in the system. In our previous example, the von Neumann entropy of ρ_S is $S_V = -\mathrm{Tr}\rho_S \ln \rho_S = 0$, since ρ_S is representing a pure state ; whereas the von Neumann entropy of the reduced density matrix ρ_S^e is $S_V = -\mathrm{Tr}\rho_S^e \ln \rho_S^e = -\left(|\alpha|^2 \ln|\alpha|^2 + |\beta|^2 \ln|\beta|^2\right) > 0$. This non-zero value of the entropy is due to the loss of information by the system into the environment. It has been conjectured that this entropy grows linearly in time with a fixed rate determined by the positive Lyapunov exponents [47].

This conjecture has been tested for several model open quantum chaotic systems. It has been shown that the entropy production rate, as a function of time, in a quartic double well with harmonic driving coupled to a sea of harmonic oscillators has at least two distinct regimes [64]. For short times this rate is proportional to the system-environment coupling strength, and for longer times there is a regime where this rate is determined by the Lyapunov exponent. In another work, the entropy production in the baker's map and Harper's map coupled to

a diffusive environment is studied [65]. A regime was found to exist where the entropy production rate is determined by the system's dynamical properties like Lyapunov exponents, folding rates, etc., and moreover, in this regime the entropy production rate becomes independent of the system-environment coupling strength. Similar results are also reported in Refs.[66, 67]. In other work, evidence has been presented that the decoherence rate (or entropy production rate) of a quantum system coupled to an environment is governed by a quantity which is a measure of both the increasingly detailed structure of the quantum distributions (Wigner function) and classical phase space distributions [68].

Very recently, it has been reported that in open quantum systems, there exists a universal scaling among the parameters (effective Planck's constant, measure of the coupling strength between system and environment, classical Lyapunov exponents) on which the quantum-classical transition of that system depends [69]. In another direction, decoherence has been discussed in an open system coupled to a nonlinear environment with finite degrees of freedom [70]. It was found that even though the environment is finite dimensional, the strong nonlinearity of it can destroy the quantum coherence. Hence there is a possibility to utilize this finite dimensional chaotic system as a model of environment, instead of infinite dimensional heat bath. The above possibility has also been discussed in a recent work. Naturally this approach is closely linked to studies like the coupled chaotic systems [71].

1.6.2 Decoherence in quantum computation and quantum information processing

Superposition principle of quantum mechanics has made a quantum system fundamentally different from a classical system. For example, as mentioned earlier, a spin-$\frac{1}{2}$ particle can be in a superposition of '*up*' and '*down*' state, whereas it is not possible for a classical coin to be in a superposition of 'head' and 'tail'. Similarly, unlike classical bit, a quantum bit or qubit can be in a superposition of $|0\rangle$ and $|1\rangle$ state. Due to this superposition of a single qubit, a quantum register, consists of N qubits, can be in a superposition of 2^N number of states. On the other hand, a classical register, consists of N classical bits, can only be in one single state at a

particular moment. That means, superposition principle of quantum mechanics automatically provides a kind of parallelism by which a quantum computer can solve certain hard problems more efficiently and sometime in a much less amount of operations. For example, Grover's quantum search algorithm needs on average $\sim \sqrt{N}$ operations to search an entity from a given unsorted database of size N. In contrary, a classical search algorithm needs on average $N/2$ operations to perform the identical task [42].

However there is a very big problem. The above mentioned efficiency of a quantum computer over its classical counterpart is valid only when the quantum computer is completely isolated from its surrounding. If it is not, then the decoherence invalidates the quantum superposition and thus turns a quantum computer into a classical computer. Therefore, due to the decoherence, a quantum computer can loose its potential power. So decoherence is really a very big threat to the operation of quantum computer.

Let us now see how decoherence can affect quantum computers. Assume a very simple situation in which a qubit in the state $|0\rangle$ undergoes successively and without decoherence two Hadamard operations Hd:

$$|\psi_{in}\rangle = |0\rangle \xrightarrow{Hd} \frac{1}{\sqrt{2}}\big(|0\rangle + |1\rangle\big) \xrightarrow{Hd} |0\rangle = |\psi_{fin}\rangle. \tag{1.18}$$

In terms of density matrix, the above sequence can be written as

$$\rho_{in} = \begin{pmatrix} 1 & 0 \\ 0 & 0 \end{pmatrix} \xrightarrow{Hd} \frac{1}{2}\begin{pmatrix} 1 & 1 \\ 1 & 1 \end{pmatrix} \xrightarrow{Hd} \begin{pmatrix} 1 & 0 \\ 0 & 0 \end{pmatrix} = \rho_{fin}. \tag{1.19}$$

If we perform a measurement on the final state, we will get $|0\rangle$ state with probability one. Let us now assume that decoherence occurs in between the two Hadamard operations and wipes out completely the off-diagonal terms. In this case, the sequence of operations will be

$$\rho_{in} = \begin{pmatrix} 1 & 0 \\ 0 & 0 \end{pmatrix} \xrightarrow{Hd} \frac{1}{2}\begin{pmatrix} 1 & 1 \\ 1 & 1 \end{pmatrix} \xrightarrow{Deco.} \frac{1}{2}\begin{pmatrix} 1 & 0 \\ 0 & 1 \end{pmatrix} \xrightarrow{Hd} \frac{1}{2}\begin{pmatrix} 1 & 0 \\ 0 & 1 \end{pmatrix} = \rho_{fin}. \tag{1.20}$$

Now ρ_{fin} is not represents a qubit in $|0\rangle$ state, but rather a statistical mixture of $|0\rangle$ and $|1\rangle$ states. If we now perform a measurement on the qubit, we will get either $|0\rangle$ or $|1\rangle$ with equal probabilities.

The above example of decoherence in a quantum computer is definitely an oversimplification. Actually decoherence is a continuous process that progressively eliminates the off-diagonal elements. In a more realistic situation, a quantum computer consists of S qubits which interacts with an environment in thermal equilibrium, the off-diagonal elements of the density matrix decay exponentially fast at a rate γS [72], i.e.

$$\rho_{ij}(t) \sim \rho_{ij}(0)\, \mathrm{e}^{-\gamma S t}, \tag{1.21}$$

where $\gamma = 1/\tau_{deco}$ is a constant which is determine by the coupling of a single qubit and the environment. The stronger the coupling, the higher γ and consequently the smaller the decoherence time τ_{deco}.

Even though the decoherence establishes an important limit, it is important to note that its effects vary from one problem to another. For example, in Shor's factoring algorithm the goal is to determine the period of the function $f(x) = a^x \bmod N$ where this period is hidden in the quantum superposition of the computer [41]. Definitely the decoherence irreversibly transfers some information from the quantum computer to the environment, but as long as the single desired piece of information is retained, it is useful. Thus decoherence should be taken into account both by the quantum hardware engineers and quantum software designers.

Decoherence is a major obstacle to the realization of quantum computer. However some error correction codes exist which may be utilize to mitigate errors due to decoherence. Until now, in the experimental front, we have only realized 5 qubits [73]. That means, Grover's search algorithm [42] can be experimentally implemented for a database of only $N = 2^5 = 32$ entries. Experimentalists are working hard to improve the present scenario, but still they have to march a very long distance.

1.7 Motivation for the thesis

The title of the present thesis suggests that a major portion of the thesis is devoted into the study of quantum chaos. As we have mentioned earlier, the most accepted

definition of quantum chaos is that, a quantum chaotic system is a system whose underlying classical dynamics is chaotic. That means quantum mechanical study of classically chaotic systems is the subject matter of quantum chaos. Therefore, a very good understanding of classical chaotic dynamics is prerequisite for the understanding of quantum chaos.

A system which does not have sufficient number of invariants is called nonintegrable system. Chaos is the property shown by these kind of systems. On the other hand, the systems having sufficient number of invariants are called integrable system. In many of the cases one can consider a nonintegrable system as a perturbed integrable system. Therefore, to understand the nonintegrable systems, we should have thorough understanding of the integrable systems. In the first part of the thesis we have presented our study on time-depended nonlinear integrable systems.

We have already discussed about the importance of the study of the effect of chaos on entanglement. Most of the results have emphasized that in general chaos produces more entanglement than any regular systems. However its opposite phenomenon has also been observed in the weakly coupled chaotic systems. Therefore, more studies are required to safely make any general statement.

Let us now return back to the discussion of a recent work which has motivated a major portion of my thesis [52]. In this work, the author has studied entanglement in coupled standard map. Following is the stepwise summary of this work:

- constructed unitary operator U of the form $U = [U_1(k_1) \otimes U_2(k_2)]U(b)$ corresponding to coupled standard map, where $U_i(k_i)$'s are the time evolution operators corresponding to individual standard maps and $U(b)$ is the interaction between two standard maps. k_i's are the parameters of each standard map which determines chaos in the system. The parameter b is the coupling strength between two standard maps. If the Hilbert space dimension of the each standard map is N, then U is a $N^2 \times N^2$ matrix.
- determined the eigenvectors $\{|e_i\rangle\}$ of U, where $i = 1, \ldots N^2$.
- constructed reduced density matrix for each $\{|e_i\rangle\}$, i.e. $\rho^{(i)}_{1,2} = \mathrm{Tr}_{2,1}(|e_i\rangle\langle e_i|)$ where 1 and 2 represent different subsystems.

- determined the von Neumann entropy $S_V^{(i)}$ for each $|e_i\rangle$.
- determined the average von Neumann entropy $\overline{S}_V = \frac{1}{N^2}\sum_{i=1}^{N^2} S_V^{(i)}$.
- studied $\overline{S}_V$ versus coupling strength b, for different Hilbert space dimensions N.

This study shows that entanglement increased with coupling strength, but after a certain magnitude of coupling strength corresponding to the emergence of complete chaos, the entanglement saturated. At this saturation the von Neumann entropy $S_V \sim \ln 0.59N$ where N is the Hilbert space dimension of the participating subsystems. This saturation value is clearly less than the maximum possible value $S_V = \ln N$. Similar saturation was also observed for a time evolving state which was initially unentangled.

Since these results indicate that the Hilbert space dimension and chaos have roles in the saturation of entanglement, hence coupled large spins are attractive models. A coupled kicked tops model has already been used in chaos-entanglement context and we generalize it to include the case of unequal spins. Moreover kicked top is a very well studied model of both classical and quantum chaos. Using this model, we study entanglement production for strongly chaotic and strongly coupled cases and we observe the saturation of entanglement with magnitude $S_V = \ln(\gamma N)$, where N is the Hilbert space dimension of the smaller subsystem and γ is the parameter depends on the subsystems Hilbert space dimensions. For equal dimensional case $\gamma \sim 0.6$, this is very close to the saturation value observed in case of coupled standard maps. So our results indicate that the entanglement saturation is an universal phenomenon.

Random matrix theory (RMT) has explained many universal phenomena of chaotic systems. Therefore, it is very natural to expect that RMT will able to explain the entanglement saturation. Later our expectation turns out to be correct and using RMT we indeed able to estimate the entanglement saturation for both equal and unequal Hilbert space dimensions of the participating subsystems.

As we have mentioned that the entanglement saturation is a property of two strongly chaotic subsystems which are very strongly coupled. We have also studied entanglement for different underlying classical dynamics, like (nearly) regular, mixed and chaotic cases ; and also for different coupling strengths. Our study

shows that the coupling strength between two subsystems is a very crucial parameter for the entanglement production. As an example, for the weakly coupled cases, the entanglement production corresponding to regular systems is significantly more than the chaotic systems. However, for the strongly coupled cases, we observe completely opposite behavior of the entanglement production.

Until now, we have discussed the effect of underlying classical dynamics on the entanglement production for the initially pure state. However, we are also interested to investigate the effect of underlying classical dynamics on the entanglement production corresponding to the initially mixed state. Absence of any unique measure is a major obstacle to study the mixed state entanglement. Recently, *Werner and Vidal* have proposed a computable measure of entanglement called *Log-negativity* [74]. However, this measure also has a restriction which we mention in Chapter 6. Nevertheless, we use the log-negativity measure to study the effect of different underlying classical dynamics on the entanglement production of the initially unentangled mixed state which is evolving under the coupled tops time evolution operator. We find that the presence of chaos, in general, enhances the mixed state entanglement production. In case of pure state, the subsystem entropies (like the von Neumann entropy and the linear entropy) are the measures entanglement. But these are no more the measures for the mixed state entanglement. However, the subsystem entropies are still very important quantities to investigate. Moreover, our studies show that the production of the subsystem entropies and the entanglement production have some similar qualitative properties. Existence of a statistical upper bound is one such property which is common in both the above mentioned quantities. We use RMT to estimate the statistical upper bounds (or the saturation value) of the subsystem linear entropy.

Beside the above study of the state entanglement, we also study the operator entanglement as a measure of the entangling power of a given operator. We basically study the entangling power of a unitary time-evolution operator corresponding to the coupled kicked tops, for different underlying classical dynamics of the individual top and for different coupling strengths between the tops. The operator entanglement production shows some properties which are similar to the state entanglement production.

1.7.1 Outline of the thesis

Including this present introductory chapter, the thesis is divided into *six* more chapters. In Chapter 2, we discuss about our study on time dependent integrable system. In the remaining chapters we discuss about entanglement and decoherence in coupled chaotic systems where coupled kicked tops is used extensively as a model system. Therefore, in Chapter 3, we discuss about coupled and single kicked top. We also present the derivation of the correct classical map of the coupled kicked tops. Chapter 4 is devoted to the study of the entanglement saturation. In this chapter we give a detail RMT calculations of the entanglement saturation. In Chapter 5, we present our detail study of entanglement production in coupled kicked tops. We also make an attempt to relate complexity of a state with its entanglement. In Chapter 6, we discuss the mixed state entanglement and the operator entanglement. Finally we summarize the thesis.

Chapter 2

Time dependent nonlinear integrable systems

The classical as well as quantum mechanical study of time dependent Hamiltonian systems which are generic is important. We know that for time independent Hamiltonian systems the Hamiltonian itself is an invariant. However, when the Hamiltonian is an explicit function of time, it is no more an invariant, and this of course a reflection of the nonconservation of energy. Then a natural question arises if any invariant exists or not. If it does, then the system becomes integrable for 1-degrees of freedom systems and if not, there is a possibility of more complicated behavior like *chaos*. Various methods have been used to obtain approximate invariants for time dependent problems, e.g., the adiabatic approximation, the sudden approximation, time dependent perturbation techniques, etc. But here we are interested in the determination of exact invariants.

The most widely studied time dependent integrable Hamiltonian is the time dependent harmonic oscillator (TDHO). It has long been a problem of considerable interest because of its varied applications in different areas of physics. The Hamiltonian of this system is given by

$$H(t) = \frac{1}{2}\,p^2 + \frac{1}{2}\,\omega^2(t)\,q^2, \tag{2.1}$$

where p and q are canonical conjugate variables. The adiabatic invariant for this system was originally given at the first Solvay Congress in 1911 when the Hamiltonian of this system was used as an approximate Hamiltonian for the slowly lengthening pendulum [75].

The study of this 1-dimensional TDHO was greatly advanced due to the work of Lewis [76, 77] and Lewis and Riesenfeld [78]. Lewis [76] determined the exact invariant by applying Kruskal's asymptotic method [79] and showed that a previously known adiabatic invariant was in fact an exact invariant. Later Lewis and Riesenfeld [78] determined that same invariant by starting with the assumption of the existence of an explicitly time dependent, homogeneous and quadratic invariant of the form given by

$$I(t) = \frac{1}{2}\,[\,\alpha(t)\,p^2 \,+\, \beta(t)\,q^2 \,+\, 2\,\gamma(t)\,p\,q\,], \tag{2.2}$$

where the coefficients $\alpha(t), \beta(t)$, and $\gamma(t)$ are time dependent real functions and $I(t)$ satisfies the condition

$$\frac{dI}{dt} \equiv \frac{\partial I}{\partial t} + \{I, H(t)\} = 0. \tag{2.3}$$

Here $\{\,,\,\}$ denotes the usual Poisson bracket. From Eq.(2.2), we have

$$\frac{dI(t)}{dt} = \frac{1}{2}\left[(\,\dot\alpha \,-\, 2\,\omega^2(t)\,\gamma)\,q^2 \,+\, (\,\dot\beta \,+\, 2\,\gamma\,)\,p^2 \,+\, 2\,(\,\dot\gamma \,+\, \alpha \,-\, \omega^2(t)\,\beta\,)\,p\,q\right], \tag{2.4}$$

where the dots denote time derivative of the variables. In order to satisfy Eq.(2.3), the coefficients of the dynamical variables should be individually equal to zero. Therefore,

$$\begin{aligned} \dot\alpha &= 2\,\omega^2(t)\,\gamma \\ \dot\beta &= -\,2\,\gamma \\ \dot\gamma &= -\,\alpha \,+\, \omega^2(t)\,\beta. \end{aligned} \tag{2.5}$$

It is convenient to define $\beta(t) = \sigma^2(t)$, where $\sigma^2(t)$ is a real function of time. Substituting this in the above set of equations, we get,

$$\gamma = -\,\sigma\,\dot\sigma \tag{2.6}$$

$$\text{and}\quad \alpha = \dot\sigma^2 \,+\, \sigma\,\ddot\sigma \,+\, \omega^2(t)\,\sigma^2. \tag{2.7}$$

From the first of Eq.(2.5) and from last two equations we get,

$$\begin{aligned} \frac{d}{dt}\left(\dot\sigma^2 \,+\, \sigma\,\ddot\sigma \,+\, \omega^2(t)\,\sigma^2\right) \,+\, 2\,\omega^2(t)\,\sigma\,\dot\sigma &= 0 \\ \Rightarrow \sigma\,\frac{d}{dt}\,(\,\ddot\sigma \,+\, \omega^2(t)\,\sigma\,) \,+\, 3\,\dot\sigma\,(\,\ddot\sigma \,+\, \omega^2(t)\,\sigma\,) &= 0. \end{aligned} \tag{2.8}$$

After Integrating the above expression with respect to time t, we get,

$$\ddot{\sigma} + \omega^2(t)\,\sigma = \frac{c}{\sigma^3}, \tag{2.9}$$

where c is an arbitrary real constant of integration. From Eq.(2.7) and Eq.(2.9), we get

$$\alpha = \dot{\sigma}^2 + \frac{c}{\sigma^2} \tag{2.10}$$

We have expressed all the time dependent functions (α, β, γ) in terms of a single time dependent function $\sigma(t)$ and its derivatives. Substituting these in Eq.(2.2), we get,

$$I = \frac{1}{2}\left[\left(\dot{\sigma}^2 + \frac{c}{\sigma^2}\right) q^2 + \sigma^2 p^2 + 2\sigma\,\dot{\sigma}\,p\,q\right], \tag{2.11}$$

with Eq.(2.9) as a subsidiary condition. The absence of a time subscript on I indicates that it is a constant over time. If we again define,

$$\sigma(t) = c^{\frac{1}{4}}\rho(t) \tag{2.12}$$

where $\rho(t)$ is a new auxiliary function of time. In terms of $\rho(t)$, time dependent functions (α, β, γ) become

$$\begin{aligned} \alpha(t) &= c^{\frac{1}{2}}\left(\dot{\rho}^2 + \frac{1}{\rho^2}\right) \\ \beta(t) &= c^{\frac{1}{2}}\,\rho^2 \\ \gamma(t) &= -2\,c^{\frac{1}{2}}\,\rho\,\dot{\rho}. \end{aligned} \tag{2.13}$$

Substituting above expressions in Eq.(2.2) and discarding the constant multiplicative factor $c^{\frac{1}{2}}$, we get

$$I = \frac{1}{2}\left[\rho^2 p^2 + \left(\dot{\rho}^2 + \frac{1}{\rho^2}\right) q^2 - 2\,\rho\,\dot{\rho}\,p\,q\right], \tag{2.14}$$

with $\rho(t)$ satisfying the subsidiary condition

$$\ddot{\rho} + \omega^2(t)\,\rho - \frac{1}{\rho^3} = 0. \tag{2.15}$$

This more complicated, nonlinear, differential equation represented an advance due to the reason that any particular solution $\rho(t)$ of the above equation would give

the exact invariant I for all initial conditions of p and q. The above is the method followed by Lewis and Riesenfeld [78] to get the expression of the invariant I and the corresponding subsidiary condition for the 1-dimensional TDHO.

Lewis [76] attempted to give an interpretation of $I(t)$ as the most general homogeneous quadratic invariant possible for the Hamiltonian of the 1-dimensional TDHO. A more natural and physical interpretation has been suggested by Eliezer and Gray [80] in terms of a 2-dimensional auxiliary motion, i.e., in terms of a 2-dimensional uncoupled TDHO. They showed that the above subsidiary condition Eq.(2.15) is the radial equation of motion for this 2-dimensional system and the invariant $I(t)$ is proportional to the conserved angular momentum of this auxiliary motion. Günther and Leach [81] interpreted $I(t)$ in terms of canonical transformations and under their transformation the invariant $I(t)$ became the Hamiltonian of the 1-dimensional time independent harmonic oscillator of unit frequency.

We have interpreted the form of $I(t)$ chosen by LR [78] from the Lie-algebraic point of view. The Hamiltonian of the 1-dimensional TDHO is formed by the dynamical variables $\frac{1}{2}p^2$ and $\frac{1}{2}q^2$. These two dynamical variables together with pq are generators of the closed su$(1,1)$ algebra under the Poisson bracket operation and $I(t)$ was chosen in [78] as the linear combination of the generators of that closed algebra with time dependent coefficients.

The integrability of the 1-dimensional TDHO is not surprising, because this is a linear system. We know, 1-dimensional time dependent Hamiltonians usually lead to nonintegrability, e.g., a simple pendulum whose length varies in time. Except for the adiabatic or small oscillation approximations, this was the problem posed by Lorentz at the above mentioned Solvay congress and the solutions have the possibility of displaying chaos.

Now a natural question is if there exist 1-dimensional time dependent nonlinear Hamiltonians which are also integrable ? In fact, the singular oscillator with a centrifugal force potential provides an important example whose kinematics is still within the su$(1,1)$ algebra. In Sec. 2.1, first, we describe the general Hamiltonian of the singular oscillator and then an important special case constitutes the rest of the section. Sec. 2.2 is devoted to the quantum dynamical study of this special case of the singular oscillator.

2.1 The classical singular oscillator

For the determination of an invariant for the 1-dimensional TDHO, the subsidiary condition Eq. (2.15) has to be integrated with *some* initial conditions, that is we should be able to determine a particular solution. The subsidiary condition, derived in Eq.(2.15), is a nonlinear, time dependent, equation and its integrability is not immediately obvious. Let us assume ρ as a position variable, say q, then Eq. (2.15) is the equation of motion corresponding to the Hamiltonian given by,

$$\mathcal{H}(t) \,=\, \frac{1}{2}\,\left(p^2 \,+\, \frac{k}{q^2}\right) \,+\, \frac{1}{2}\,\omega^2(t)\,q^2, \tag{2.16}$$

with $k \,=\, 1$. This is another time dependent Hamiltonian which has also been studied for long [82, 83]. The new nonlinear force in the system is a *'Centrifugal force'* and it appears in many integrable systems, including the celebrated Calogero-Sutherland-Moser [84] many-body Hamiltonian.

The above Hamiltonian is formed by the dynamical variables $\frac{1}{2}\,(p^2 \,+\, k/q^2)$ and $\frac{1}{2}\,q^2$. These two dynamical variables together with $p\,q$, also form su$(1,1)$ closed algebra. Now from our algebraic interpretation of $I(t)$, we can assume the invariant of this nonlinear Hamiltonian to be of the form

$$I(t) = \frac{1}{2}\,\alpha(t)\,\left(p^2 + \frac{k}{q^2}\right) \,+\, \frac{1}{2}\,\beta(t)\,q^2 \,+\, 2\,\gamma(t)\,p\,q. \tag{2.17}$$

Again by the same substitutions and identical procedure we get

$$I = \frac{1}{2}\,\rho^2\,\left(\,p^2 \,+\, \frac{k}{q^2}\,\right) \,+\, \frac{1}{2}\,\left(\,\dot{\rho}^2 \,+\, \frac{1}{\rho^2}\,\right)\,q^2 \,-\, \rho\,\dot{\rho}\,p\,q\,, \tag{2.18}$$

with the same subsidiary condition given in Eq.(2.15). But now the equation of motion and the subsidiary condition are the *same* nonlinear equation. However the fact that we need only one particular solution of this equation to determine the invariant shows the power of this methodology and also the integrability of the above Hamiltonian in Eq.(2.16). In Fig. 2.1 we have shown a special case corresponding to $\omega^2(t) \,=\, 1 \,+\, \cos\,(\sqrt{2}\,t)$ where the existence of the invariant is reflected in the regular structure.

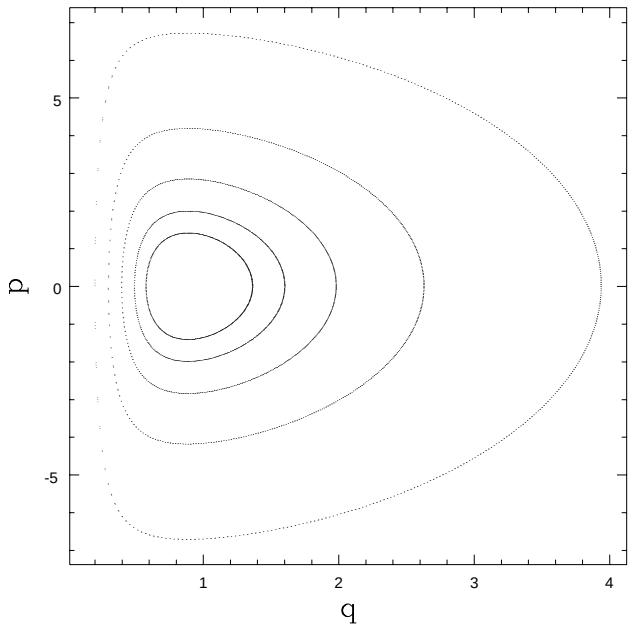

Figure 2.1: Stroboscopic picture of the time dependent harmonic oscillator with a singular perturbation ; the integrable behavior is evident. All quantities shown are dimensionless.

2.1.1 The kicked singular oscillator

Let us now consider a special form of the time dependent frequency

$$\omega^2(t) = \omega^2 T \sum_n \delta\,(t - nT).$$

This form of $\omega^2(t)$, in case of the singular oscillator, allows us to construct a nonlinear integrable map by integrating the Hamilton's equations of motion in between two consecutive kicks. Study of integrable maps are important for the following reason. First, the dynamics of a mapping is more simple than the dynamics of a continuous system since it involves direct iterations. Second, if one want to study numerically any integrable continuous system, it is absurd to use nonintegrable numerical schemes that destroy the basic properties of the system. Therefore, for a numerical studies of any integrable system, one has to find a discrete integrable version of the system. The discrete map we discuss below, or extensions thereof, for instance, may be used in the numerical studies of the Calogero-Sutherland-Moser model. Lastly, we may argue that the discrete sys-

tems are more fundamental ones since they contain continuous ones as special limits.

Now we are interested in the Hamiltonian,

$$H(t) = \frac{1}{2}\left(p^2 + \frac{k}{q^2}\right) + \frac{1}{2}\omega^2 T q^2 \sum_n \delta(t - nT) \tag{2.19}$$

and the corresponding Hamilton's equations of motion are

$$\dot{p} = \frac{k}{q^3} - \omega^2 T q \sum_n \delta(t - nT) \tag{2.20a}$$

$$\dot{q} = p \tag{2.20b}$$

The equation of motion of the system is given by

$$\ddot{q} + \omega^2 T q \sum_n \delta(t - nT) - \frac{k}{q^3} = 0. \tag{2.21}$$

This equation is the same as that of the subsidiary condition given in Eq.(2.15), except for the constant k. If we integrate Hamilton's equations of motion from just after the nth kick to just after the $(n+1)$th kick and define new scaled variables

$$p \to k^{1/4} T^{-1/2} p \quad \text{and} \quad q \to k^{1/4} T^{1/2} q,$$

the phase space map of the system will be

$$q_{n+1} = \sqrt{p_n^2 + \frac{1}{q_n^2} + q_n^2 + 2 q_n p_n} \tag{2.22a}$$

$$p_{n+1} = \frac{p_n^2 + \frac{1}{q_n^2} + p_n q_n}{q_{n+1}} - \Omega^2 q_{n+1}, \tag{2.22b}$$

where $\Omega = \omega T$. Here we want to point out that if we would have considered TDHO with this special form of $\omega^2(t)$ and have followed the above procedure then we would have got the well known linear map. The linear map can also be obtained from the above nonlinear map by simply removing $1/q^2$ term, or equivalently by substituting $k = 0$ in Eq. (2.20a). After integrating the corresponding Hamilton's equations of motion in between two consecutive kicks, we get,

$$q_{n+1} = p_n + q_n \tag{2.23a}$$

$$p_{n+1} = p_n - \Omega^2 q_{n+1}. \tag{2.23b}$$

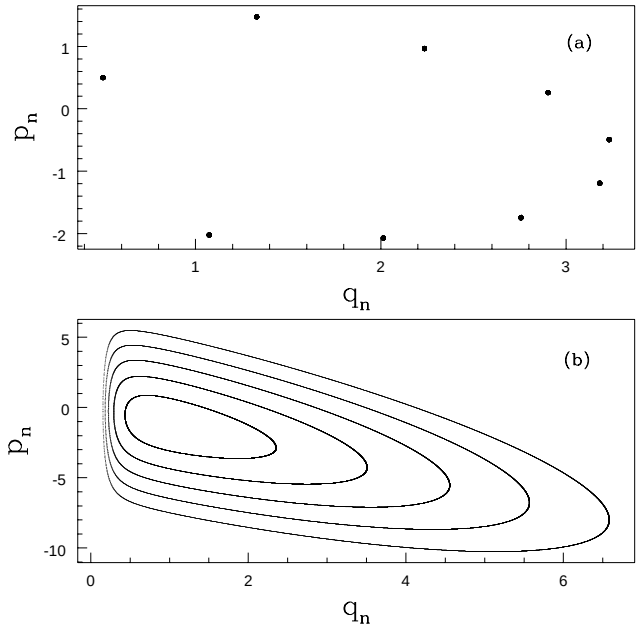

Figure 2.2: (a) Period-9 orbit of the nonlinear map for the case $\Omega^2 = 2\,[\,1 - \cos(2\,\pi/9)\,] \approx 0.4679$, (b) quasiperiodic orbit for the case $\Omega^2 = 2.43$. All quantities shown are dimensionless.

The linear map is very simple classically.

Let us now return back to the discussion of nonlinear map. We have plotted the above nonlinear phase space map in Fig. 2.2. The phase space map clearly shows regular behavior of the nonlinear map. This rather complicated looking discrete map has a very simple behavior, reflecting the fact that this and a linear map have common algebraic antecedents. Moreover, the property of the linear map that exclusively quasiperiodic or entirely periodic behavior exists for different values of the parameter has also been observed for the nonlinear map. For $0 < \Omega^2 < 4$ the motion is bounded and stable and for all other values the motion is unbounded and unstable, in both the maps. The invariant in the case of the linear map describes either an ellipse or a hyperbola. We now determine the invariant of the nonlinear map using the method of LR.

According to Eq.(2.18) the invariant of this map would be of the form,

$$I = \rho^2 \left({p_n}^2 + \frac{1}{{q_n}^2} \right) + \left(\dot{\rho}^2 + \frac{1}{\rho^2} \right) {q_n}^2 - 2\,\rho\,\dot{\rho}\,p_n\,q_n, \tag{2.24}$$

where ρ satisfies the same subsidiary condition as given in Eq. (2.15), but now

$\omega^2(t) = \omega^2 T \sum_n \delta(t - nT)$. Now we have to determine any particular solution of the subsidiary condition, and using that solution we will get the invariant of the nonlinear map Eq. (2.22). As we know, the equation of motion of this nonlinear kicked system is the same as that of the subsidiary condition for ρ, as shown in Eq. (2.21), therefore if we are able to determine *any* solution of the nonlinear map Eq. (2.22), that solution should also be the solution for ρ. Since Eq.(2.22) is a nonlinear equation, hence there are infinitely many solutions exist. But the most simple solution corresponds to the fixed point. Therefore the problem of determining the invariant has been reduced to determining the fixed point of the nonlinear mapping. That means, we have to solve the equations $q_{n+1} = q_n$ and $p_{n+1} = p_n$. The solutions of these equations give the fixed point at,

$$q^* = -\frac{2}{\Omega^{1/2}\left[4\left(4 - \Omega^2\right)\right]^{1/4}}, \tag{2.25a}$$

$$p^* = \frac{\Omega^{3/2}}{\left[4\left(4 - \Omega^2\right)\right]^{1/4}}. \tag{2.25b}$$

This is a particular solution of ρ and $\dot{\rho}$. Note that unlike the linear map whose fixed point at the origin is independent of the system parameters, the fixed points here move with the parameter and as the system approaches instability ($\Omega^2 \to 4$), they approach infinity. Using the above solutions, we get the invariant of the mapping within an arbitrary multiplicative constant as,

$$I = p_n^2 + \frac{1}{q_n^2} + \Omega^2 \left(q_n^2 + q_n\, p_n\right). \tag{2.26}$$

The lack of a time subscript on I indicates its constancy. This invariant is valid even when the motion is classically unstable.

2.1.2 The classical evolution operator of the kicked singular oscillator

In this section, we study the nonlinear map from a point of view that simultaneously explains its dynamics as well as sets the stage for quantum mechanical work. First we introduce the classical time evolution operator for studying the dynamics of the system. For a given dynamical variable, say V, the corresponding Liouville operator is denoted by L_V and it is defined as $L_V \equiv \{V, *\}$, where $\{*, *\}$ denotes the usual Poisson bracket.

We know the dynamical equation for any dynamical variable, say f, is given by,

$$\frac{df}{dt} = -\{H, f\} \equiv -L_H f, \tag{2.27}$$

where H is the Hamiltonian of the system and L_H is the Liouville operator corresponding to H. Let us now define $A \equiv \frac{1}{2}(p^2 + \frac{k}{q^2}), B \equiv \frac{1}{2}q^2$ and $\{A, B\} = -p\,q \equiv -2\,C$, i.e., $C = -\frac{1}{2}p\,q$. We also know, the triad (A, B, C) form the closed su$(1,1)$ algebra. Then we can write,

$$L_H = \left[L_A + \omega^2\,T\,L_B \sum_n \delta(t - nT)\right], \tag{2.28}$$

where L_A and L_B are the Liouville operators corresponding to A and B respectively. These Liouville operators together with L_C, the Liouville operator corresponding to C, forms the same su$(1,1)$ algebra as that of (A, B, C) but now under the Lie bracket operation, i.e., $[L_A, L_B] = -2\,L_C, [L_C, L_A] = L_A$ and $[L_C, L_B] = -L_B$.

In terms of these Liouville operators, Eq. (2.27) will become,

$$\frac{df}{dt} = -L_H\,f = -\left[L_A + \omega^2\,T\,L_B \sum_n \delta(t - nT)\right] f. \tag{2.29}$$

Integrating the above equation Eq. (2.29) in between the time $t = 0$ to $t = T$, we get the classical time evolution operator from just after zero time to just after the first kick. We write $f\,(q\,(t = T), p(t = T)) = F\,f\,(q\,(t = 0),\, p\,(t = 0))$ where

$$F = \exp\left(-\omega^2\,T\,L_B\right) \exp\left(-L_A\,T\right) \tag{2.30}$$

is called *Perron-Frobenius* operator. The Perron-Frobenius operator can also be regarded as the classical Flouquet operator. To understand the dynamics for time n, we have to determine the power F^n. The one parameter Abelian group of the powers completely specifies the dynamics at all time. However, F is itself a product of the exponential of two noncommuting operators which do not even commute with their commutator L_C.

We now apply a recent operator method, following Rau [85], to derive the classical time evolution operator at any time. The general procedure of this method is straight forward. Suppose we have any general time dependent Hamiltonian of

the form,

$$\mathcal{H}(t) \;=\; \sum_{i=1}^{n} a_i(t) H_i, \tag{2.31}$$

where $(a_i(t),\, i \;=\; 1, \ldots, n)$ are a set of linearly independent general complex function of time and the dynamical variables $(H_i,\, i \;=\; 1, \ldots, n)$ are the generators of any $n-$dimensional closed Lie algebra. Corresponding Liouville operators $(L_{H_i},\, i \;=\; 1, \ldots, n)$, as we have already mentioned, would also form that same algebra under Lie bracket operation. Then the corresponding classical time evolution operator $F(t)$ can be expressed in the product form :

$$F(t) \;=\; \prod_{j=1}^{n} \exp[b_j(t)\, L_{H_j}]. \tag{2.32}$$

Therefore, for the singular oscillator case, we can start with the time evolution operator of the form :

$$F(t) \;=\; \exp[X(t)\, L_B]\; \exp[Y(t)\, L_C]\; \exp[Z(t)\, L_A], \tag{2.33}$$

where $X(t), Y(t)$ and $Z(t)$ are real functions of time. From the initial condition $F(0) \;=\; \mathbf{1}$, we have $X(0) \;=\; Y(0) \;=\; Z(0) \;=\; 0$. Substituting this product form of $F(t)$ in Eq. (2.29), and repeatedly applying the Campbell-Baker-Hausdorff (CBH) formula we can cast it into a form such that $F(t)$ is pushed to the extreme right in the LHS of the equation Eq. (2.29). This yields a set of first order differential equations for the introduced functions of time :

$$\begin{aligned} \dot{X} \;&=\; -X^2 - \omega^2\, T \sum_n \delta(t - nT), \\ \dot{Y} \;&=\; 2\, X, \\ \dot{Z} \;&=\; -e^{-Y}. \end{aligned} \tag{2.34}$$

In the equation Eq. (2.33) we can choose the exponential operators in different orders, but we find that this leads to sets of differential equations whose solutions may not even exist for such kicked systems.

Integrating the above equations in between two consecutive kicks and rescaling

$$x = T\, X, \;\; y = Y, \;\; \text{and} \;\; z = \frac{Z}{T},$$

we get a nonlinear mapping, a "coefficient" mapping for the new dimensionless variables (x, y, z):

$$x_{n+1} = \frac{x_n}{1+x_n} - \Omega^2, \tag{2.35a}$$

$$y_{n+1} = y_n - \log\left[(1+x_n)^2\right], \tag{2.35b}$$

$$z_{n+1} = z_n + \frac{1}{\Omega^2}(x_{n+1} - x_n). \tag{2.35c}$$

To be explicit the n-th power of the operator F is

$$F^n = \exp[x_n\, T\, L_B]\ \exp[y_n\, L_C]\ \exp[z_n\, L_A/T]. \tag{2.36}$$

From the initial condition $F^0 = \mathbf{1}$, we have $x_0 = y_0 = z_0 = 0$. The time development is now entirely buried in the scalar functions x_n, y_n, and z_n.

The most important of the recursion equations in Eq. (2.35) is the first one. We have solved this nonlinear map by constructing an auxiliary *two dimensional* linear map. This is not entirely surprising as lurking behind the one dimensional nonlinear singular oscillator is a two dimensional linear one. This gives a new insight into the often stated close relationship between the harmonic oscillator and the singular oscillator.

Let us first define $s_n \equiv 1 + x_n$, and in terms of s_n, Eq. (2.35a) becomes

$$s_{n+1} = \eta - \frac{1}{s_n}, \tag{2.37}$$

where $\eta \equiv 2 - \Omega^2$, and from the initial condition $x_0 = 0$, we have $s_0 = 1$. Construct the auxiliary linear map:

$$\begin{pmatrix} a_{n+1} \\ b_{n+1} \end{pmatrix} = \begin{pmatrix} \eta & -1 \\ 1 & 0 \end{pmatrix} \begin{pmatrix} a_n \\ b_n \end{pmatrix}, \tag{2.38}$$

with initial conditions $a_0 = b_0 = 1$. We identify $s_n \equiv a_n/b_n$.

To get the general form of s_n, we have to diagonalize the matrix

$$M \equiv ((\eta, -1), (1, 0)).$$

The eigenvalues of M are,

$$\lambda_\pm = \frac{1}{2}\left(\eta \pm \sqrt{\eta^2 - 4}\right). \tag{2.39}$$

Whether $\lambda_\pm$ is real or complex is dependent on η. Therefore just as for the linear map we have to study separately three different regions for the parameter η, these are :

Case 1 : $\eta^2 < 4$, i.e., $0 < \Omega^2 < 4$

In this case the eigenvalues of M are complex-conjugate of each other, *i.e.*, we can write

$$\lambda_\pm = \exp(\pm i\sigma), \quad \text{where } \sigma \equiv \cos^{-1}(\eta/2) = \cos^{-1}\left(\frac{2-\Omega^2}{2}\right).$$

The dynamics is stable and bounded. After diagonalizing the matrix M, we determine a_n and b_n to finally get:

$$x_n = \cos\sigma - \sin\sigma \tan\left[(2n-1)\frac{\sigma}{2}\right] - 1. \tag{2.40}$$

In terms of x we can obtain the solution for y and z as :

$$y_n = -2\sum_{k=0}^{n-1} \log|1+x_k|, \tag{2.41}$$

$$z_n = \frac{x_n}{\Omega^2}. \tag{2.42}$$

When $\sigma = 2\pi m/N$, where m and N are coprime integers, one sees, after some algebra, that

$$x_n = x_{n+N}, \quad y_n = y_{n+N}, \quad z_n = z_{n+N}.$$

Therefore for these particular values of σ (or of the corresponding value of Ω), the above three-dimensional map for the coefficients is *exactly* periodic. To be explicit at these values of the parameter

$$F^N = \mathbf{1}, \tag{2.43}$$

the Perron-Frobenius operator becomes unity at time N. The quantum equivalence to be discussed below will be complete and the Flouquet unitary operator will become unity at the same time. Fig. 2.3 shows the coefficients for a periodic case. Since the coefficient z is proportional to x, it would follow the same behavior as x. This map in Eq. (2.22) would also be periodic with the same period, and corresponds to the phase space shown in Fig. 2.2(a). For other values of Ω, this map is quasi-periodic. Equivalently, the phase space map Eq. (2.22) also displays the above behavior for corresponding values of Ω. This shows that our operator

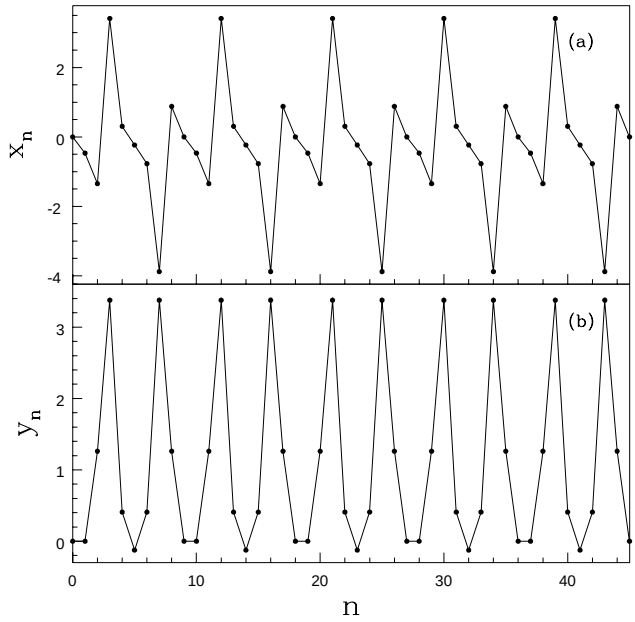

Figure 2.3: The coefficients of the time-evolution operator showing the period-9 behavior for the same Ω^2 as in Fig. 2.2(a). Shown are the x (a) and y (b) coefficients. All quantities shown are dimensionless.

approach for studying the classical map is in one-to-one correspondence with the phase space dynamics. Fig. 2.4 shows the coefficients for a quasi-periodic case, corresponding to the phase space in Fig. 2.2(b). Again the behavior of z is same as x.

Case 2 : $\eta^2 > 4$, i.e., $\Omega^2 > 4$ or $\Omega^2 < 0$

We can divide this case into two parts. They are :

(a) $\eta > 2$, i.e., $\Omega^2 < 0$:

In this part the eigenvalues of M are real and positive. Therefore we can take

$$\lambda_{\pm} = \exp(\pm\sigma), \text{ where } \sigma \equiv \cosh^{-1}(\eta/2) = \cosh^{-1}\left(\frac{2-\Omega^2}{2}\right).$$

In this part the dynamics is unstable and unbounded (hyperbolic). Again following procedures as outlined above, we get

$$x_n = \cosh\sigma + \sinh\sigma \tanh\left[(2n-1)\frac{\sigma}{2}\right] - 1. \tag{2.44}$$

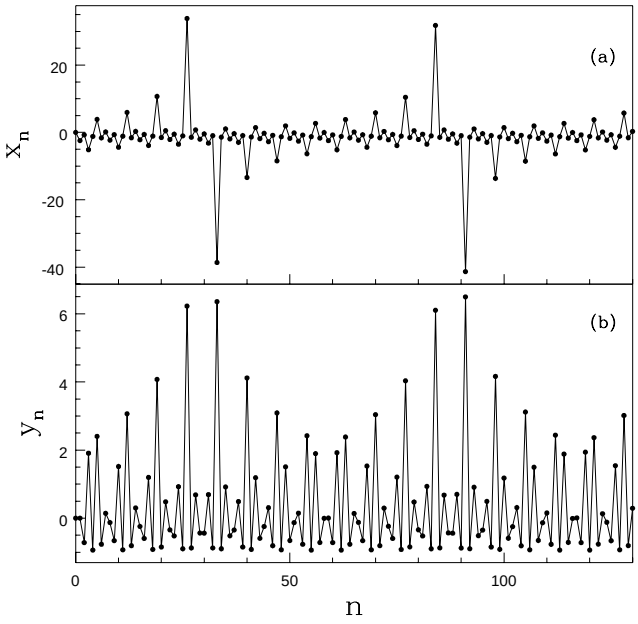

Figure 2.4: The coefficients of the time-evolution operator showing the quasi-periodic behavior for the same Ω^2 as in Fig. 2.2(b). Shown are the x (a) and y (b) coefficients. All quantities shown are dimensionless.

In this case the solution for y and z would also be the same as that given in Eq. (2.41). However, the basic properties of x, y and z would change due to the unstable and unbounded dynamics, and this is evident from the above equations. For large n, both x and z asymptotically reach a constant value that depends on the magnitude of Ω.

$$x_\infty = \lambda_+ - 1, \quad z_\infty = x_\infty/\Omega^2.$$

However, y would increase linearly with n, when n is large.

(b) $\eta < -2$, i.e., $\Omega^2 > 4$.

Here both the eigenvalues of M are real and negative. Thus we can take

$$\lambda_\pm = -\exp(\pm\sigma) \text{ where } \sigma \equiv \cosh^{-1}(|\eta|/2) = \cosh^{-1}\left(\frac{|2-\Omega^2|}{2}\right).$$

In this part the dynamics is still unstable and unbounded; it corresponds, in the linear map, to hyperbolic fixed point with reflections. On following the above

procedures, we get

$$x_n = -\cosh\sigma - \sinh\sigma \coth\left[(2n-1)\frac{\sigma}{2}\right] - 1. \tag{2.45}$$

The solutions for y and z still remain the same, and their behavior for large values of n are qualitatively same as that of the previous part.

Case 3: $\eta^2 = 4$, i.e., $\Omega^2 = 0$ or $\Omega^2 = 4$

These cases correspond to the marginal ones separating the stable and unstable motions. We can divide this case also into two parts. They are :

(a) $\eta = 2$, i.e., $\Omega^2 = 0$.

Here the eigenvalues of M are equal, $\lambda_\pm = 1$. The kick is not operating on the system. This implies that in the expression of the time-evolution operator F, $x = y = 0$. Therefore F contains only one exponential and hence the coefficient z would increase linearly with time. This can also be seen as a limiting case; as from Eq. (2.35a), $(x_{n+1} - x_n) \to -\Omega^2$ and the Eq. (2.35c) gives $z_n = -n$.

(b) $\eta = -2$, i.e., $\Omega^2 = 4$.

Again, the eigenvalues of M are equal, but now $\lambda_\pm = -1$. We can get the solution for the coefficients quite easily and these are given by,

$$x_n = -\frac{2n+1}{2n-1} - 1, \tag{2.46a}$$

$$y_n = -2\log|2n-1|, \tag{2.46b}$$

$$z_n = \frac{x_n}{\Omega^2}. \tag{2.46c}$$

For large n, the coefficients x and z asymptotically reach constant values (-2 and $-1/2$), while the magnitude of y increases logarithmically. Thus this marginal case straddling the stable and the reflective hyperbolic cases would have *power law* behaviors in time for phase space variables.

2.2 Quantum dynamics of the kicked singular oscillator

Quantum mechanical studies of the time-dependent singular oscillator have been carried out for some time now, for instance in [83] where complete analytical

solutions were given. We have exploited our algebraic method to the special case of the kicked oscillator to lay bare properties such as exact periodicity and quasi-periodicity. In fact, except for a change of terminology, the mathematics is already complete in the previous section.

During the study of the classical nonlinear map, we introduced the classical time evolution operator to show the one-to-one correspondence between the nonlinear and the linear map. While classically this is not the usual approach to dynamics, in the case of quantum dynamics, the most natural and popular way is to study the quantum time evolution operator $\hat{U}(t)$. Thus our classical approach generalizes most easily to the quantum. Previous work [86] that points out exact quantum-classical correspondence in the case of the su$(1,1)$ algebra for the coefficients of the invariant is easily understood in our approach.

We define the operators as in the classical case:

$$\hat{A} \equiv \frac{1}{2}\left(\hat{p}^2 + \frac{1}{\hat{q}^2}\right), \quad \hat{B} \equiv \frac{1}{2}\hat{q}^2, \quad \text{and } [\hat{A},\hat{B}] = -\frac{i}{2}\hbar\,(\hat{p}\,\hat{q} + \hat{q}\,\hat{p}) \equiv 2\,\hbar\,\hat{C},$$

where $(\hat{A},\hat{B},\hat{C})$ form the closed $SU(1,1)$ algebra which is given by $[\hat{A},\hat{B}] = 2\,\hbar\,\hat{C}$, $[\hat{C},\hat{A}] = \hbar\,\hat{A}$ and $[\hat{C},\hat{B}] = -\hbar\,\hat{B}$. Among these operators $\hat{C}$ is anti-hermitian and the other two are hermitian. In terms of these operators our Hamiltonian would be,

$$\hat{\mathcal{H}}(t) = \hat{A} + \omega^2\,T\,\hat{B}\sum_n \delta(t - nT), \tag{2.47}$$

The time-evolution operator $\hat{U}(t)$ satisfies the equation,

$$i\,\hbar\,\frac{d\hat{U}(t)}{dt} = \hat{\mathcal{H}}(t)\,\hat{U}(t), \tag{2.48}$$

where $\hat{U}(0) = \mathbf{1}$ and $\hat{U}(t)$ is unitary.

The quantum Flouquet operator $\hat{U}(t = T)$, which we denote simply as $\hat{U}$, is given by

$$\hat{U} = \exp\left(-\frac{i}{\hbar}\,\omega^2\,T\,\hat{B}\right)\exp\left(-\frac{i}{\hbar}\,T\,\hat{A}\right). \tag{2.49}$$

For the complete dynamics, as usual, we have to determine the powers $\hat{U}^n$. Again we apply Rau's [85] method for the derivation of the time evolution operator at

any arbitrary time. We start with the time evolution operator of the form,

$$\hat{U}(t) = \exp\left[\frac{i}{\hbar}X(t)\,\hat{B}\right] \quad \exp\left[\frac{1}{\hbar}Y(t)\,\hat{C}\right] \quad \exp\left[\frac{i}{\hbar}Z(t)\,\hat{A}\right], \tag{2.50}$$

where $X(t), Y(t)$ and $Z(t)$ are real functions of time, so that $\hat{U}(t)$ remains unitary. From the initial condition $\hat{U}(0) = \mathbf{1}$, we have $X(0) = Y(0) = Z(0) = 0$. Substituting the above $\hat{U}(t)$ in Eq. (2.48), following identical procedures as given for the classical dynamics, we get

$$\begin{aligned} \dot{X} &= -X^2 - \omega^2 T \sum_n \delta(t - nT), \\ \dot{Y} &= 2X, \\ \dot{Z} &= -e^{-Y}. \end{aligned} \tag{2.51}$$

These set of equations for the quantum coefficients are *identical* to the equations for the classical coefficients as given in Eq. (2.34). Therefore we would get an identical map for the quantum coefficients as for the classical coefficients Eq. (2.35). Since these two maps are identical, their stability properties are identical, i.e., quantum dynamics exactly follows its classical counterpart. Thus when the classical Perron-Frobenius operator becomes identity as in Eq. (2.43) the Flouquet operator also becomes identity. The various cases discussed classically, including the marginal and the reflective hyperbolic cases have exact quantum counterparts. Thus as far as time evolution is concerned the quantal problem is already solved.

Chapter 3

Coupled Kicked Tops

In the previous chapter, we have discussed about our work on the integrable systems. Now, from this chapter onwards, we will discuss about the nonintegrable systems. The principal goal of our study of nonintegrable systems, especially of the chaotic systems, is to observe the effect of classical dynamics on the quantum entanglement. It has been observed that, in general, entanglement production is higher for the stronger chaotic cases. However, an earlier work [52] showed that though there exists a maximum kinematical limit for the entanglement, dynamically it is not possible to create it by using chaotic dynamics. There exists a *statistical* upper bound on entanglement, which depends on the Hilbert space dimension of the system. Since the Hilbert space dimension is the crucial parameter for the above mentioned saturation of the entanglement, a nonintegrable large spin system is an ideal model for our study.

A kicked top is one such system which has been studied extensively as a model for both classical and quantum chaotic system [87]. If we fix the spin size of this system, say at j, then we are also fixing its Hilbert space dimension $N = 2j + 1$. Moreover, due to the finite dimensional Hilbert space, we need not to artificially truncate the corresponding time evolution operator during any numerical study. We know, for the entanglement production, the system should have at least two interacting subsystems. Therefore we consider the coupled kicked tops as the model system for our study. Moreover, this system has already been used in the context of 'chaos and entanglement' in Ref.[50], but in this reference the corresponding classical map presented was unfortunately incorrect. Moreover, the

map was not even *canonical*, a fundamental property of a Hamiltonian system. Hence we derive the correct classical map corresponding to the coupled kicked tops which satisfy canonical properties. We devote this chapter to present our derivation of the classical map and to discuss the dynamical properties of both coupled kicked tops and single kicked top. The classical map of the single kicked top can be derived simply from the coupled kicked tops map by putting the coupling strength between two tops equal to *zero*.

We divide this chapter into three sections. In Section 3.1, we present Hamiltonian of the single kicked top and of the coupled kicked tops. We derive the classical map of this system in the large spin limit by defining the quantum time evolution corresponding to the coupled kicked tops. In Section 3.2, we discuss about the classical dynamical behaviors of the single top for different parameter values. Finally, in Section 3.3, we discuss how the stability of some of the fixed points and the short periodic orbits of the single top change with the system parameter and how these changes lead to regular $\longrightarrow$ chaos transition. We only discuss the stability of some of those fixed points and periodic orbits which are clearly visible by naked eyes.

3.1 Derivation of the classical map corresponding to coupled kicked tops

The single kicked top is a spin system, characterized by an angular momentum vector $\mathbf{J} = (J_x, J_y, J_z)$, where these components obey the usual $SU(3)$ angular momentum algebra, i.e. $[J_i, J_j] = i\,\varepsilon_{ijk}\,J_k$. Here we set Planck's constant to unity. The dynamics of the top is governed by the Hamiltonian [87] :

$$H(t) = p\,J_y + \frac{k}{2j}\,J_z^2 \sum_{n=-\infty}^{+\infty} \delta\,(t - n). \tag{3.1}$$

The first term describes free precession of the top around y-axis with angular frequency p, and the second term is due to periodic δ-function kicks. Each such kick results in a torsion about z-axis by an angle proportional to J_z, and the proportionality constant is a dimensionless constant $k/2j$. Now, to study the entanglement between two tops, we consider the Hamiltonian of the coupled kicked

tops which can be written, following Ref. [50], as :

$$\begin{aligned} \mathcal{H}(t) &= H_1(t) + H_2(t) + H_{12}(t) && (3.2)\\ \text{where } H_i(t) &\equiv p_i J_{y_i} + \frac{k_i}{2j} J_{z_i}^2 \sum_n \delta(t-n), && (3.3)\\ H_{12}(t) &\equiv \frac{\epsilon}{j} J_{z_1} J_{z_2} \sum_n \delta(t-n), && (3.4) \end{aligned}$$

where $i = 1, 2$. Here $H_i(t)$'s are the Hamiltonians of the individual tops, and $H_{12}(t)$ is the coupling between the tops using spin-spin interaction term with a coupling strength of ϵ/j. All these angular momentum operators obey standard commutation relations. For the rest of the thesis we will only concentrate to the case $p_1 = p_2 = \pi/2$. This special choice of the angular frequencies will simplify both the quantum and classical maps. Since J_i^2 and J_{z_i}'s are four mutually commuting operators, the simultaneous eigenvectors of these operators we take as our basis. In general, this basis is denoted by $|j_1, m_1; j_2, m_2\rangle = |j_1, m_1\rangle \otimes |j_2, m_2\rangle$, where $J_i^2|j_i, m_i\rangle = j_i(j_i+1)|j_i, m_i\rangle$ and $J_{z_i}|j_i, m_i\rangle = m_i|j_i, m_i\rangle$. The individual top angular momentums, j_1 and j_2, could in general be different.

The time evolution operator, defined in between two consecutive kicks, corresponding to this coupled Hamiltonian is given by,

$$U_T = U_{12}^{\epsilon}(U_1 \otimes U_2) = U_{12}^{\epsilon}\left[(U_1^k U_1^f \otimes (U_2^k U_2^f)\right], \tag{3.5}$$

where the different terms are given by,

$$\begin{aligned} U_i^f \equiv \exp\left(-i\frac{\pi}{2} J_{y_i}\right) \quad ; \quad U_i^k &\equiv \exp\left(-i\frac{k}{2j} J_{z_i}^2\right),\\ U_{12}^{\epsilon} &\equiv \exp\left(-i\frac{\epsilon}{j} J_{z_1} J_{z_2}\right), \end{aligned} \tag{3.6}$$

and as usual $i = 1, 2$.

The corresponding classical map of the coupled kicked tops discussed above can be obtained from the quantum description with the Heisenberg picture in which the angular momentum operators evolve as:

$$\mathbf{J}(n+1) = U_T^{\dagger} \mathbf{J}(n) U_T. \tag{3.7}$$

Let us now determine the explicit form of the angular momentum evolution equation for each component of the angular momentum. Here we present the time-

evolution of different components of the angular momentum vector $\mathbf{J_1}$ corresponding to first subsystem are (see *Appendix*):

$$\begin{aligned} J'_{x_1} \equiv U_T^\dagger J_{x_1} U_T &= \frac{1}{2}(J_{z_1} + iJ_{y_1}) \exp\left[i\frac{k}{j}\left(-J_{x_1} + \frac{1}{2}\right)\right] \otimes \exp\left(-i\frac{\epsilon}{j}J_{x_2}\right) \\ &+ \frac{1}{2}\exp\left[-i\frac{k}{j}\left(-J_{x_1} + \frac{1}{2}\right)\right](J_{z_1} - iJ_{y_1}) \otimes \exp\left(i\frac{\epsilon}{j}J_{x_2}\right), \quad (3.8a) \\ J'_{y_1} \equiv U_T^\dagger J_{y_1} U_T &= \frac{1}{2i}(J_{z_1} + iJ_{y_1}) \exp\left[i\frac{k}{j}\left(-J_{x_1} + \frac{1}{2}\right)\right] \otimes \exp\left(-i\frac{\epsilon}{j}J_{x_2}\right) \\ &- \frac{1}{2i}\exp\left[-i\frac{k}{j}\left(-J_{x_1} + \frac{1}{2}\right)\right](J_{z_1} - iJ_{y_1}) \otimes \exp\left(i\frac{\epsilon}{j}J_{x_2}\right), \quad (3.8b) \end{aligned}$$

$$J'_{z_1} \equiv U_T^\dagger J_{z_1} U_T = -J_{x_1}. \quad (3.8c)$$

The time-evolution of the components of $\mathbf{J_2}$ can be obtained by interchanging the index 1 and 2 in the above expressions. We proceed by rescaling the angular momentum operator as $(X_i, Y_i, Z_i) \equiv (J_{x_i}, J_{y_i}, J_{z_i})/j$, for $i = 1, 2$. Components of this rescaled angular momentum vector satisfy the commutation relations, $[X_i, Y_i] = iZ_i/j, [Y_i, Z_i] = iX_i/j$ and $[Z_i, X_i] = iY_i/j$. Therefore, in $j \to \infty$ limit, components of this rescaled angular momentum vector will commute and become classical c-number variables. Consequently, in this large-j limit, we obtain the classical map corresponding to coupled kicked tops as,

$$\begin{aligned} X'_1 &= Z_1 \cos\Delta_{12} + Y_1 \sin\Delta_{12} && (3.9a) \\ Y'_1 &= -Z_1 \sin\Delta_{12} + Y_1 \cos\Delta_{12} && (3.9b) \\ Z'_1 &= -X_1 && (3.9c) \\ X'_2 &= Z_2 \cos\Delta_{21} + Y_2 \sin\Delta_{21} && (3.9d) \\ Y'_2 &= -Z_2 \sin\Delta_{21} + Y_2 \cos\Delta_{21} && (3.9e) \\ Z'_2 &= -X_2 && (3.9f) \end{aligned}$$

where

$$\Delta_{12} \equiv kX_1 + \epsilon X_2 \ ; \ \text{ and } \ \Delta_{21} \equiv kX_2 + \epsilon X_1. \quad (3.10)$$

The difference between the map presented above and which was derived in [50] lies in the form of the angles Δ_{12} and Δ_{21}. However, these minute differences

are very important. The above map is canonical. It satisfies all Poisson bracket relations like $\{X_i', Y_i'\} = Z_i'$, $\{Y_i', Z_i'\} = X_i'$ and $\{Z_i', X_i'\} = Y_i'$, where $i = 1, 2$; and Poisson brackets of any two dynamical variables corresponding to different tops are equal to *zero*. In contrast the classical map presented in [50], satisfies the first three Poisson bracket relations, but the Poisson brackets of any two dynamical variables corresponding to different tops are nonzero and they are proportional to the coupling strength ϵ, implying that the map is canonical only in the uncoupled limit.

3.2 Dynamical properties of the single kicked top

We have already mentioned that the classical map corresponding to the single kicked top can trivially be obtained from the expressions of the classical map corresponding to the coupled kicked tops by substituting the coupling strength ϵ equal to zero. Therefore, from Eq.(3.9) and Eq.(3.10), we get the classical map corresponding to the single kicked top, whose Hamiltonian is given in Eq.(3.1) (where $p = \pi/2$), and that map is given by

$$X' = Z\cos kX + Y\sin kX \tag{3.11a}$$

$$Y' = -Z\sin kX + Y\cos kX \tag{3.11b}$$

$$Z' = -X. \tag{3.11c}$$

We shall sometime use the shorthand $\overline{\mathbf{X}}' = \mathbf{F}(\mathbf{X})$ for the above map. From the above expressions, it is clear that the variables (X, Y, Z) lie on the sphere of radius unity, i.e., $X^2 + Y^2 + Z^2 = 1$. This constraint on the dynamical variables restricted the classical motion to the two-dimensional surface of a unit sphere. Following the usual procedure, we can parameterize the dynamical variables in terms of the polar angle θ and the azimuthal angle ϕ as $X = \sin\theta\cos\phi$, $Y = \sin\theta\sin\phi$ and $Z = \cos\theta$. In Fig.3.1, we show a schematic diagram of a unit sphere and also show the relation between the Cartesian coordinates (X, Y, Z) and the spherical coordinates (ϕ, θ). In terms of this new (ϕ, θ) variables, the above map looks very complicated, and therefore we do not display that map. Moreover, during our numerical iterations we use the above three-dimensional form of the map,

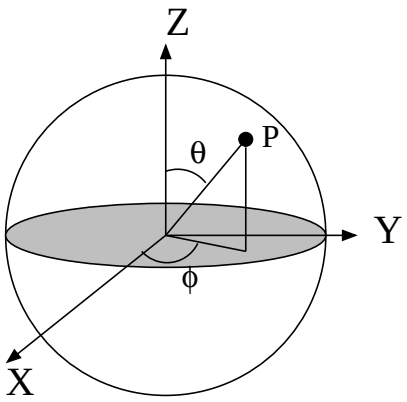

Figure 3.1: Schematic diagram of a sphere. This show the relation between the spherical coordinates (ϕ, θ) with the Cartesian coordinates (X, Y, Z). At $z = \pm 1$, $\theta = 0$ and π, but ϕ is undefined.

and after every iteration we get back the corresponding (ϕ, θ) from the relations $\phi = \tan^{-1}(Y/X)$ and $\cos\theta = Z$, where ϕ and $\cos\theta$ are the canonical coordinates on the sphere.

In Fig.3.2, we present the phase space diagrams of the single top for different values of the parameter k. For $k = 1.0$, as shown in Fig.3.2(a), the phase space is mostly covered by regular orbits, without any visible stochastic region. As we further increase the parameter, regular region becomes smaller. Fig.3.2(b) is showing the phase space for $k = 2.0$. Still the phase space is mostly covered by the regular region, but now we can observe a thin stochastic layer at the separatrix. For the change in the parameter value from $k = 2.0$ to $k = 3.0$, there is significant change in the phase space. At $k = 3.0$, shown in Fig.3.2(c), the phase space is of a truly mixed type. The size of the chaotic region is now very large with few regular islands. Fig.3.2(d) is showing the phase space for $k = 6.0$. Now the phase space is mostly covered by the chaotic region, with very tiny regular islands.

3.3 The transition from regular to chaotic dynamics: A detailed study

In Fig.3.2, we show the transition of the dynamics of the single (uncoupled) top from highly regular to highly chaotic with the increment of the parameter k. We

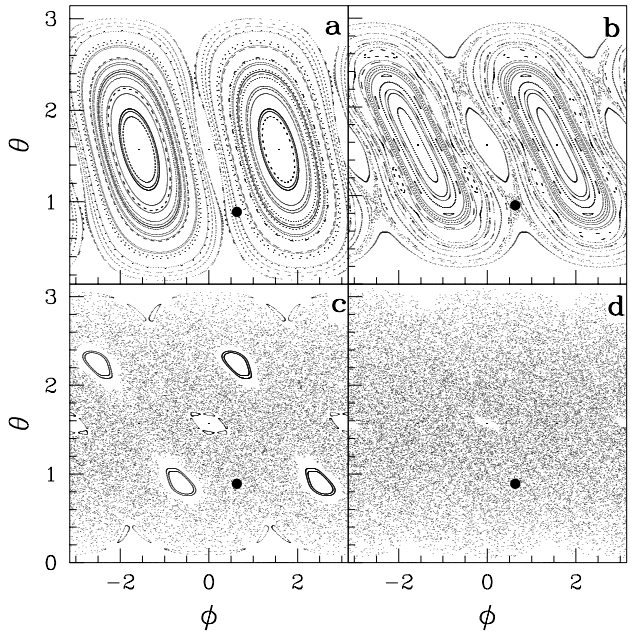

Figure 3.2: Phase space pictures of the single top, corresponding to different parameter values, are presented. (a) $k = 1$. Phase space is mostly covered by the regular region. (b) $k = 2$. The phase space is still very much regular, but now a thin stochastic layer can be observed at the separatrix. (c) $k = 3$. The phase space is truly mixed type. Few regular elliptic islands are visible inside the chaotic region. (d) $k = 6$. The phase space is almost covered by the chaotic region with few tiny elliptic islands. The solid circle (•) is the point at which we will construct the initial wavepacket during our study of the pure state entanglement production (Chapters 4 and 5).

now elaborately study the changes in the stability properties of some of the fixed points and the short periodic orbits as a function of the parameter k. A stable to unstable transition of the periodic points leads to chaos. Therefore, this study will give us better understanding of the classical dynamics of the kicked top. Let us first look at the fixed points of the map $\mathbf{F}$. There are two *trivial* fixed points at $\overline{\mathbf{X}} = \big(0, \pm 1, 0\big)$ which exist for any arbitrary values of k. On (ϕ, θ) surface these points are at $\big(\pm\pi/2, \pi/2\big)$. The *non-trivial* fixed points appear at sufficiently larger value of k. We determine the non-trivial fixed points by substituting $\overline{\mathbf{X}}' = \mathbf{F}(\overline{\mathbf{X}}) = \overline{\mathbf{X}}$ in Eq.(3.11) and we get

$$z = -x, \quad y = x \cot\left(\frac{kx}{2}\right). \tag{3.12a}$$

Substituting the above expressions in the constraint $x^2 + y^2 + z^2 = 1$, we get an

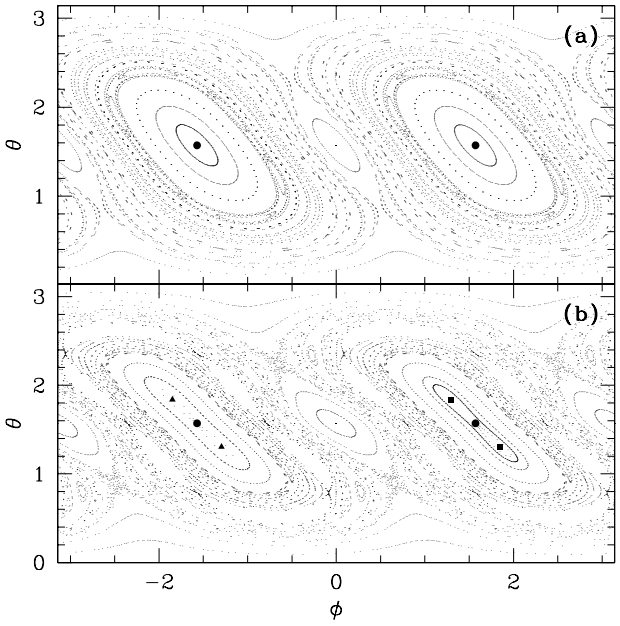

Figure 3.3: Phase space pictures of the single top, corresponding to two different parameter values, are presented. (a) $k = 1.5$. The phase space is predominantly regular. Solid circles (•) are representing the trivial fixed points. (b) $k = 2.1$. The phase space is still regular, but now a thin stochastic layer can be observed at the separatrix. Two trivial fixed points (•) have become unstable. One of the trivial fixed point bifurcates into a pair of new fixed points (■), which we call non-trivial fixed points. The other trivial fixed point bifurcates into a period-2 orbit (▲). The trivial period-4 $\left[\left(\phi;\theta = 0,\pi\right),\left(\phi = 0,\pi \text{ or } -\pi;\theta = \pi/2\right)\right]$ orbit is also clearly visible in both the cases. Note that the points at $\phi = \pi$ and at $\phi = -\pi$, are basically same points on the surface of the sphere.

algebraic equation for the x-coordinate as

$$f(x) = 0, \text{ where } f(x) \equiv \frac{\sin^2 \frac{kx}{2}}{1 + \sin^2 \frac{kx}{2}} - x^2. \tag{3.12b}$$

We get the non-trivial fixed points at different values of k by substituting the numerical solutions of Eq.(3.12b) in Eq.(3.12a).

To understand the stability properties of these fixed points we need to linearize the map $\overline{\mathbf{X}}' = \mathbf{F}(\mathbf{X})$ around those fixed points. The constraint $x^2 + y^2 + z^2 = 1$ fixes one eigenvalue of the linearized map $\mathbf{F}'(\overline{\mathbf{X}})$ at *unity* and hence this is irrelevant for stability. This implies that the motion is restricted on a two-dimensional space (surface of the sphere $x^2 + y^2 + z^2 = 1$). From the other two eigenvalues,

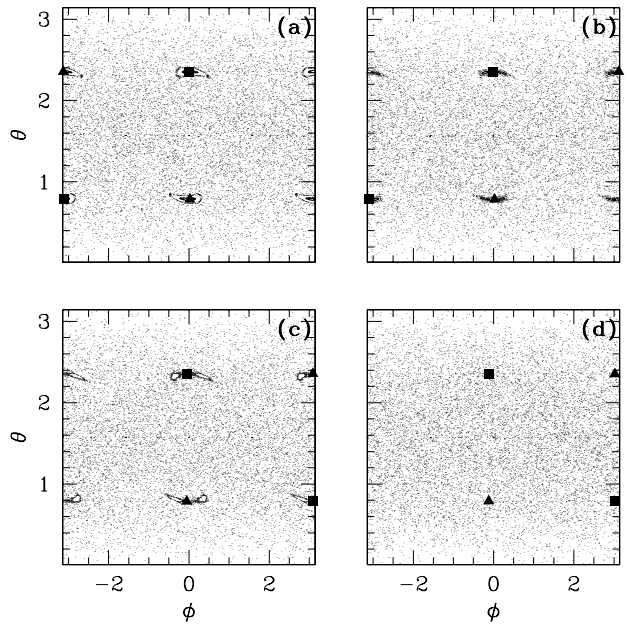

Figure 3.4: Phase space pictures of the single top are presented for the following parameter values. (a) $k = 4.4$. The non-trivial fixed points (■) and the period-2 orbit (▲) are stable. (b) $k = 4.5$. The non-trivial fixed points and the period-2 orbit have become unstable, and they bifurcate into *new* periodic points. (c) $k = 4.6$. Remnant of the non-trivial fixed points and the period-2 orbit are still visible due to the presence of the new stable periodic points. (d) $k = 4.8$. The new periodic points have also become unstable, and there are no sign of any remnant of the non-trivial fixed points and the period-2 orbit. The trivial period-4 orbit is unstable for all the above parameter values and therefore we do not see it.

we get the stability condition

$$\left|\,\mathrm{Tr}\;\mathbf{F}'(\overline{\mathbf{X}})\;-\;1\,\right| = \left|\,kx\;+\;\cos kx\;-\;1\,\right| \;<\; 2. \tag{3.13}$$

The above stability condition shows, that the trivial fixed points are stable only for $k \leq 2$. In Fig.3.3, we show these trivial fixed points for the parameter values $k = 1.5$ and $k = 2.1$. At $k = 1.5$ these fixed points are stable, shown in Fig.3.3(a) and at $k = 2.0$ these fixed points are marginally stable, shown in Fig.3.2(b). But at $k = 2.1$, we can see in Fig.3.3(b) that these fixed points have become unstable and each point has bifurcated into a pair of new stable points. However, the periodicity of these two pairs of new stable points are different. A pair of points which appears due to the bifurcation of the trivial fixed point at $(\pi/2, \pi/2)$ are two new fixed points. We mark these fixed points by the solid squares in Fig.3.3(b). These

two fixed points are actually the first set of non-trivial fixed points which satisfy Eq.(3.12) and we can go from the one fixed point to the other fixed point by a rotation of π about y-axis. Using MATHEMATICA 4, we solve the nonlinear algebraic equation given in Eq.(3.12b) and get the solution $x = \pm 0.263550$. Substituting this solution in Eq.(3.12a), we get $y = 0.927945$, $z = \mp 0.263550$. In spherical coordinates (ϕ, θ), location of the non-trivial fixed points are $(1.294069, 1.837497)$ and $(1.847524, 1.304096)$. On the other hand, the trivial fixed point at $(-\pi/2, \pi/2)$ bifurcates into a period-2 orbit which is marked by the solid triangles in Fig.3.3(b). The period-2 points can be obtained from the non-trivial fixed points by a rotation of $-\pi$ about z-axis, where *negative* sign implies *anti-clockwise* rotation. Therefore the period-2 points exist at $(0.263550, -0.927945, 0.263550)$ and $(-0.263550, -0.927945, -0.263550)$. In terms of the spherical coordinates, the period-2 points are located at $(-1.847524, 1.837497)$ and $(-1.294069, 1.304096)$. Stability analysis shows that the above mentioned non-trivial fixed points and the period-2 orbit become unstable when $k > \sqrt{2}\pi \simeq 4.442883$ [87]. For $k = 3.0$, shown in Fig.3.2(c), we can clearly observe the stable non-trivial fixed points and the period-2 orbit. In Fig.3.4, we present *four* phase space diagrams for the parameter values $k = 4.4, 4.5, 4.6$ and 4.8. At $k = 4.4 (< \sqrt{2}\pi)$, shown in Fig.3.4(a), we observe the stable non-trivial fixed points (marked by solid squares) and the period-2 orbit (marked by solid triangles). But at $k = 4.5 (> \sqrt{2}\pi)$, shown in Fig.3.4(b), we now see that each above mentioned stable point has become unstable (marked as usual by solid squares and solid triangles) and has bifurcated into a pair of new stable periodic points. Now at $k = 4.6$, presented in Fig.3.4(c), due to the presence of the new stable points, we at least identify the unstable non-trivial fixed points and the unstable period-2 orbit. However, at $k = 4.8$, we do not see any remnant of those fixed points and the period-2 orbit by the naked eye. That means, with an increment of the parameter k from 4.6 to 4.8, all the new periodic points have also become unstable.

Let us now discuss the stability of a trivial period-4 orbit $(0, 0, 1) \xrightarrow{\mathbf{F}} (1, 0, 0) \xrightarrow{\mathbf{F}} (0, 0, -1) \xrightarrow{\mathbf{F}} (-1, 0, 0) \xrightarrow{\mathbf{F}} (0, 0, 1)$. In terms of spherical coordinates, these points are located at $(\phi, \theta = 0) \xrightarrow{\mathbf{F}} (\phi = 0, \theta = \pi/2) \xrightarrow{\mathbf{F}} (\phi, \theta = \pi) \xrightarrow{\mathbf{F}} (\phi = \pm\pi, \theta = \pi/2) \xrightarrow{\mathbf{F}} (\phi, \theta = 0)$. When $\theta = 0$ and $\theta = \pi$, ϕ can take

any arbitrary values in between $(-\pi, \pi)$. These points are actually two poles on the z-axis (See Fig.3.1 for clarification). A comparison between Fig.3.1 and all the other figures [Fig.3.2 - Fig.3.4] shows that the two poles at $z \pm 1$ have become two lines at $\theta = 0$ and $\theta = \pi$ where $\phi \in [-\pi, \pi]$. In Figs. 3.2 and 3.3, we clearly observe the presence of the above mentioned period-4 orbit. From the stability analysis, it can be shown that this period-4 orbit exists for all values of k, but it is stable only for $(2\cos k + k \sin k)^2 < 4$ [87]. In Fig. 3.4, we are not observing the period-4 orbit. Because, in the parameter range $k \in [4.4, 4.8]$, this period-4 orbit is not stable. However, at $k = 6.0$, the period-4 orbit has again become stable and we observe its reappearance in Fig.3.2(d). These disappearances and the reappearances of the period-4 orbit will go on with the increment of the parameter k.

Appendix

Derivation of the classical map corresponding to coupled kicked tops :

Let us define ladder operators,

$$J_{1\pm} \equiv J_{x_1} \pm J_{y_1} \qquad ; \qquad J_{1+} = J_{1-}$$
$$J_{1+}|m_1\rangle = C_{m_1}|m_1+1\rangle \quad \text{and} \quad J_{1-}|m_1\rangle = D_{m_1}|m_1-1\rangle \tag{3.14a}$$

where C_{m_1} and D_{m_1} are known functions of j and m_1 and $|m_1\rangle$ are the standard angular momentum basis states. We can write $J_{x_1} = (J_{1+} + J_{1-})/2$ and $J_{y_1} = (J_{1+} - J_{1-})/2i$. Therefore,

$$J'_{x_1} \otimes I_2 = \frac{1}{2}U_T^\dagger (J_{1+} \otimes I_2) U_T + \frac{1}{2}U_T^\dagger (J_{1-} \otimes I_2) U_T, \tag{3.14b}$$
$$J'_{u_1} \otimes I_2 = \frac{1}{2i}U_T^\dagger (J_{1+} \otimes I_2) U_T - \frac{1}{2i}U_T^\dagger (J_{1-} \otimes I_2) U_T, \tag{3.14c}$$

where the terms present at the right hand side are the Hermitian conjugate of each other. Therefore, it is sufficient to determine only one term. Here we will

calculate the first term explicitly. We have

$$U_T^\dagger(J_{1+}\otimes I_2) = (U_1\otimes U_2)^\dagger U_{12}^{\epsilon\dagger}(J_{1+}\otimes I_2)U_{12}^{\epsilon}(U_1\otimes U_2). \tag{3.14d}$$

In $|m_1,m_2\rangle$ basis, $U_{12}^{\epsilon\dagger}(J_{1+}\otimes I_2)U_{12}^{\epsilon}$ is,

$$\begin{aligned}
&\langle m_1,m_2|U_{12}^{\epsilon\dagger}(J_{1+}\otimes I_2)U_{12}^{\epsilon}|n_1,n_2\rangle \\
&= \exp\left[i\frac{\epsilon}{j}(m_1-n_1)m_2\right]\langle m_1|J_{1+}|n_1\rangle\delta_{m_2n_2} \\
&= \exp\left[i\frac{\epsilon}{j}(m_1-n_1)m_2\right]C_{n_1}\delta_{m_1,n_1+1}\delta_{m_2n_2} \\
&= \exp\left[i\frac{\epsilon}{j}m_2\right]C_{n_1}\delta_{m_1,n_1+1}\delta_{m_2n_2}.
\end{aligned} \tag{3.14e}$$

The above expression can also be written as,

$$\begin{aligned}
\langle m_1,m_2|U_{12}^{\epsilon\dagger}(J_{1+}\otimes I_2)U_{12}^{\epsilon}|n_1,n_2\rangle &= \langle m_1,m_2|J_{1+}\otimes\exp\left(i\frac{\epsilon}{j}J_{z_2}\right)|n_1,n_2\rangle \\
\Rightarrow U_{12}^{\epsilon\dagger}(J_{1+}\otimes I_2)U_{12}^{\epsilon} &= J_{1+}\otimes\exp\left(i\frac{\epsilon}{j}J_{z_2}\right).
\end{aligned} \tag{3.14f}$$

Therefore,

$$\begin{aligned}
U_T^\dagger(J_{1+}\otimes I_2)U_T &= (U_1\otimes U_2)^\dagger\left[J_{1+}\otimes\exp\left(i\frac{\epsilon}{j}J_{z_2}\right)\right](U_1\otimes U_2) \\
&= (U_1^\dagger J_{1+}U_1)\otimes\left[U_2^\dagger\exp\left(i\frac{\epsilon}{j}J_{z_2}\right)U_2\right]
\end{aligned} \tag{3.14g}$$

Now,

$$\begin{aligned}
U_1^\dagger J_{1+}U_1 &= U_1^{f\dagger}U_1^{k\dagger}J_{1+}U_1^kU_1^f \\
&= U_1^{f\dagger}J''_{1+}U_1^f, \quad \text{where} \quad J''_{1+}\equiv U_1^{k\dagger}J_{1+}U_1^k.
\end{aligned} \tag{3.14h}$$

In $\{|m_1\rangle\}$ basis, J''_{1+} can be written as,

$$\begin{aligned}
\langle m_1|J''_{1+}|n_1\rangle &= \langle m_1|U_1^{k\dagger}J_{1+}U_1^k|n_1\rangle, \\
&= \exp\left[i\frac{k}{2j}\left(m_1^2-n_1^2\right)\right]\langle m_1|J_{1+}|n_1\rangle, \\
&= \exp\left[i\frac{k}{2j}\left(m_1^2-n_1^2\right)\right]C_{n_1}\delta_{m_1,n_1+1}, \\
&= \exp\left[i\frac{k}{j}\left(n_1+\frac{1}{2}\right)\right]C_{n_1}\delta_{m_1,n_1+1}, \\
&= \langle m_1|J_{1+}\exp\left[i\frac{k}{j}\left(J_{z_1}+\frac{1}{2}\right)\right]|n_1\rangle \\
\Rightarrow J''_{1+} &= J_{1+}\exp\left[i\frac{k}{j}\left(J_{z_1}+\frac{1}{2}\right)\right]
\end{aligned} \tag{3.14i}$$

Therefore,

$$U_1^\dagger J_{1+} U_1 = U_1^{f\dagger} J_{1+} \exp\left[i\frac{k}{j}\left(J_{z_1}+\frac{1}{2}\right)\right] U_1^f. \tag{3.14j}$$

The operator U_1^f is the rotation operator about $y-$axis with angle $\pi/2$, therefore $U_1^{f\dagger}(J_{x_1}, J_{y_1}, J_{z_1})U_1^f = (J_{z_1}, J_{y_1}, -J_{x_1})$. Hence we have

$$U_1^\dagger J_{1+} U_1 = (J_{z_1} + iJ_{y_1}) \exp\left[i\frac{k}{j}\left(-J_{x_1}+\frac{1}{2}\right)\right]. \tag{3.14k}$$

Now we will calculate the other term of Eq.(3.14g), i.e.,

$$\begin{aligned} U_2^\dagger \exp\left(i\frac{\epsilon}{j}J_{z_2}\right) U_2 &= U_2^{f\dagger} U_2^{k\dagger} \exp\left(i\frac{\epsilon}{j}J_{z_2}\right) U_2^k U_2^f \\ &= U_2^{f\dagger} \exp\left(i\frac{\epsilon}{j}J_{z_2}\right) U_2^f \quad [\text{ since } \left[U_2^k, J_{z_2}\right] = 0] \\ &= \exp\left(-i\frac{\epsilon}{j}J_{x_2}\right) \quad \left[\text{ since } U_2^f \text{ is rotation matrix}\right]. \end{aligned} \tag{3.14l}$$

Substituting all the above results in Eq. (3.14g), we get,

$$U_T^\dagger (J_{1+}\otimes I_2) U_T = (J_{z_1} + iJ_{y_1}) \exp\left[i\frac{k}{j}\left(-J_{x_1}+\frac{1}{2}\right)\right] \otimes \exp\left(-i\frac{\epsilon}{j}J_{x_2}\right). \tag{3.14m}$$

By taking Hermitian conjugate of the above expression, we determine

$$U_T^\dagger (J_{1-}\otimes I_2) U_T = \exp\left[-i\frac{k}{j}\left(-J_{x_1}+\frac{1}{2}\right)\right] (J_{z_1} - iJ_{y_1}) \otimes \exp\left(i\frac{\epsilon}{j}J_{x_2}\right). \tag{3.14n}$$

Substituting, last two expressions in Eq.(3.14b) and in Eq.(3.14c), we will get Eq.(3.8a) and Eq.(3.8b).

Let us now derive the time evolution of J_{z_1}.

$$\begin{aligned} J'_{z_1}\otimes I_2 &= U_T^\dagger (J_{z_1}\otimes I_2) U_T \\ &= (U_1\otimes U_2)^\dagger U_{12}^{\epsilon\dagger} (J_{z_1}\otimes I_2) U_{12}^\epsilon (U_1\otimes U_2) \\ &= (U_1^\dagger \otimes U_2^\dagger)(J_{z_1}\otimes I_2)(U_1\otimes U_2) \quad [\text{since } [U_{12}^\epsilon, J_{z_1}\otimes I_2] = 0] \\ &= U_1^\dagger J_{z_1} U_1 \\ &= U_1^{f\dagger} U_1^{k\dagger} J_{z_1} U_1^k U_1^f \\ &= U_1^{f\dagger} J_{z_1} U_1^f \quad [\text{since } [U_1^k, J_{z_1}] = 0] \\ &= \exp\left(i\frac{\pi}{2}J_{y_1}\right) J_{z_1} \exp\left(-i\frac{\pi}{2}J_{y_1}\right) \\ \text{Therefore, } J'_{z_1} &= -J_{x_1}. \end{aligned} \tag{3.14o}$$

Thus we get Eq.(3.8c).

Chapter 4

Quantum Entanglement and Random Matrix Theory (RMT)

In the introductory chapter we have discussed extensively about chaos, entanglement and the effects of the former on the later. Saturation of entanglement among the participating subsystems is one interesting property shown by the coupled chaotic systems. This was first observed during a study of entanglement in coupled standard map [52]. The saturation of entanglement is observed in the eigenstates of the coupled chaotic systems and also in the time evolving states evolving under coupled chaotic dynamics. The saturation value depends on the Hilbert space dimensions of the participating subsystems and is less than its maximum possible value. This result also implies that, though there exists a maximum kinematical limit for entanglement, dynamically it is not possible to create it by using generic Hamiltonian evolutions on unentangled states. We want to emphasize that these upper bounds are *statistical* and are more unlikely to be violated the larger the Hilbert space dimension.

Since the Hilbert space dimension and chaos have roles in this bound for entanglement, a coupled kicked tops is an attractive model. The single and coupled kicked top has already been discussed in the previous chapter ; we generalize it here to include the case of unequal spins and symmetry breaking terms. The

Hamiltonian of the coupled top system used is :

$$\begin{aligned} H(t) &= \frac{\pi}{2}J_{y_1} + \frac{k}{2j_1}(J_{z_1}+\alpha_1)^2 \sum_{n=-\infty}^{\infty}\delta(t-n) \\ &+ \frac{\pi}{2}J_{y_2} + \frac{k}{2j_2}(J_{z_2}+\alpha_2)^2 \sum_{n=-\infty}^{\infty}\delta(t-n) \\ &+ \frac{\epsilon}{\sqrt{j_1 j_2}}J_{z_1}J_{z_2}\sum_{n=-\infty}^{\infty}\delta(t-n). \end{aligned} \tag{4.1}$$

The J_{y_r} terms describe free precession of each top and the remaining terms are due to periodic δ-function kicks. The first two such terms are torsion about $z-$axis and the final term describes the spin-spin coupling. When either of the constants, α_1 or α_2, is not zero the parity symmetry $RH(t)R^{-1} = H(t)$, where $R = \exp\left(i\pi J_{y_1}\right) \otimes \exp\left(i\pi J_{y_2}\right)$, is broken. The dimensionality of the Hilbert spaces are $N = 2j_1 + 1$ and $M = 2j_2 + 1$. The unitary time evolution operator corresponding to this Hamiltonian is given by :

$$U_T = \left(U_1 \otimes U_2\right) U_{12}^{\epsilon} = \left[\left(U_1^f U_1^k\right) \otimes \left(U_2^f U_2^k\right)\right] U_{12}^{\epsilon}, \tag{4.2}$$

where the different terms are given by

$$U_i^f \equiv \exp\left(-\frac{i\pi}{2}J_{y_i}\right), \quad U_i^k \equiv \exp\left(-\frac{ik}{2j_i}\left(J_{z_i}+\alpha_i\right)^2\right), \quad U_{12}^{\epsilon} \equiv \exp\left(-\frac{i\epsilon}{\sqrt{j_1 j_2}}J_{z_1}J_{z_2}\right) \tag{4.3}$$

and $i = 1, 2$. There exists an antiunitary generalized time reversal symmetry,

$$\left[\exp\left(i\pi J_{x_1}\right)\,\exp\left(i\pi J_{y_1}/2\right)\right] \otimes \left[\exp\left(i\pi J_{x_2}\right)\,\exp\left(i\pi J_{y_2}/2\right)\right] K$$

where K is complex conjugation operator, from which we can expect the applicability of results concerning the Gaussian orthogonal ensemble (GOE).

4.1 Initial States

Entanglement production of time evolving states under U_T has been studied for two different initial states.

(1) The initial state is a product of a generalized $SU(2)$ coherent state or the directed angular momentum states placed in the chaotic sea of phase space. This is

completely unentangled state, i.e., $S_V = 0$ and $S_R = 0$. This state corresponding to individual tops is given in $|j_i, m_i\rangle$ basis as :

$$\langle j_i, m_i | \theta_0^i, \phi_0^i \rangle = \left(1 + |\gamma|^2\right)^{-j_i} \gamma^{j_i - m_i} \sqrt{\binom{2j_i}{j_i + m_i}} \tag{4.4}$$

where $\gamma \equiv \exp\left(i\phi_0\right) \tan\left(\theta_0/2\right)$. Now on we will write $|j_i, m_i\rangle$ as $|m_i\rangle$ for notational simplification. Explicitly in $|m_i\rangle$ basis the initial product state can be written as

$$\begin{aligned} |\psi(0)\rangle &= \sum_{m_1=-j_1}^{+j_1} \sum_{m_2=-j_2}^{+j_2} \langle m_1, m_2 | \psi(0)\rangle |m_1, m_2\rangle \\ &= \sum_{m_1=-j_1}^{+j_1} \sum_{m_2=-j_2}^{+j_2} \langle m_1 | \theta_0^1, \phi_0^1\rangle \langle m_2 | \theta_0^2, \phi_0^2\rangle \end{aligned} \tag{4.5}$$

where $\langle m_i | \theta_0^i, \phi_0^i \rangle$ can be obtained from Eq.(4.4).

(2) The initial state is maximally entangled state, i.e., $S_V = \ln N$ and $S_R = 1 - \left(1/N\right)$. In $|m_1, m_2\rangle$ basis, this state can be written as

$$\langle m_1, m_2 | \psi(0)\rangle = \frac{1}{N} \delta_{m_1, m_2}. \tag{4.6}$$

4.2 Numerical Scheme

We now evolve the above initial states $|\psi(0)\rangle$ by the coupled top time evolution operator U_T as $|\psi(n)\rangle = U_T|\psi(n-1)\rangle = U_T^2|\psi(n-2)\rangle = \ldots = U_T^n|\psi(0)\rangle$. The numerical iteration scheme for the above evolutions, following [50], is

$$\left\langle s_1, s_2 \middle| \psi(n) \right\rangle = \exp\left(-i\frac{\epsilon}{j} s_1 s_2\right) \sum_{m_1=-j_1}^{+j_1} \sum_{m_2=-j_2}^{+j_2} \left\langle s_1 \middle| U_1 \middle| m_1 \right\rangle \left\langle s_2 \middle| U_2 \middle| m_2 \right\rangle \left\langle m_1, m_2 \middle| \psi(n-1) \right\rangle \tag{4.7}$$

where

$$\langle s_1 | U_1 | m_1 \rangle = \exp\left(-i\frac{k}{2j_1} s_1^2\right) d_{s_1 m_1}^{(j_1)}\left(\frac{\pi}{2}\right). \tag{4.8}$$

$d_{s_1 m_1}^{(j_1)}\left(\frac{\pi}{2}\right)$ is the Wigner rotation matrix [89] :

$$d_{s_1 m_1}^{(j_1)}\left(\frac{\pi}{2}\right) = \frac{(-1)^{s_1 - m_1}}{2^{j_1}} \binom{2j_1}{j_1 - s_1}^{1/2} \binom{2j_1}{j_1 + m_1}^{-1/2} \sum_k (-1)^k \binom{j_1 - s_1}{k} \binom{j_1 + s_1}{k + s_1 - m_1}. \tag{4.9}$$

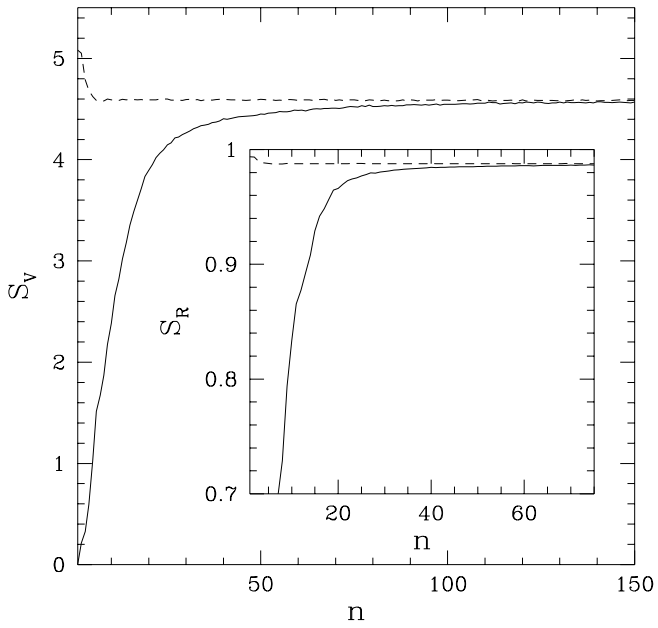

Figure 4.1: Entanglement saturation of a completely unentangled initial state (solid line) and a maximally entangled initial state (dotted line) under time evolution operator U_T. Here $k = 3, \epsilon = 0.1$ and the phases $\alpha_1 = \alpha_2 = 0.47$. Inset shows similar behavior of linear entropy.

The main problem in calculating the Wigner rotation matrix lies in the calculation of the above sum. Defining that sum as V_{m_1}, and starting from $V_{-j} = 1$ and $V_{-j+1} = 2\,s_1$, we can get the other V_{m_1} recursively by using the following relation [90]

$$(j - m_1 + 1)V_{m_1-1} - 2s_1V_{m_1} + (j + m_1 + 1)V_{m_1+1} = 0.$$

Besides Wigner rotation matrix can be expressed in terms of Jacobi polynomials and of different Hypergeometric functions [91]. However, we have followed the above recursive scheme.

4.3 Numerical Results

These initial states are evolved under U_T, and the results are displayed in Fig. 4.1. Here we have taken stronger coupling strength, compared to the value taken in [50]. Because, our goal is to study entanglement saturation and strong coupling

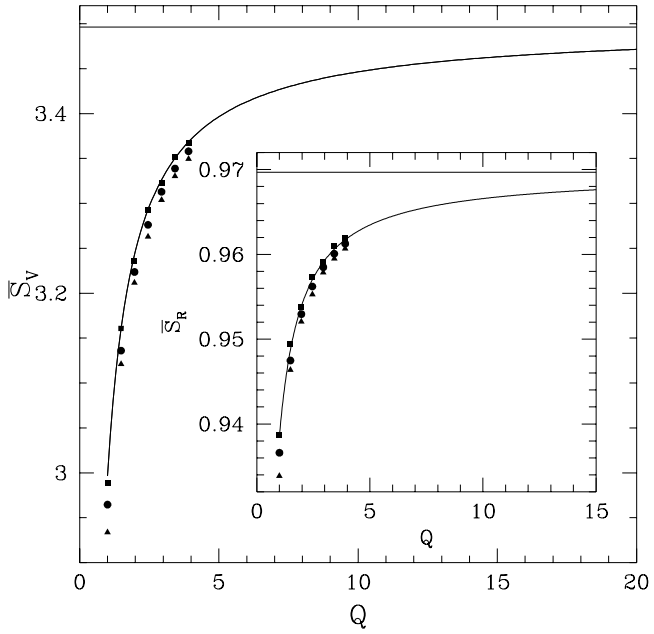

Figure 4.2: The spectral average of the entanglement present in eigenstates of U_T ($k = 9, \epsilon = 10$) as a function of $Q = M/N$, where $N = 2j_1 + 1 = 33$. Solid triangles are kicked top results with parity symmetry ($\alpha_1 = \alpha_2 = 0$) and solid circles are the corresponding results without symmetry ($\alpha_1 = \alpha_2 = 0.47$). Solid squares are the result of corresponding RMT Monte Carlo simulations and solid line is the theoretical curve Eq. (4.12a). Horizontal line is the maximum possible entanglement ($\ln(N)$). Inset shows the behavior of the linear entropy.

will help us achieve entanglement saturation within a short time. In the first case, initially both the von Neumann entropy and the linearized entropy ($S_R = 1 - \mathrm{Tr}_1(\rho_1^2)$), are zero, but with time evolution both entropies start increasing and saturate, apart from small fluctuations, at values *less* than the maximum possible $\left(\ln N\right)$.

For the von Neumann entropy the saturation value is $\sim \ln(0.6N)$ and for the linear entropy it is approximately $1 - 2/N$, where N is the dimension of each subsystems. This is the dynamical bound for entanglement of a system consists of two equal dimensional subsystems, while the maximum kinematical limits are $\ln N$ and $1 - 1/N$ respectively. The saturation value of von Neumann entropy of this time evolved state is same as that obtained for stationary states of completely chaotic coupled standard maps [52]. In the second case, the initial state is maximally entangled and time evolution forces this state to partially disentangle till

the entropy reaches the above mentioned values.

This study shows that the saturation of entanglement is a universal phenomenon, it depends only on the Hilbert space dimensions, and not on dynamical characteristics of the system, apart from the presence of complete chaos. The effect of dimension on entanglement saturation has been studied by keeping the dimension of the first subsystem constant at N and increasing the dimension M of the second subspace from $M = N$ to some large value. Thus we may think of the second system as tending towards a complex bath with a quasi-continuous spectrum. It is observed that the entanglement saturation increases with M and finally gets saturated at the maximum possible kinematical limit, as shown in Fig. 4.2. For example the von Neumann entropy starting from $\ln(0.6N)$ increases asymptotically to $\ln N$, while the linear entropy starting from $1 - 2/N$ tends to $1 - 1/N$.

4.4 Analytical formulation using RMT

RMT has been successful in calculating many important universal statistical properties of quantum chaotic systems. Here we can also develop a complete analytical understanding of these limits via RMT modeling. A typical stationary state of a quantum chaotic system shares properties of the eigenvectors of random matrices. Let us assume that some product basis $\{ |\phi_n^{(1)}\rangle |\phi_m^{(2)}\rangle \}$ has been used to write any state $|\psi\rangle$ as

$$|\psi\rangle = \sum_{n=1}^{N} \sum_{m=1}^{M} a_{nm} |\phi_n^{(1)}\rangle |\phi_m^{(2)}\rangle.$$

The components a_{nm} are real for stationary states of time reversal symmetric systems. Now the reduced density matrix (RDM) corresponding to first subsystem is

$$\rho_1 = \mathrm{Tr}_2 |\psi\rangle\langle\psi| = \sum_{n,l=1}^{N} \sum_{m=1}^{M} a_{nm} a_{lm} |\phi_n^{(1)}\rangle\langle\phi_m^{(1)}| = AA^T, \tag{4.10}$$

where $a_{nm} = \big[A\big]_{nm}$ and A is a $N \times M$ rectangular matrix. Similarly we can show, the RDM corresponding to second subsystem $\rho_2 = A^T A$. Obviously ρ_1 is a N-dimensional matrix, whereas ρ_2 is a M-dimensional matrix. The assumptions of

quantum chaos imply that A can be taken to have random independent entries, a member of the Laguerre ensemble. The RDMs then have the structure of correlation matrices [92], from where we directly use results for the density of states. Such matrices have also been studied since the early days of RMT as they have a non-negative spectrum [93]. The distribution of the eigenvalues of such matrices is known and thus this is the distribution of the eigenvalues of RDMs. The density of the eigenvalues of the RDM ρ_1 is given by

$$\begin{aligned} f(\lambda) &= \frac{NQ}{2\pi}\frac{\sqrt{(\lambda_{max}-\lambda)(\lambda-\lambda_{min})}}{\lambda} \\ \lambda_{min}^{max} &= \frac{1}{N}\left(1+\frac{1}{Q}\pm\frac{2}{\sqrt{Q}}\right), \end{aligned} \tag{4.11}$$

where $\lambda \in [\lambda_{min}, \lambda_{max}]$, $Q = M/N$ and $Nf(\lambda)d\lambda$ is the number of eigenvalues within λ to $\lambda + d\lambda$. This has been derived under the assumption that both M and N are large. Note that this predicts a range of eigenvalues for the RDMs that are of the order of $1/N$. For $Q \neq 1$, the eigenvalues of the RDMs are bounded away from the origin, while for $Q = 1$ there is a divergence at the origin. All of these predictions are seen to be borne out in numerical work with coupled tops. Fig. 4.3 shows how well the above formula fits the eigenvalue distribution of actual reduced density matrices. This figure also shows that the probability of getting an eigenvalue outside the range $[\lambda_{min}, \lambda_{max}]$ is indeed very small. The sum in S_V can be replaced by an integral over the density $f(\lambda)$:

$$S_V \sim -\int_{\lambda_{min}}^{\lambda_{max}} f(\lambda)\lambda \ln\lambda \, d\lambda \equiv \ln(\gamma N) \tag{4.12a}$$

The integral in γ can be evaluated to a generalized hypergeometric function and the final result is :

$$\gamma = \frac{Q}{Q+1}\exp\left[\frac{Q}{2(Q+1)^2}\,{}_3F_2\left\{1,1,\frac{3}{2};2,3;\frac{4Q}{(Q+1)^2}\right\}\right] \tag{4.12b}$$

When the two subsystems are of equal dimension, that is $Q = 1$, then above expression gives $\gamma = \exp(-0.5) \sim 0.6$ and so the corresponding von Neumann entropy is $\ln(0.6N)$. This is also the saturation value obtained in previous numerical work for the stationary states and time evolving states of a coupled standard map

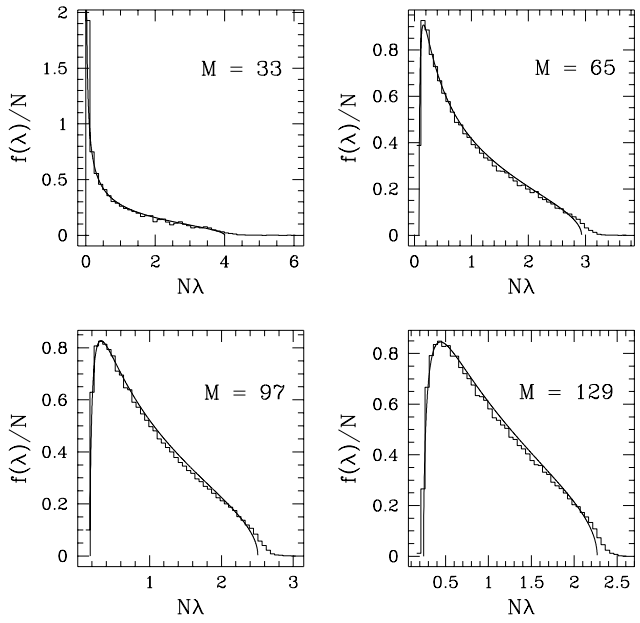

Figure 4.3: Distribution of the eigenvalues of the RDMs of coupled kicked tops, averaged over all the eigenstates ($N = 2j_1 + 1 = 33$). Solid curves corresponds to the theoretical distribution function Eq. (4.11).

[52], reflecting universality. In another extreme case, when the Hilbert space dimension of the second subsystem is very large compared to that of the first, that is $Q \gg 1$, then $\gamma \sim 1$ and hence the corresponding von Neumann entropy is $\ln(N)$. Therefore, the analytical formulation based on RMT is able to explain the saturation behavior of the von Neumann entropy or quantum entanglement very accurately.

Fig. 4.3 also compares the Eq. (4.12a) to both RMT simulations and kicked top results. We expect that the deviations of the quantum calculations are due to finite size effects. The presence of parity symmetry results in a somewhat smaller entanglement, as seen in this figure, a fact that needs further study. For time evolving states and stationary states of system without time reversal symmetry the RDMs are complex Hermitian matrices. The entanglement bounds discussed here are also valid for these cases as the entanglement depends only on the density of states of the RDMs. However, spectral fluctuations of the RDMs (such as *their* NNSD) corresponding to these states can be distinct. Indeed, in

the correlation matrix approach to atmospheric data, such a difference has been recently noted [94].

The linear entropy can also be derived as above, but using direct RMT results, without taking recourse to the distribution above, is also possible in this case. Thus we may write:

$$\mathrm{Tr}\rho^2 = \sum_{j,k=1}^{N} \sum_{\alpha,\beta=1}^{M} a_{j\alpha} a_{k\alpha} a_{k\beta} a_{j\beta} \tag{4.13}$$

Substituting RMT ensemble average values [95] of

$$\left\langle a_{j\alpha}^2 a_{j\beta}^2 \right\rangle = \left\langle a_{j\alpha}^2 a_{k\alpha}^2 \right\rangle = \frac{1}{MN(MN+2)}, \quad \left\langle a_{j\alpha}^4 \right\rangle = \frac{3}{MN(MN+2)}$$

$$\text{and} \quad \left\langle a_{j\alpha} a_{k\alpha} a_{k\beta} a_{j\beta} \right\rangle = 0,$$

where $j \neq k$ and $\alpha \neq \beta$ in the above expressions, we find that:

$$S_R = 1 - \mathrm{Tr}\rho_1^2 = 1 - \frac{M+N+1}{MN+2}. \tag{4.14}$$

When the dimension of the two subsystems are equal, that is $M = N$, then in the large N limit $S_R \sim 1 - 2/N$. This is the saturation value of the linear entropy approximately obtained in case of time evolving states of coupled kicked tops. Similarly, when the Hilbert space dimension of the second subsystem is very large compared to the dimension of first subsystem, that is $M \gg N$, $S_R \sim 1 - 1/N$. This is the maximum possible value of linear entropy.

4.5 Discussion on some Related Works

- A recent related work calculates the mean entanglement of pure states for the case $M = N$ by using a RMT model that allows specification of the joint probability distribution of the eigenvalues of the reduced density matrices [96].

- There is also an early work that studies the subsystem entropy for random pure states [97]. In this work, the author conjecture that the exact general

formula for the von Neumann entropy is

$$S_V = \sum_{k=M+1}^{NM} \frac{1}{k} - \frac{N-1}{2M}, \tag{4.15}$$

where $N \leq M$ are the Hilbert space dimensions of the participating subsystems. The above formula is valid for any arbitrary values of N and M. Later, three different proof have been given for the above conjecture [98].

In our derivation, we have used eigenvalue distribution of the reduced density matrices that is valid for large N and M limit. We have to take large N and M limit in Eq.(4.15) to compare it with our derivation. Let us first substitute $l = k - M$. In terms of this new discrete variable, Eq.(4.15) will become

$$\begin{aligned} S_V &= \sum_{l=1}^{M(N-1)} \frac{1}{l+M} - \frac{N-1}{2M} \\ &= \frac{1}{M} \sum_{l=1}^{M(N-1)} \frac{1}{1+\left(\frac{l}{M}\right)} - \frac{N-1}{2M}. \end{aligned} \tag{4.16}$$

Now we define $x \equiv l/M$ and $\delta \equiv 1/M$, where $\delta \to 0$ in large M limit. We can now convert the above sum approximately into an integral in the large M limit as,

$$\begin{aligned} S_V &\sim \lim_{\delta \to 0} \int_{\delta}^{N-1} \frac{dx}{1+x} - \frac{N}{2M} \quad \left[\text{taking} \frac{1}{2M} \simeq 0\right] \\ &= \ln N - \frac{1}{2Q} \quad \left[\text{where } Q = \frac{M}{N}\right] \\ &= \ln \gamma N \ \text{ where } \gamma = \exp\left(-\frac{1}{2Q}\right). \end{aligned} \tag{4.17}$$

For $M = N$ case, when $Q = 1$, the above result exactly coincides with our result $S_V = \ln \gamma N$ where $\gamma = \exp(-0.5) \simeq 0.6$ and for any arbitrary values of Q, the above result is very good approximation of Eq.(4.12b). In the asymptotic limit $Q \to \infty$, two results coincide at $\gamma = 1$.

- In Eq.(4.14), we have presented the saturation value of the linear entropy S_R corresponding to GOE case using RMT. Random matrix calculation of the purity $\mathcal{P}$ $\left(\text{where } S_R = 1 - \mathcal{P}\right)$ for Gaussian unitary ensemble (GUE) case

has already been derived in [99] and also very recently in [96]. According to these calculations, for GUE case,

$$S_R \,=\, 1 \,-\, \mathcal{P} \,=\, 1 \,-\, \frac{M+N}{MN+1}. \tag{4.18}$$

However for large M and N limit, GOE and GUE results coincide at

$$S_R \,\simeq\, 1 \,-\, \frac{M+N}{MN}. \tag{4.19}$$

The above value of S_R can also be obtained using the universal distribution of the eigenvalues of the RDM. This implies that the universal distributions of the eigenvalues of the RDM, which is valid for large M and N, are same for both GOE and GUE cases.

- We have seen that, for any arbitrary initial state, the strongly chaotic systems produce a large amount of entanglement, which is less than the maximum possible value. Here we show that a very simple system can produce maximally entangled state, but it is so for a very special initial unentangled state. We consider a pair of spin particles which are interacting with each other via spin-spin interaction operator

$$U(t) \,=\, \exp\left(-\,i\,\frac{\epsilon\,t}{j}\,J_{z_1}\,\otimes\,J_{z_2}\right). \tag{4.20}$$

and they have no individual dynamics. The above interaction operator is same as that we consider for the coupled kicked top case. Consider an initial product state of the form

$$|\psi(0)\,\rangle \,=\, \frac{1}{2j\,+\,1}\sum_{m_1,m_2=-j}^{+j}|m_1,\,m_2\,\rangle. \tag{4.21}$$

Now we evolve this state by the above evolution operator. At any arbitrary time t, we get

$$|\psi(t)\,\rangle \,=\, U(t)|\psi(0)\,\rangle \,=\, \frac{1}{2j\,+\,1}\sum_{m_1,m_2=-j}^{+j}\exp\left(-\,i\frac{\epsilon\,t}{j}\,m_1\,m_2\right)|m_1,\,m_2\,\rangle. \tag{4.22}$$

Now we determine the entanglement of the above state. The RDM corresponding to the first subsystem at time t is

$$\begin{aligned}\rho_1(t) &= \mathrm{Tr}_2\left(|\psi(t)\rangle\langle\psi(t)|\right) \\ &= \sum_{m_2=-j}^{+j}\langle m_2|\psi(t)\rangle\langle\psi(t)|m_2\rangle \\ &= \frac{1}{(2j+1)^2}\sum_{m_1,n_1=-j}^{+j}\sum_{m_2=-j}^{+j}\exp\left[i\frac{\epsilon\,t}{j}m_2\,(m_1-n_1)\right]|m_1\rangle\langle n_1|.\end{aligned} \tag{4.23}$$

Any element of the RDM $\rho_1(t)$ is

$$\begin{aligned}\left[\rho_1(t)\right]_{m_1n_1} &= \frac{1}{(2j+1)^2}\sum_{m_2=-j}^{+j}\exp\left[i\frac{\epsilon\,t}{j}m_2\,(n_1-m_1)\right] \\ &= \frac{1}{(2j+1)^2}\left[1+2\,\mathbb{R}e\sum_{m_2=1}^{j}\exp\left\{i\frac{\epsilon\,t}{j}m_2\,(n_1-m_1)\right\}\right].\end{aligned} \tag{4.24}$$

The diagonal elements of $\rho_1(t)$ are constants (they will not change with the time evolution) and they are all equal the inverse of the dimension of the Hilbert space of the first subsystem, i.e.,

$$\left[\rho_1(t)\right]_{m_1m_1} = \frac{1}{2j+1}. \tag{4.25}$$

After performing the sum present in Eq.(4.24), we get the off-diagonal elements of $\rho_1(t)$ as

$$\left[\rho_1(t)\right]_{m_1n_1} = \frac{1}{(2j+1)^2}\,\frac{\sin\left[\frac{\epsilon t}{2j}(2j+1)(m_1-n_1)\right]}{\sin\left[\frac{\epsilon t}{2j}(m_1-n_1)\right]}. \tag{4.26}$$

We find from the above expression that, when

$$\left(\frac{2j+1}{2j}\right)\epsilon\,t = k\,\pi \tag{4.27}$$

and k is any integer, the off-diagonal elements of $\rho_1(t)$ are all *zero*. That means, for any coupling strength ϵ, the RDM $\rho_1(t)$ is diagonal at the time

$$t = \left(\frac{2j}{2j+1}\right)\frac{k\pi}{\epsilon}. \tag{4.28}$$

We know that the diagonal elements of $\rho_1(t)$ are all constants and they are equal to $1/(2j+1)$. Therefore, the corresponding von Neumann entropy of the RDM $\left(\rho_1(t)\right)$ is equal to $\ln(2j+1)$. This is the maximum possible value of the entanglement. Let us now consider the time t is such that

$$\frac{\epsilon\, t}{2j} = l\pi \tag{4.29}$$

where l is any integer. For these time, the numerator and the denominator of Eq.(4.26) are both zero. Using L'Hospital's rule, we find the off-diagonal elements of $\rho_1(t)$ are all equal to $1/(2j+1)$, when

$$t = 2j\left(\frac{l\pi}{\epsilon}\right). \tag{4.30}$$

Only one eigenvalue of this RDM is nonzero, which is equal to unity, and the remaining all the eigenvalues are zero, and therefore the corresponding von Neumann entropy is also zero. This implies complete disentanglement.

So we observe that the above mentioned very simple system can create maximally entangled state starting from a special unentangled (product) initial state. However, the entanglement of this state does not remain fix at this maximum possible value for all the time, rather the entanglement comes down from that value and becomes completely unentangled state. This changes of the entanglement property goes on periodically with the time evolution.

Appendix

Derivation of the parameter γ

The density of the eigenvalues of the reduced density matrix (RDM) is given by

$$f(\lambda) = \frac{NQ}{2\pi}\frac{\sqrt{(\lambda_{\max}-\lambda)(\lambda-\lambda_{\min})}}{\lambda}$$

$$\lambda_{\min}^{\max} = \frac{1}{N}\left(1+\frac{1}{Q}\pm\frac{2}{\sqrt{Q}}\right)$$

where $\lambda \in [\lambda_{\min}, \lambda_{\max}]$ and $Q = M/N$. N is the Hilbert space dimension of the first subsystem and M is the same of the second subsystem. $N f(\lambda) d\lambda$ is the number of eigenvalues within λ to $\lambda + d\lambda$.

The von Neumann entropy S_V of the RDM is given by

$$S_V = -\mathrm{Tr}\, \rho_1 \ln \rho_1 = -\mathrm{Tr}\, \rho_2 \ln \rho_2,$$

where ρ_1 and ρ_2 are the RDM corresponding to first and second subsystem respectively. The nonzero eigenvalues $\{\lambda_i\}$ are same for both RDMs. Here we have assumed $N \geq M$. Therefore in the eigenbasis of the RDM, the von Neumann entropy is

$$S_V = -\sum_{i=1}^{N} \lambda_i \ln \lambda_i.$$

For large value of N, we can replace the above sum by an integral over the density $f(\lambda)$:

$$\begin{aligned} S_V &\sim -N \int_{\lambda_{\min}}^{\lambda_{\max}} f(\lambda)\, \lambda \ln \lambda\, d\lambda \\ &\sim -\frac{N^2 Q}{2\pi} \int_{\lambda_{\min}}^{\lambda_{\max}} \sqrt{(\lambda_{\max} - \lambda)(\lambda - \lambda_{\min})}\, \ln \lambda\, d\lambda. \end{aligned} \tag{4.31a}$$

Let us now define $x \equiv N\lambda$, and therefore $d\lambda = dx/N$. We have also defined $x_{\max} = N\lambda_{\max}$ and $x_{\min} = N\lambda_{\min}$. Substituting these in the above integral, we get

$$\begin{aligned} S_V &\sim -\frac{Q}{2\pi} \int_{x_{\min}}^{x_{\max}} \sqrt{(x_{\max} - x)(x - x_{\min})}\, \ln\left(\frac{x}{N}\right) dx, \\ &\sim -\frac{Q}{2\pi} I_1 + \frac{Q \ln N}{2\pi} I_2 \end{aligned} \tag{4.31b}$$

where

$$I_1 \equiv \int_{x_{\min}}^{x_{\max}} \sqrt{(x_{\max} - x)(x - x_{\min})}\, \ln x\, dx \tag{4.31c}$$

$$I_2 \equiv \int_{x_{\min}}^{x_{\max}} \sqrt{(x_{\max} - x)(x - x_{\min})}\, dx \tag{4.31d}$$

The integral I_2 is equal to $2\pi/Q$. Hence we get

$$S_V \sim \ln N - \frac{Q}{2\pi} I_1 \equiv \ln \gamma N \tag{4.31e}$$

$$\text{where } \gamma \equiv \exp\left(-\frac{Q}{2\pi} I_1\right). \tag{4.31f}$$

The integral I_1 in γ can be evaluated to a generalized hypergeometric function and the final result is

$$\gamma \,=\, \frac{Q}{Q\,+\,1}\,\exp\left[\frac{Q}{2\,(\,Q\,+\,1\,)^2}\,{}_3F_2\left(\,1,\,1,\,\frac{3}{2}\,;\,2,\,3\,;\,\frac{4\,Q}{(\,Q\,+\,1\,)^2}\,\right)\right]. \tag{4.31g}$$

Now we are going to derive the above expression. For the notational simplification, we define $x_{\min} \,\equiv\, a$, and $x_{\max} \,\equiv\, b$. Therefore,

$$I_1 \,\equiv\, \int_a^b \,\ln\,x\,\sqrt{(\,b\,-\,x\,)\,(\,x\,-\,a\,)}\,dx$$

We can write

$$(\,b\,-\,x\,)\,(\,x\,-\,a\,) \,=\, p^2\,-\,(\,x\,-\,q\,)^2$$

where

$$p \,\equiv\, \frac{b\,-\,a}{2} \,=\, \frac{2}{\sqrt{Q}}\,;\;\; q \,\equiv\, \frac{b\,+\,a}{2} \,=\, 1\,+\,\frac{1}{Q}.$$

Let us substitute

$$z \,=\, x\,-\,q,\;\;\text{therefore}\;\; dz \,=\, dx.$$

Moreover, when

$$x \,=\, a\,;\;\; z \,=\, a\,-\,q \,=\, -p$$

$$x \,=\, b\,;\;\; z \,=\, b\,-\,q \,=\, p.$$

Therefore

$$I_1 \,=\, \int_{-p}^{+p} \ln\,(\,z\,+\,q\,)\,\sqrt{p^2\,-\,z^2}\,\,dz.$$

Again substitute

$$z \,=\, p\,y,\;\;\text{therefore}\;\; dz \,=\, p\,dy,$$

then

$$z \,=\, -\,p \;\Rightarrow\; y \,=\, -\,1\;\;\text{and}\;\;\; z \,=\, p \;\Rightarrow\; y \,=\, 1.$$

Hence we get,

$$\begin{aligned} I_1 &= \int_{-1}^{+1} \ln(p\,y + q)\,\sqrt{p^2 - p^2\,y^2}\,p\,dy \\ &= p^2\,\ln p \int_{-1}^{+1} \sqrt{1 - y^2}\,dy + p^2 \int_{-1}^{+1} \ln\left(y + \frac{q}{p}\right)\sqrt{1 - y^2}\,dy \\ &= \frac{1}{2}\,\pi\,p^2 \ln p + p^2 \int_{-1}^{+1} \ln\left(y + \frac{q}{p}\right)\sqrt{1 - y^2}\,dy. \end{aligned} \tag{4.31h}$$

First term of the above expression, without the factor $\ln p$, is actually same as I_2. The value of this term is $\pi\,p^2/2$, and in terms of Q this is equal to $2\,\pi/Q$. Therefore this expression also verify our earlier statement that $I_2 = 2\,\pi/Q$. Let us now determine the integral of the above expression.

$$\begin{aligned} &\int_{-1}^{+1} \ln\left(y + \frac{q}{p}\right)\sqrt{1 - y^2}\,dy \\ &= \ln\alpha \int_{-1}^{+1} \sqrt{1 - y^2}\,dy + \int_{-1}^{+1} \ln\left(1 + \frac{y}{\alpha}\right)\sqrt{1 - y^2}\,dy \\ &= \frac{\pi}{2}\,\ln\alpha + \int_{-1}^{+1} \ln\left(1 + \frac{y}{\alpha}\right)\sqrt{1 - y^2}\,dy \end{aligned} \tag{4.31i}$$

where

$$\alpha \equiv \frac{q}{p} = \frac{b + a}{b - a} = \frac{1}{2}\sqrt{Q}\left(1 + \frac{1}{Q}\right).$$

Therefore

$$\begin{aligned} I_1 &= \frac{\pi}{2}\,p^2\,\ln\alpha\,p + p^2 \int_{-1}^{+1} \ln\left(1 + \frac{y}{\alpha}\right)\sqrt{1 - y^2}\,dy \\ &= \frac{\pi}{2}\,p^2\,\ln q + p^2\,J \end{aligned} \tag{4.31j}$$

where

$$J \equiv \int_{-1}^{+1} \ln\left(1 + \frac{y}{\alpha}\right)\sqrt{1 - y^2}\,dy.$$

Let us now expand the above logarithm :

$$\begin{aligned} \ln\left(1 + \frac{y}{\alpha}\right) &= \left(\frac{y}{\alpha}\right) - \frac{1}{2}\left(\frac{y}{\alpha}\right)^2 + \frac{1}{3}\left(\frac{y}{\alpha}\right)^3 - \frac{1}{4}\left(\frac{y}{\alpha}\right) + \cdots\cdots\cdots \\ &= \sum_{k=1}^{\infty} (-1)^{k+1}\,\frac{y^k}{k\,\alpha^k}. \end{aligned} \tag{4.31k}$$

Therefore

$$\begin{aligned} J &= \sum_{k=1}^{\infty} (-1)^{k+1} \frac{1}{k\alpha^k} \int_{-1}^{+1} y^k \sqrt{1 - y^2}\, dy \\ &= \sum_{l=1}^{\infty} (-1)^{2l+1} \frac{1}{l\alpha^{2l}} \int_0^1 y^{2l} \sqrt{1 - y^2}\, dy \\ &= \sum_{l=0}^{\infty} (-1)^{2l+3} \frac{1}{(l+1)\,\alpha^{2l+2}} \int_0^1 y^{2l+2} \sqrt{1 - y^2}\, dy. \end{aligned} \tag{4.31l}$$

Hence we have

$$J = -\sum_{l=0}^{\infty} \frac{1}{(l+1)\,\alpha^{2l+2}}\, j_l \tag{4.31m}$$

where

$$j_l \equiv \int_0^1 y^{2l+2} \sqrt{1 - y^2}\, dy.$$

Now substitute

$$y = \sin\phi\,; \quad \text{therefore} \quad dy = \cos\phi\, d\phi,$$

so when

$$y = 0\,; \quad \phi = 0, \quad \text{and} \quad y = 1\,; \quad \phi = \frac{\pi}{2}.$$

Therefore we have

$$j_l = \int_0^{\frac{\pi}{2}} \sin^{2l+2}\phi\, \cos^2\phi\, d\phi.$$

We know

$$\frac{1}{2}\beta(m, n) = \int_0^{\frac{\pi}{2}} \sin^{2m-1}\phi\, \cos^{2n-1}\phi\, d\phi,$$

where $\beta(m, n)$ is the Euler β-function. In our case

$$2m - 1 = 2l + 2 \quad \Rightarrow \quad m = \frac{2l+3}{2}$$

$$2n - 1 = 2 \quad \Rightarrow \quad n = \frac{3}{2}.$$

Hence

$$j_l \;=\; \frac{1}{2}\,\beta\left(\frac{2\,l\,+\,3}{2},\,\frac{3}{2}\right) \;=\; \frac{\Gamma\left(l\,+\,\frac{3}{2}\right)\,\Gamma\left(\frac{3}{2}\right)}{2\,\Gamma(\,l\,+\,3\,)}$$

where $\Gamma(\,)$ is the Euler Γ-function. So now we have

$$\begin{aligned}
J &= -\frac{1}{2\alpha^2}\sum_{l=0}^{\infty}\frac{\Gamma\left(l\,+\,\frac{3}{2}\right)\,\Gamma\left(\frac{3}{2}\right)}{2\,\alpha^{2\,l}\,(\,l\,+\,1\,)\,\Gamma(\,l\,+\,3\,)} \\
&= -\frac{\Gamma(3/2)}{2\,\alpha^2}\sum_{l=0}^{\infty}\frac{\Gamma\left(l\,+\,\frac{3}{2}\right)\,\Gamma(\,l\,+\,1\,)}{\Gamma(\,l\,+\,3\,)\,\Gamma(\,l\,+\,2\,)}\left(\frac{1}{\alpha^2}\right)^{l} \\
&= -\frac{\Gamma(3/2)}{2\,\alpha^2}\sum_{l=0}^{\infty}\frac{\Gamma\left(l+\frac{3}{2}\right)}{\Gamma(3/2)}\,\frac{\Gamma(\,3\,)}{\Gamma(\,l\,+\,3\,)}\,\frac{\Gamma(\,2\,)}{\Gamma(\,l\,+\,2\,)}\,\frac{\Gamma(\,l\,+\,1\,)}{\Gamma(\,1\,)}\,\frac{\Gamma(3/2)}{\Gamma(\,2\,)\,\Gamma(\,3\,)}\,\left(\frac{1}{\alpha^2}\right)^{l} \\
&= -\frac{[\,\Gamma(3/2)\,]^2}{2\,\alpha^2\,\Gamma(\,3\,)}\sum_{l=0}^{\infty}\frac{\Gamma\left(l+\frac{3}{2}\right)}{\Gamma(3/2)}\,\frac{\Gamma(\,3\,)}{\Gamma(\,l\,+\,3\,)}\,\frac{\Gamma(\,2\,)}{\Gamma(\,l\,+\,2\,)}\,\frac{\Gamma(\,l\,+\,1\,)}{\Gamma(\,1\,)}\,\frac{\Gamma(\,l\,+\,1\,)}{\Gamma(\,1\,)}\,\frac{1}{l\,!}\,\left(\frac{1}{\alpha^2}\right)^{l} \\
&= -\frac{\pi}{16\,\alpha^2}\,{}_3F_2\left(1,\,1,\,\frac{3}{2};\,2,\,3\,;\,\frac{1}{\alpha^2}\right). \qquad (4.31n)
\end{aligned}$$

Substituting above expression in Eq.(4.31j) we get,

$$I_1 \;=\; \frac{\pi\,p^2}{2}\,\ln\,q\;-\;\frac{\pi\,p^2}{16\,\alpha^2}\,{}_3F_2\left(1,\,1,\,\frac{3}{2};\,2,\,3\,;\,\frac{1}{\alpha^2}\right). \qquad (4.31o)$$

Now substituting the values of p, q and α, in terms of Q, in the above expression, we obtain

$$\begin{aligned}
I_1 &= \frac{2\,\pi}{Q}\left[\ln\left(1+\frac{1}{Q}\right)\;-\;\frac{1}{2\,Q\,\left(1\,+\,\frac{1}{Q}\right)^2}\,{}_3F_2\left(1,\,1,\,\frac{3}{2};\,2,\,3\,;\,\frac{4\,Q}{(\,Q\,+\,1\,)^2}\right)\right] \\
&= \frac{2\,\pi}{Q}\left[\ln\left(\frac{Q\,+\,1}{Q}\right)\;-\;\frac{Q}{2\,(\,Q\,+\,1\,)^2}\,{}_3F_2\left(1,\,1,\,\frac{3}{2};\,2,\,3\,;\,\frac{4\,Q}{(\,Q\,+\,1\,)^2}\right)\right]. \qquad (4.31p)
\end{aligned}$$

Therefore

$$\begin{aligned}
\gamma &= \exp\left(-\frac{Q}{2\,\pi}\,I_1\right) \\
&= \exp\left[\ln\left(\frac{Q}{Q\,+\,1}\right)\;+\;\frac{Q}{2\,(\,Q\,+\,1\,)^2}\,{}_3F_2\left(1,\,1,\,\frac{3}{2};\,2,\,3\,;\,\frac{4\,Q}{(\,Q\,+\,1\,)^2}\right)\right]. \qquad (4.31q)
\end{aligned}$$

Finally we get,

$$\gamma \;=\; \frac{Q}{Q\,+\,1}\,\exp\left[\frac{Q}{2\,(\,Q\,+\,1\,)^2}\,{}_3F_2\left(1,\,1,\,\frac{3}{2};\,2,\,3\,;\,\frac{4\,Q}{(\,Q\,+\,1\,)^2}\right)\right] \qquad (4.31r)$$

Chapter 5

Entanglement Production in Coupled Chaotic Systems

In Chapter 4 we discussed about the saturation of entanglement. This is a property of the coupled chaotic systems, whose participating subsystems are strongly chaotic and they are also coupled very strongly to each other. We have already explained this property from random matrix theory (RMT) in the Chapter 4. In the present chapter, we are interested to study the entanglement production for different underlying classical dynamics, like (nearly) regular, mixed and chaotic ; and also for different coupling strengths. For this we would like to observe the possible behaviors of a time evolving wavepacket on the phase space. The phase space of the coupled kicked tops is four dimensional $\left(S^2 \times S^2\right)$, therefore it is not possible to visualize the wavepacket dynamics on such a phase space. Hence we use reduced Husimi function, the Husimi function of the reduced density matrix (RDM), to visualize the possible behaviors of a wavepacket. Using the reduced Husimi function, we study a phase space based measure of the complexity of a state [100]. We find that, in general, the complexity of a time evolving state increases with the entanglement. We also study the same measure for a state evolving under the single (uncoupled) top time evolution operator. We find that a state of a kicked top, coupled to another top, has more access of the phase space than a state corresponding to a single top. Using RMT, we explain the behaviors of this measure for the strongly chaotic cases. As we have emphasized several times that we are mainly interested in understanding the effect of chaos

on the entanglement. Therefore, as a special case, we separately study the entanglement production in coupled strongly chaotic systems. Using RMT, we derive an analytical formula for the entanglement production for this special case. We apply this formula for the entanglement production in coupled kicked tops. This formula is applicable to large coupling strengths and is also valid for sufficiently long time, while a recently reported perturbative derivation deals only with the weak coupling strength.

We organize the present chapter in the following way. We begin with the discussion on the reduced Husimi function in Sec.5.1, then we discuss about the second moment of the Husimi function in Sec.5.2. In Sec.5.3, we present our detail numerical investigation of the entanglement production in coupled kicked tops corresponding to different underlying classical dynamics and different coupling strengths. In Sec. 5.4, we study decoherence in a kicked top which is entangled with another top. Finally we present the derivation of the analytical formula for the entanglement production in coupled strongly chaotic systems.

5.1 Reduced Husimi function

The reduced Husimi function is defined in a straightforward way. Let us consider a state $|\psi\rangle$ in the angular momentum basis $|m_1, m_2\rangle$, i.e.,

$$|\psi\rangle = \sum_{m_1,m_2} a_{m_1 m_2} |m_1, m_2\rangle. \tag{5.1}$$

The Husimi function of $|\psi\rangle$ is $\left|\langle z_1; z_2|\psi\rangle\right|^2$, where

$$\langle z_1; z_2|\psi\rangle = \sum_{m_1,m_2} a_{m_1 m_2} \langle z_1|m_1\rangle \langle z_2|m_2\rangle, \tag{5.2}$$

and $|z_i\rangle \equiv |\theta_i, \phi_i\rangle$ are the directed angular momentum states (atomic coherent states) presented in Eq.(4.4). We define reduced Husimi function corresponding

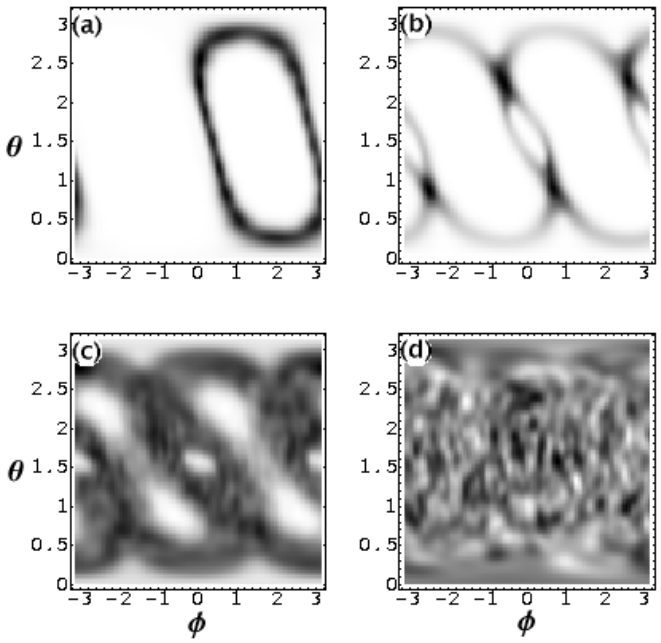

Figure 5.1: Reduced Husimi functions of the time evolving state, evolving under U_T, are presented corresponding to the time at which the entanglement production is saturated. (a) $k = 1.0$. The wavepacket is spread over the elliptic orbits. (b) $k = 2.0$. The wavepacket is spread over the separatrix. It is also showing strong localization at the unstable period-4 orbit. (c) $k = 3.0$. The wavepacket is spread over the whole chaotic region. (d) $k = 6.0$. At this parameter value, the phase space is mostly covered by the chaotic region, see Fig.3.2. Consequently, the wavepacket is spread over almost whole phase space.

to first subspace as,

$$\rho_{1H}(z_1) = \int_{z_2} \left| \langle\, z_1; z_2 | \psi \,\rangle \right|^2 d\mu(z_2), \tag{5.3}$$

where $d\mu(z_2)$ is the Haar measure :

$$d\mu(z_2) \;=\; \frac{2j+1}{4\pi} \sin\theta_2 \, d\theta_2 \, d\phi_2. \tag{5.4}$$

Since the phase space of a kicked top is the surface of a sphere of unit radius, the total phase space area is 4π. Therefore for the kicked top whose Hilbert space dimension is $N = 2j + 1$, volume of the Planck cell is $4\pi/(2j + 1)$. Hence the above mentioned Haar measure $d\mu(z)$ is equal to the number of Planck cells present in the infinitesimal area $dz \;=\; \sin\theta \, d\theta \, d\phi$. The integration of $d\mu(z)$ over whole phase space will give total number of Planck cells $N = 2j + 1$ present in the whole phase

space. We can also write the above expression, Eq. (5.3), as,

$$\rho_{1H}(\theta_1,\phi_1) = \left\langle \theta_1,\phi_1 \left| \frac{2j+1}{4\pi} \left[\int_{\theta_2}\int_{\phi_2} \left\langle\, \theta_2,\ \phi_2 \,|\, \psi \,\right\rangle \left\langle\, \psi \,|\, \theta_2,\ \phi_2 \,\right\rangle \sin\theta_2\, d\theta_2\, d\phi_2 \right] \right| \theta_1,\phi_1 \right\rangle . \tag{5.5}$$

The above integral can easily be identified as the partial trace of the density matrix $|\psi\,\rangle\,\langle\,\psi|$ over the second subspace, hence it gives the reduced density matrix (RDM) corresponding to the first subspace. Therefore,

$$\rho_{1H}(\theta_1,\phi_1) = \langle\theta_1,\phi_1|\rho_1|\theta_1,\phi_1\rangle, \tag{5.6}$$

where ρ_1 is the RDM of the first subspace. Therefore, the reduced Husimi function is just the Husimi function of the RDM. We can write $\rho_1 = \sum_{i=1}^{N} \lambda_i |e_i\rangle\langle e_i|$, where λ_i's are the eigenvalues of ρ_1 and $|e_i\rangle$'s are the corresponding eigenstates. These $|e_i\rangle$'s are also called Schmidt vectors. Therefore,

$$\rho_{1H}(\theta_1,\phi_1) = \sum_{i=1}^{N} \lambda_i \left|\langle\theta_1,\phi_1|e_i\rangle\right|^2. \tag{5.7}$$

Thus the reduced Husimi function can also be expressed as the weighted sum of the Husimi functions of the Schmidt vectors, where the weight factors are the eigenvalues of the RDM. In an identical fashion, we can define reduced Husimi function for the second subspace, and is given by,

$$\rho_{2H}(\theta_2,\phi_2) = \sum_{i=1}^{N} \lambda_i \left|\langle\theta_2,\phi_2|d_i\rangle\right|^2, \tag{5.8}$$

where $|d_i\,\rangle$'s are the Schmidt vectors of the second subspace.

In Fig.5.1, we show the reduced Husimi functions of the time evolving state evolving under the time evolution operator corresponding to coupled kicked tops.

5.2 Second moment of Husimi function

Reduced Husimi function technique is useful for the visualization of the behavior of the time evolving state on the phase space. Moreover, we want a quantitative phase space based measure of the complexity of any state to relate it with the entanglement. There already exists a good measure of that complexity based on

the Husimi distribution function, $\rho_H = \langle z\,|\rho|z\,\rangle$, called 'classical entropy' or Wehrl entropy [101] and that is given by

$$S(\rho_H) = \int d\mu(z)\,\rho_H \ln \rho_H \tag{5.9}$$

But it is difficult to determine the above quantity due to the presence of the logarithmic function. Therefore, following a recent proposal [100], we consider inverse of the 'second moment of the Husimi function' $W_2(\rho_H)$ as a measure complexity of quantum states. This measure is defined as,

$$W_2(\rho_H) = \frac{1}{M_2(\rho_H)} \tag{5.10}$$

$$\text{where } M_2(\rho_H) = \int d\mu(z)\,\rho_H^2. \tag{5.11}$$

The quantity W_2 actually represents the amount of the phase space effectively occupy by the Husimi function of the state ρ and its unit is the Planck's cell volume. We note that a similar kind of quantity, based on the Wigner function, has already been introduced and studied as a measure of the complexity of quantum states in phase space [102] many years ago.

We now define a quantity $\Delta N_{\text{eff}} \equiv W_2(\rho_H)/N$ as the fraction of the total number of Planck cells $(N = 2j + 1)$ occupied by the state ρ. Since the total number of Planck cells is also equal to the Hilbert space dimension, we can define ΔN_{eff} also as the rough measure of the fraction of the Hilbert space occupied by the above state. The above definitions of ΔN_{eff} are valid for the single top. For the coupled tops, phase space is 4-dimensional. Here we define ΔN_{eff} for any one of its subspaces. However, the only difference between these two cases is that ρ is a pure state for the single top whereas for the coupled tops, ρ is a mixed state. Here we study the time evolution of ΔN_{eff} for the single top and also for the coupled tops.

5.2.1 Single top

In the single top case, we again consider $SU(2)$ coherent state $\big|\psi(0)\big\rangle = |\theta_0, \phi_0\rangle$, which we have already defined in the previous chapter, Eq.(4.4), as the initial state. We construct this state at the point $(\theta_0,\, \phi_0) = (0.89,\, 0.63)$, and evolve it with

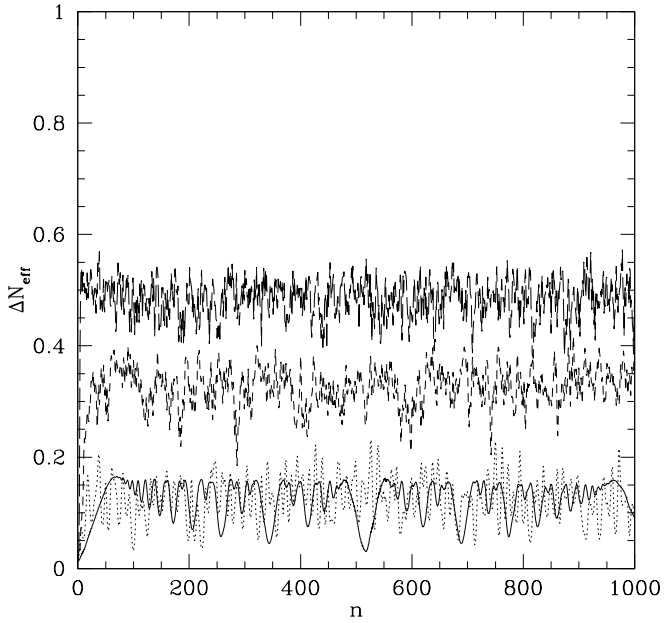

Figure 5.2: Evolution of $\Delta N_{\rm eff}$ is presented for the single top. For the nonchaotic cases ($k = 1.0$ and $k = 2.0$), denoted respectively by solid and dotted line, maximum value of $\Delta N_{\rm eff}$ is very less. That means, the time evolving state has very little access over the phase space. However, for chaotic cases ($k = 3.0$ and $k = 6.0$), maximum value of $\Delta N_{\rm eff}$ is also not large. For the strongly chaotic case ($k = 6.0$), the average value of the maxima is about 0.5.

repeated applications of the single top evolution operator U. The time evolution operator U, defined between two consecutive kicks, is given as

$$U = \exp\left(-i\frac{\pi}{2}J_y\right)\exp\left(-i\frac{k}{2j}J_z^2\right). \tag{5.12}$$

For the single top case, $\Delta N_{\rm eff}$ at time n is

$$\begin{aligned} \Delta N_{\rm eff} &= \frac{1}{(2j+1)M_2[|\psi(n)\rangle]} \\ \text{where} \quad M_2\Big[|\psi(n)\rangle\Big] &= \int d\mu(z)\big|\langle\, z|\psi(n)\,\rangle\big|^4 \end{aligned} \tag{5.13}$$

and $\big|\psi(n)\big\rangle = U^n\big|\psi(0)\big\rangle$. In Fig.5.2, we show time evolution of $\Delta N_{\rm eff}$ for different k-values. For $k = 1.0$, the initial state is inside the elliptic region, and therefore, time evolution of this state is governed by the elliptic orbits on which it is initially placed. Since the evolution of this state is in some sense trapped by the elliptic orbits, it has little or no access to many parts of the phase space. Consequently,

the maximum value of $\Delta N_{\rm eff}$ is very small. After reaching its maxima, there are many oscillations in the time evolution of $\Delta N_{\rm eff}$ due to partial and full revival of the time evolving state $\big|\psi(n)\big\rangle$. This particular issue of quantum revival of the time evolving state in such mixed systems warrant a separate study. Now at $k = 2.0$, the initial state is inside a stochastic layer present at the separatrix and consequently its dynamics is restricted by and large to be inside that stochastic layer. Naturally, for this case, the maxima of $\Delta N_{\rm eff}$ is also small. For $k = 3.0$, the phase space is of a truly mixed type, with a significant measure of chaotic orbits. In this case, the initial state is inside the chaotic region. Therefore, time evolution of this state is governed by the chaotic dynamics and this state has access over chaotic region of the phase space. Since the size of the chaotic region is large, hence the maxima of $\Delta N_{\rm eff}$ is also larger (~ 0.35). Finally, when $k = 6.0$, the phase space is mostly covered by the chaotic region, with few visible tiny regular islands. The time evolving state has now almost full access over the phase space. However, we observe that $\Delta N_{\rm eff}$ reaches maximum around 0.5 and then fluctuates around that value. This imply, for the strong chaotic case, the time evolving *pure* state has access over only half of the phase space. We explain this typical behavior of $\Delta N_{\rm eff}$ for strongly chaotic case by RMT in the following way.

In the angular momentum basis $\{|m\rangle\}$,

$$\begin{aligned} M_2\Big[\big|\psi(n)\big\rangle\Big] &= \sum_{i,k}\sum_{l,m} \big\langle\, i \,\big|\, \psi(n)\,\big\rangle \big\langle\, \psi(n) \,\big|\, k\,\big\rangle \big\langle\, l \,\big|\, \psi(n)\,\big\rangle \big\langle\, \psi(n) \,\big|\, m\,\big\rangle \\ &\times \int d\mu(z) \big\langle\, z \,\big|\, i\,\big\rangle \big\langle\, k \,\big|\, z\,\big\rangle \big\langle\, z \,\big|\, l\,\big\rangle \big\langle\, m \,\big|\, z\,\big\rangle. \end{aligned} \tag{5.14}$$

After performing the above integral, see *Appendix A*,

$$\begin{aligned} M_2\Big[\big|\psi(n)\big\rangle\Big] &= \sum_{i,k}\sum_{l,m} \big\langle\, i \,\big|\, \psi(n)\big\rangle \big\langle\, \psi(n) \,\big|\, k\big\rangle \big\langle\, l \,\big|\, \psi(n)\,\big\rangle \big\langle\, \psi(n) \,\big|\, m\,\big\rangle \\ &\times F\big(\,2j;\, i,k,l,m\,\big)\,\delta_{i+l,k+m} \end{aligned} \tag{5.15}$$

where

$$\begin{aligned} F\big(\,2j;\, i,k,l,m\,\big) &= \frac{2j+1}{(4j+1)!}\sqrt{\binom{2j}{j-i}\binom{2j}{j-k}\binom{2j}{j-l}\binom{2j}{j-m}} \\ &\times \big(\,2j-i-l\,\big)!\,\big(\,2j+i+l\,\big)! \end{aligned} \tag{5.16}$$

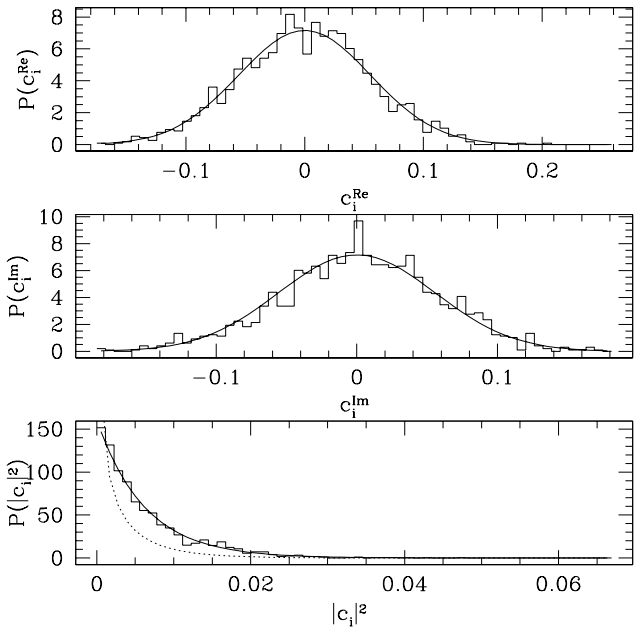

Figure 5.3: Distribution of the components of the time evolving state, evolving under strongly chaotic single top dynamics, is presented. Top and middle windows are showing that the real and the imaginary part of the components of the time evolving state are Gaussian distributed random numbers with *zero* mean and the variance is $1/\sqrt{N}$, where $N = 2j + 1$ is the Hilbert space dimension of the top. In this case $j = 80$. Bottom window is showing that the distribution of the square of the absolute values of the components of the time evolving state are exponentially distributed. This is a typical property of the components of a GUE distributed vector. Dotted line representing the GOE (Porter-Thomas) distribution.

Let us now assume, in the angular momentum basis,

$$\left|\,\psi(n)\,\right\rangle \;=\; \sum_{m} c_m \left|\,m\,\right\rangle. \tag{5.17}$$

In Fig.5.3, we present the distribution of the real and the imaginary part of the coefficients c_m. They are indeed Gaussian distributed random numbers. Moreover, in that figure, we also present the distribution of $|c_m|^2$. This figure shows that $|c_m|^2$ are exponentially distributed, which is a typical property of the elements of a Gaussian unitary ensemble (GUE) distributed random vector. Therefore, we can assume that the distribution of $\{c_m\}$ are GUE type. For GUE case, RMT average of a quantity identical to $M_2\Big[\left|\psi(n)\right\rangle\Big]$ has been calculated in a recent publication

[103], and according to that,

$$\Big\langle\, M_2\Big[\,|\psi(n)\rangle\Big]\,\Big\rangle \;=\; \frac{2}{N+1}, \quad \text{where} \;\; N \;=\; 2j+1, \tag{5.18}$$

where the angular bracket $\langle \ldots \rangle$ represents RMT averaged value. Using the above expression, we get

$$\langle\, \Delta N_{\text{eff}} \,\rangle \;=\; \frac{N+1}{2N} \;=\; \frac{1}{2}\left(1+\frac{1}{N}\right) \tag{5.19}$$

and for large N limit,

$$\langle\, \Delta N_{\text{eff}} \,\rangle \;\simeq\; 0.5. \tag{5.20}$$

This is the saturation value of ΔN_{eff}, which we observe in strongly chaotic case $k = 6.0$.

5.2.2 Coupled tops

In the last section, we have presented reduced Husimi function technique to visualize the behaviors of the time evolving state of the coupled tops on any one of its subspaces. However, to measure the complexity of this state in any one of its subspaces, we have to define ΔN_{eff} in a subspace. We define ΔN_{eff} for a given subspace as

$$\Delta N_{\text{eff}} \;=\; \frac{1}{(2j+1)M_2\big(\rho_{iH}\big)} \tag{5.21}$$

$$\text{where} \quad M_2\big(\rho_{iH}\big) \;=\; \int d\mu(z_i)\,\langle\, z_i \,|\, \rho_i \,|\, z_i \,\rangle, \tag{5.22}$$

and $i = 1, 2$ representing different subspaces. In Fig.5.4, we present the time evolution of the above mentioned ΔN_{eff} for different dynamics (different k values) and for different coupling strengths ϵ. When coupling strength is very weak ($\epsilon = 10^{-4}$), time evolution of ΔN_{eff} for different dynamics are practically identical to that which we have observed in the case of single tops. Therefore, for this coupling strength, effect of the dynamics of one top on the other top is very small and two tops are very close to two uncoupled systems. For other coupling strengths, the maxima of ΔN_{eff} has not changed much for the nonchaotic cases ($k = 1.0$, and $k = 2.0$). When $\epsilon = 10^{-3}$, for the chaotic cases ($k = 3.0$, and $k = 6.0$), ΔN_{eff} first

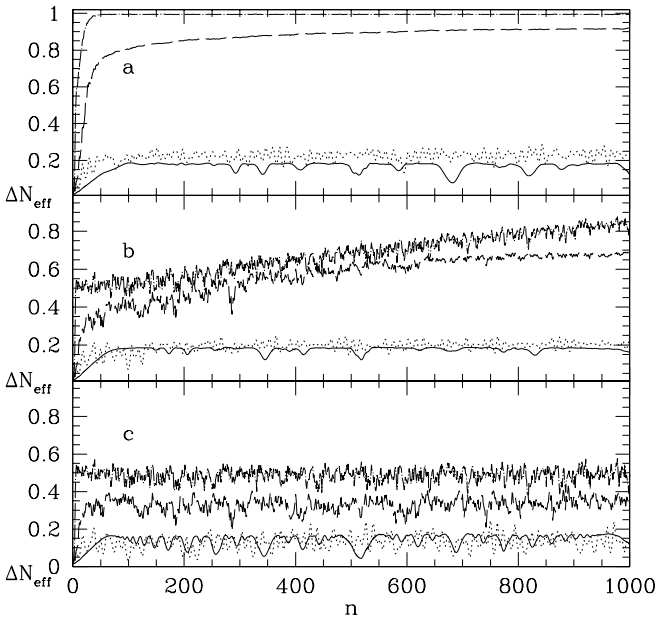

Figure 5.4: Evolution of $\Delta N_{\rm eff}$ corresponding to coupled kicked tops is presented. Solid lines and dotted lines are representing the results corresponding to nonchaotic cases ($k = 1.0$ and $k = 2.0$ respectively). Dashed lines are representing the mixed case ($k = 3.0$) and dash-dot lines are showing the results corresponding to strongly chaotic case ($k = 6.0$). The top window representing the results for the stronger coupling strength ($\epsilon = 10^{-2}$), middle window is showing the results for the intermediate coupling strength ($\epsilon = 10^{-3}$) and the bottom window is for the weak coupling case ($\epsilon = 10^{-4}$).

reaches the saturation value which is observed in the case of single tops and then it increases approximately linearly with time. However, for the stronger coupling ($\epsilon = 10^{-2}$), it is not possible to divide the time evolution of $\Delta N_{\rm eff}$, for the chaotic cases, into two distinct time regimes. In these cases, $\Delta N_{\rm eff}$ saturates at much higher values than the maxima of $\Delta N_{\rm eff}$ observed in single top. For the strongly chaotic case $k = 6.0$, $\Delta N_{\rm eff}$ saturates at a value that is very slightly less than unity. We again apply RMT to explain this saturation of $\Delta N_{\rm eff}$, which we now proceed to do.

In the angular momentum basis, second moment of the Husimi function of the reduced state, say for the first subsystem, at time n is,

$$M_2(\rho_{1H}) = \sum_{i,k} \sum_{l,m} (\rho_1)_{ik} (\rho_1)_{lm} \int d\mu(z_1) \langle z_1 | i \rangle \langle k | z_1 \rangle \langle z_1 | l \rangle \langle m | z_1 \rangle. \qquad (5.23)$$

After performing the above integral, we have,

$$M_2(\rho_{1H}) = \sum_{i,k}\sum_{l,m}(\rho_1)_{ik}\,(\rho_1)_{lm}F\left(2j;i,k,l,m\right)\delta_{i+l,k+m} \tag{5.24}$$

where $F\left(2j;i,k,l,m\right)$ has already been given in Eq. (5.16). If we write down above expression in the eigenbasis of the RDM ρ_1, then we have,

$$\begin{aligned}
M_2(\rho_{1H}) &= \sum_{\alpha,\beta=1}^{N}\lambda_\alpha\,\lambda_\beta\sum_{i,k}\sum_{l,m}\langle\, i\,|\,\phi_\alpha\,\rangle\langle\,\phi_\alpha\,|\,k\,\rangle\langle\,l\,|\,\phi_\beta\,\rangle\langle\,\phi_\beta\,|\,m\,\rangle \\
&\times\ F\left(2j;i,k,l,m\right)\delta_{i+l,k+m} \\
&= \Bigg[\sum_{\alpha}\lambda_\alpha^2\sum_{i,k}\sum_{l,m}\langle\, i\,|\,\phi_\alpha\,\rangle\langle\,\phi_\alpha\,|\,k\rangle\langle\,l\,|\,\phi_\alpha\,\rangle\langle\,\phi_\alpha\,|\,m\,\rangle \\
&\times\ F\left(2j;i,k,l,m\right)\delta_{i+l,k+m}\Bigg] \\
&+ \Bigg[\sum_{\substack{\alpha,\beta\\ \alpha\neq\beta}}\lambda_\alpha\,\lambda_\beta\sum_{i,k}\sum_{l,m}\langle\, i\,|\,\phi_\alpha\,\rangle\langle\phi_\alpha\,|\,k\,\rangle\langle\,l\,|\,\phi_\beta\,\rangle\langle\,\phi_\beta\,|\,m\rangle \\
&\times\ F\left(2j;i,k,l,m\right)\delta_{i+l,k+m}\Bigg] \\
&\equiv \sum_{\alpha}\lambda_\alpha^2 Q_{\alpha\alpha}^2+\sum_{\substack{\alpha,\beta\\ \alpha\neq\beta}}\lambda_\alpha\lambda_\beta Q_{\alpha\beta}^2
\end{aligned} \tag{5.25}$$

$$\text{where}\quad Q_{\alpha\alpha}^2 = \sum_{i,k}\sum_{l,m}\langle\, i\,|\,\phi_\alpha\rangle\langle\,\phi_\alpha\,|\,k\rangle\langle\,l\,|\,\phi_\alpha\,\rangle\langle\,\phi_\alpha\,|\,m\,\rangle\,F\left(2j;i,k,l,m\right), \tag{5.26}$$

$$\text{and}\quad Q_{\alpha\beta}^2 = \sum_{i,k}\sum_{l,m}\langle\, i\,|\,\phi_\alpha\,\rangle\langle\,\phi_\alpha|\,k\rangle\langle\,l\,|\,\phi_\beta\,\rangle\langle\,\phi_\beta\,|\,m\,\rangle\,F\left(2j;i,k,l,m\right), \tag{5.27}$$

where $\left\{\lambda_\alpha,\,|\phi_\alpha\rangle\right\}$ are the eigenvalues and the eigenvectors of the RDM ρ_1. In Fig.5.5, we present the distribution of the real and the imaginary part of the components of the eigenvectors $\left\{|\phi_\alpha\rangle\right\}$ of the RDM ρ_1. This figure shows that the real and the imaginary part of $\left\{|\phi_\alpha\rangle\right\}$ are Gaussian distributed random numbers. Moreover, Fig.5.5 also shows that the distribution of the absolute square of the components of $\{|\phi_\alpha\rangle\}$ is GUE type. Therefore, from the recent calculation [103], we can again use RMT average values of $Q_{\alpha\alpha}^2$ and $Q_{\alpha\beta}^2$ to get RMT average value of

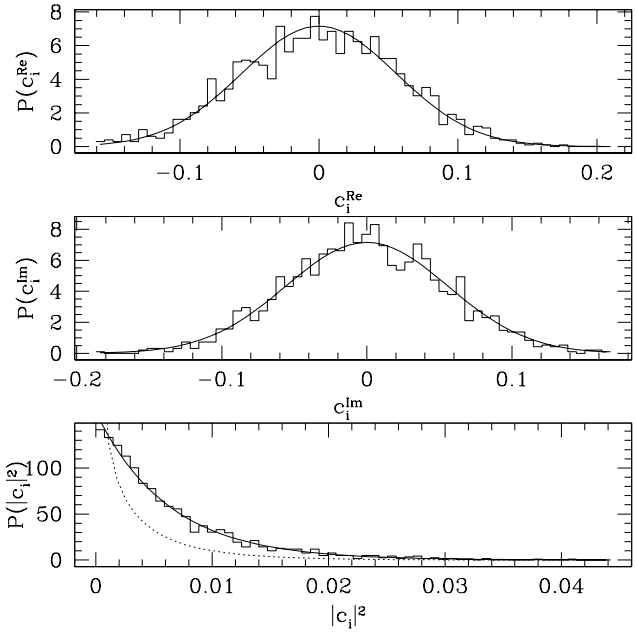

Figure 5.5: Distribution of the components of the eigenvectors of the RDM, corresponding to which entanglement production has reached the statistical bound. The top and the middle window shows that the real and the imaginary part of the components of these eigenvectors of RDM are Gaussian distributed random numbers with *zero* mean and the variance is $1/\sqrt{N}$. Here $N = 2j+1 = 161$. The bottom window is showing that the distribution of the absolute square of the eigenvectors of the RDM are exponentially distributed. Therefore, the eigenvectors of the RDM are GUE distributed. Dotted line representing the GOE (Porter-Thomas) distribution.

$M_2(\rho_{1H})$ as,

$$\begin{aligned}
\langle M_2(\rho_{1H})\rangle &= \frac{2}{N+1}\left\langle \sum_\alpha \lambda_\alpha^2 \right\rangle + \frac{1}{N+1}\left\langle \sum_{\substack{\alpha,\beta \\ \alpha\neq\beta}} \lambda_\alpha\lambda_\beta \right\rangle \\
&= \frac{2}{N+1}\left\langle \sum_\alpha \lambda_\alpha^2 \right\rangle + \frac{1}{N+1}\left[1 - \left\langle \sum_\alpha \lambda_\alpha^2 \right\rangle\right] \\
&= \frac{1}{N+1}\left(1 + \left\langle \sum_\alpha \lambda_\alpha^2 \right\rangle\right). \qquad (5.28)
\end{aligned}$$

We know from our derivation in previous chapter, Eq.(4.14),

$$\left\langle \sum_\alpha \lambda_\alpha^2 \right\rangle = \frac{2N+1}{N^2+2}. \qquad (5.29)$$

Therefore, we have,

$$\langle M_2(\rho_{1H})\rangle \;=\; \frac{1}{N+1}\left(1+\frac{2N+1}{N^2+2}\right). \tag{5.30}$$

Hence,

$$\begin{aligned}\langle \Delta N_{\rm eff}\rangle &= \frac{1}{N\langle M_2(\rho_{1H})\rangle}\\ &= \frac{(N+1)(N^2+2)}{N(N^2+2N+3)}.\end{aligned} \tag{5.31}$$

In the large N limit,

$$\langle \Delta N_{\rm eff}\rangle = \frac{N+1}{N+2} + \mathcal{O}\left(\frac{1}{N^2}\right) \lesssim 1.0. \tag{5.32}$$

This is the saturation value of $\Delta N_{\rm eff}$, which we observe in the strongly chaotic ($k = 6.0$) and strongly coupled ($\epsilon = 10^{-2}$) case. We emphasize that this is nearly twice that of pure states in a single top. Thus roughly speaking the effect of strongly coupling to another chaotic system doubles the phase space access of a state.

5.3 Entanglement production : Numerical results

In Fig.5.6, we present our results for the entanglement production in coupled kicked tops for the spin $j = 80$. As we go from top to bottom window, coupling strength is decreasing by a factor of *ten*. Top window corresponds to $\epsilon = 10^{-2}$, middle one is showing the results for $\epsilon = 10^{-3}$ and the bottom window corresponds to the case $\epsilon = 10^{-4}$. For each coupling strength, we study entanglement production for four different single top parameter values, whose corresponding classical phase space picture has already been shown in Fig.3.2.

5.3.1 Coupling $\epsilon = 10^{-2}$

Let us first discuss the case of stronger coupling $\epsilon = 10^{-2}$, whose results are presented in Fig.5.6(a). It shows that there exists a saturation of S_V for $k = 1.0$ and $k = 2.0$, which are much smaller than the saturation value corresponding to highly chaotic cases such as when $k = 6.0$. The saturation value of S_V for

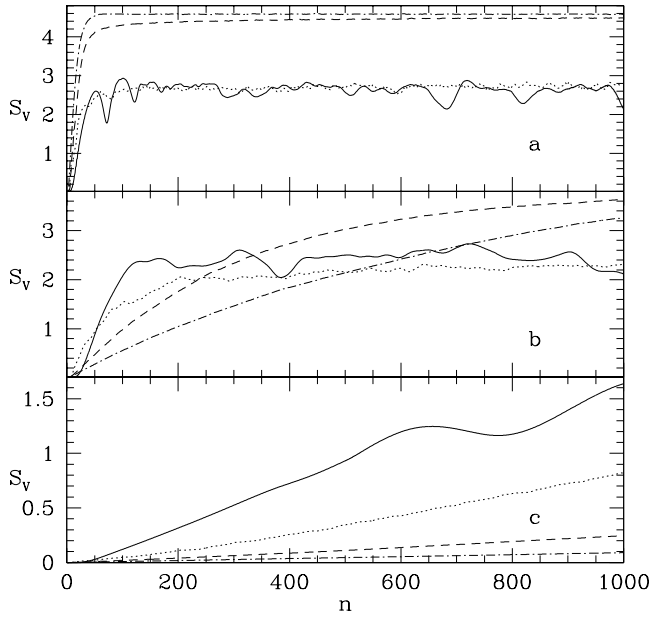

Figure 5.6: Time evolution of the von Neumann entropy in coupled kicked tops is presented for different coupling strengths and for different underlying classical dynamics. (a) $\epsilon = 10^{-2}$. (b) $\epsilon = 10^{-3}$. (c) $\epsilon = 10^{-4}$. Solid line represents $k = 1.0$, dotted line corresponds to $k = 2.0$, dashed line is for $k = 3.0$ and dash-dot line represents $k = 6.0$.

$k = 6.0$ is the statistical bound $S_V = \ln(N) - \frac{1}{2} \simeq 4.57$ (where $N = 161$), which can be understood from random matrix theory. See previous chapter. However for $k = 3.0$, corresponding to a mixed classical phase space, S_V is still less than the above mentioned saturation value, indicating the influence of the regular regions.

These two distinct behaviors of the entanglement saturation can be understood from the underlying classical dynamics. For $k = 1.0$, the initial unentangled state is the product of the coherent wavepacket placed inside the elliptic region [see Fig.3.2(a)] of each top. This initially unentangled state will become more and more entangled under the repeated application of the coupled top unitary operator U_T. Moreover, if one observes the evolution of the reduced Husimi function corresponding to each top, then it can be seen that the initially localized wavepacket starts moving along the classical elliptic orbits on which it was initially placed and simultaneously it also spreads along those orbits.

However, one can observe some initial oscillations in the entanglement production, which is due to the fact that the entanglement production is mostly

determined by the spreading of the wavepacket along θ-direction. As we know $\cos\theta_i = \lim_{j\to\infty}(J_{z_i}/j)$, therefore the spreading of the wavepacket along θ-direction determines how many eigenstates of J_{z_i}, which are also our basis states, are participating to construct the wavepacket. Larger amount of spreading of the wavepacket along the θ-direction causes greater number of basis states to participate in the wavepacket. Moreover, coupling between two tops is via interaction between J_{z_1} and J_{z_2}. Therefore, this interaction term will couple greater number of basis states and consequently leads to higher entanglement.

Initially, the spreading of the wavepacket sometimes may become parallel to the ϕ-direction and therefore its spreading along θ-direction become less. Consequently, one can observe a dip in the entanglement production. Finally, the wavepacket spreads all over the elliptic orbits and the entanglement production reaches its saturating maxima. In Fig.5.1(a), we show the reduced Husimi function of the wavepacket corresponding to the maxima (saturation) of the entanglement production. After reaching its saturation, there are again many dips in the entanglement production. These dips are also due to the small spreading of the wavepacket along θ-direction. However, the localization of the wavepacket along θ-direction are now happening due to fractional or full revival of the wavepacket. These revivals are actually the single top behaviors which persists even under the interaction with other top. The quantum revivals of the wavepacket are interesting phenomena of any quantum system and therefore it requires separate study, especially in this rather more complex setting.

At $k = 2.0$, the center of the initial coherent state was inside the separatrix. Therefore, in its time evolution, the spreading of the wavepacket was restricted to be inside the separatrix region. Finally, the wavepacket spread over the separatrix region, and the entanglement production arrived at its saturation. The corresponding reduced Husimi function has been shown in Fig.5.1(b). Moreover, the reduced Husimi function shows that even though the wavepacket has spread over the whole separatrix region, its spread is not uniform. The wavepacket is strongly localized at the unstable period-4 orbit. This strong localization of the wavepacket is also a single top behavior which may also warrant separate study.

At $k = 3.0$ and $k = 6.0$, the initial wavepackets were inside the chaotic region.

However, the saturation of the entanglement production are different for these two cases. This can be understood as the phase space of the kicked top is more mixed type for $k = 3.0$ than the case $k = 6.0$. Therefore, the size of the chaotic region is less for $k = 3.0$ than its size corresponding to $k = 6.0$. Consequently, the wavepacket can spread over less of the phase space for $k = 3.0$ than $k = 6.0$. In Fig.5.1(c), we have shown the spreading of the wavepacket corresponding to this case. At $k = 6.0$, since the phase space is almost fully chaotic, the wavepacket can spread over almost whole phase space. In Fig.5.1(d), we have shown reduced Husimi function corresponding to this strongly chaotic case.

5.3.2 Coupling $\epsilon = 10^{-3}$

Entanglement production corresponding to this coupling strength is presented in Fig.5.6(b). For the nonchaotic cases ($k = 1.0$ and $k = 2.0$), the saturation value of the entanglement production is less than the entanglement saturation observed in the stronger coupling case ($\epsilon = 10^{-2}$). For weaker coupling, the influence of one subsystem on the other subsystem becomes less, and the individual subsystems behave more like isolated quantum systems. Consequently, pure quantum effects play dominant role in the evolution of the wavepacket. In Fig.5.7, we show reduced Husimi function for $k = 1.0$ and $k = 2.0$ at the time $n = 384$ when the entanglement production saturated. For $k = 1.0$, the reduced Husimi function is showing that the wavepacket has spread over the elliptic orbits, but not uniformly. Now for $k = 2.0$, at the entanglement saturation, the wavepacket has spread as usual over the whole separatrix region. Moreover, it also shows localization at the same unstable period-4 orbit. However, the difference is that the wavepacket is now more localized at a particular periodic point of that period-4 orbit which was very close to the initial wavepacket. As we have seen in Fig. 5.4b, within our observational time ($n = 1000$), ΔN_{eff} has not reached any saturation value for the mixed and as well as for the chaotic cases. Moreover, for the strong chaos case, $k = 6.0$, the ΔN_{eff} was well short of unity even after the observational time and consequently the wavepacket has not got access over whole Hilbert space within this time of observation. Therefore, the entanglement production is well short of the known statistical bound $\ln(N) - \frac{1}{2}$.

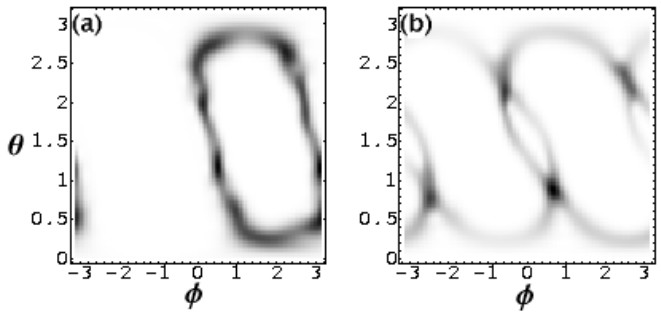

Figure 5.7: Reduced Husimi functions of the time evolving wavepacket are presented corresponding to the time $n = 384$ at which the entanglement production gets saturated. (a) $k = 1.0$. The wavepacket is spread over the elliptic orbits, but the spreading is not uniform. (b) $k = 2.0$. The wavepacket is spread over the separatrix and shows strong localization on the unstable period-4 orbit. Here $\epsilon = 10^{-3}$.

5.3.3 Coupling $\epsilon = 10^{-4}$

The entanglement production for this very weak coupling regime has been presented in Fig.5.6(c). The entanglement production for this weak coupling has recently been explained by perturbation theory [53]. However, the formula for the entanglement production presented in that work is not valid for arbitrarily long times. In Section 5.5 we present an approximate formula for the entanglement production in coupled strongly chaotic systems. This formula explains the entanglement production for the case $k = 6.0$. Here we have also observed that entanglement production is much larger for the nonchaotic cases than the chaotic cases. Rather, we can say that, for weakly coupled cases, the presence of chaos actually suppresses entanglement production.

5.4 Decoherence in coupled chaotic systems

When we consider observation at one of the two subsystems of any coupled quantum system, we see different consequences due to the entanglement between the two subsystems. One important effect is the disappearance of quantum interferences and this effect is known as decoherence. In case of coupled kicked tops, we are interested to study the decoherence in one top due to its interaction with the other top. More precisely, we are interested to observe the effect of different underlying classical dynamics on decoherence.

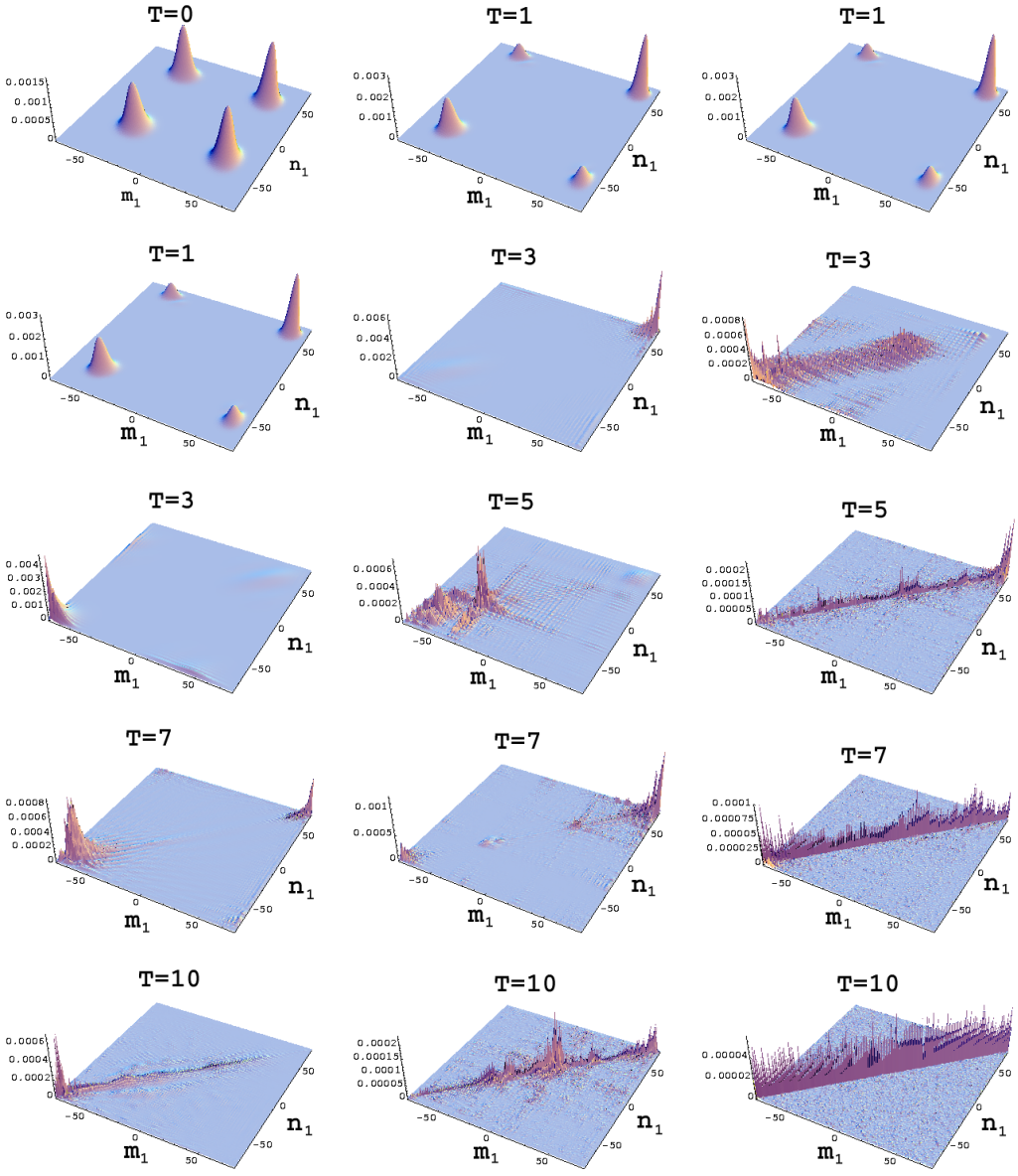

Figure 5.8: Time evolution of an initial reduced density matrix (corresponding to the first subsystem) shown in the left topmost figure. The left, middle and right panels correspond to the cases $k = 2.0$ (nearly regular), $k = 3.0$ (mixed) and $k = 6.0$ (chaotic) respectively. Coupling strength $\epsilon = 0.1$. $|\rho_1(m_1, n_1)|^2$ is plotted along z-axis.

In this study, as usual, we start with product states, but now the states corresponding to each subsystem are linear superposition of two coherent states placed at the two different points on the phase space. This choice of initial state gives rise to large off-diagonal parts in the initial reduced density matrix (RDM). See the left topmost figure of Fig.5.8. These off-diagonal parts are the consequence of the quantum interferences. We now study the evolution of the initial RDM under the coupled top time evolution operator for three different underlying classical dynamics, like nearly regular ($k = 2.0$), mixed ($k = 3.0$) and chaotic ($k = 6.0$) cases. Here we keep the coupling strength fixed at $\epsilon = 0.1$. Fig. 5.8 shows that the off-diagonal parts of the RDM for all the three different kind of dynamics are significantly reduced, even after one time step. For later times, the RDM corresponding to strongly chaotic case ($k = 6.0$) rapidly become diagonally dominant. That means, for the strongly chaotic case, decoherence rate is very fast. In contrast, for the mixed classical dynamics, the RDM also becomes diagonally dominant, but its rate is slower than the strongly chaotic case. For nearly regular case, the RDM also shows similar tendency to become effectively diagonal, but the rate is much slower than the other two cases. These results indicate that the decoherence rate becomes faster with the presence of stronger chaos in the system. Enhancement of the decoherence rate in the presence of chaos has also been observed in coupled standard map [52], however, in this reference, the dynamics of the individual subsystems were kept fixed and the decoherence was studied for two different coupling strengths. For the stronger coupling, when the over all system was chaotic, a faster decoherence rate was observed. In our study, we are not concern about the over all dynamics of the coupled systems. Therefore we keep the coupling strength constant and study the effect of the dynamics of the individual subsystems on the decoherence rate.

5.5 Entanglement production in coupled strongly chaotic systems : An analytical study

We have already mentioned that, due to the relatively simpler form, it is easier to derive an approximate formula for the time evolution of the linear entropy S_R.

Hence we now present an analytical formalism for the time evolution of S_R in coupled strongly chaotic systems.

Let us assume, the initial state is a product state, given as $|\psi(0)\rangle = |\phi_1(0)\rangle \otimes |\phi_2(0)\rangle$, where $|\phi_i(0)\rangle$'s are the states corresponding to individual subsystems. In general, the time evolution operator of a coupled system is of the form $U \equiv U_\epsilon U_0 = U_\epsilon(U_1 \otimes U_2)$, where U_ϵ is the coupling time evolution operator and U_i's are the time evolution operators of the individual subsystems. Furthermore, we assume

$$U_\epsilon = \exp(-i\epsilon H_{12}) \tag{5.33}$$

where $H_{12} = h^{(1)} \otimes h^{(2)}$, and the $h^{(i)}$ are Hermitian local operators. For simplicity, we derive our formalism in the eigenbasis of $h^{(i)}$'s, i.e., $h^{(i)}\big|e_\alpha^{(i)}\big\rangle = e_\alpha\big|e_\alpha^{(i)}\big\rangle$, where $\big\{e_\alpha^{(i)},\, \big|e_\alpha^{(i)}\big\rangle\big\}$ are the eigenvalues and the corresponding eigenvectors of $h^{(i)}$.

The one step operation of U on $|\psi(0)\rangle$ will give,

$$\big\langle e_\alpha^{(1)}, e_\beta^{(2)}\big|\psi(1)\big\rangle = \exp\left(-i\,\epsilon\, e_\alpha^{(1)}\, e_\beta^{(2)}\right)\big\langle e_\alpha^{(1)},\, e_\beta^{(2)}\big|\psi_0(1)\big\rangle, \tag{5.34}$$

where $|\psi(1)\rangle$ is the time evolving state of the full coupled system at time $n = 1$ and $|\psi_0(1)\rangle$ is the same for the uncoupled system. From the above expression, one can get the RDM corresponding to one subsystem by tracing over the other subsystem. The RDM corresponding to first subsystem is given by,

$$\begin{aligned}\big[\rho_1(1)\big]_{\alpha\beta} &= \left\langle e_\alpha^{(1)}\middle|\rho_1(1)\middle|e_\beta^{(1)}\right\rangle = \sum_\gamma \left\langle e_\alpha^{(1)},\, e_\gamma^{(2)}\middle|\psi(1)\right\rangle \left\langle\psi(1)\middle|e_\beta^{(1)},\, e_\gamma^{(2)}\right\rangle \\ &= \sum_\gamma \exp\left[-i\epsilon\left(e_\alpha^{(1)} - e_\beta^{(1)}\right)e_\gamma^{(2)}\right]\left\langle e_\alpha^{(1)},\, e_\gamma^{(2)}\middle|\psi_0(1)\right\rangle\left\langle\psi_0(1)\middle|e_\beta^{(1)},\, e_\gamma^{(2)}\right\rangle\end{aligned} \tag{5.35}$$

Here we now assume that, $|\psi_0(1)\rangle$ is a random vector. Consequently we can further assume that the components of $|\psi_0(1)\rangle$ are uncorrelated to the exponential term coming due to the coupling. Hence we have,

$$\begin{aligned}\big[\rho_1(1)\big]_{\alpha\beta} &\simeq \frac{1}{N}\sum_\gamma \left\langle e_\alpha^{(1)},\, e_\gamma^{(2)}\middle|\psi_0(1)\right\rangle\left\langle\psi_0(1)\middle|e_\beta^{(1)},\, e_\gamma^{(2)}\right\rangle \sum_\delta \exp\left[-i\epsilon\left(e_\alpha^{(1)} - e_\beta^{(1)}\right)e_\gamma^{(2)}\right] \\ &= \frac{1}{N}\big[\rho_{10}(1)\big]_{\alpha\beta}\sum_\gamma \exp\left[-i\epsilon\left(e_\alpha^{(1)} - e_\beta^{(1)}\right)e_\gamma^{(2)}\right],\end{aligned} \tag{5.36}$$

where N is the Hilbert space dimension of the first subsystem and ρ_{10} is the density matrix corresponding to the uncoupled top. If we proceed one more time

step, then at the time $n = 2$ we have,

$$\begin{aligned} \left[\rho_1(2)\right]_{\alpha\beta} &\simeq \frac{1}{N}\left|p(\epsilon)\right|^2 \left[\rho_{10}(2)\right]_{\alpha\beta} \sum_{\gamma} \exp\left[-i\epsilon\left(e_\alpha^{(1)} - e_\beta^{(1)}\right)\right] \\ \text{where} \quad p(\epsilon) &= \frac{1}{N^2}\sum_{\alpha,\beta} \exp\left(-i\epsilon\, e_\alpha^{(1)}\, e_\beta^{(2)}\right). \end{aligned} \tag{5.37}$$

If we use the above assumptions up to any arbitrary time n, we obtain

$$\left[\rho_1(n)\right]_{\alpha\beta} = \frac{1}{N}\left|p(\epsilon)\right|^{2(n-1)} \left[\rho_{10}(n)\right]_{\alpha\beta} \sum_{\gamma} \exp\left[-i\epsilon\left(e_\alpha^{(1)} - e_\beta^{(1)}\right) e_\gamma^{(2)}\right]. \tag{5.38}$$

From the above expression, it is straightforward to calculate Linear entropy and that is given as,

$$S_R(n) \simeq 1 - \frac{1}{N^4}|p(\epsilon)|^{4(n-1)} \sum_{\alpha,\beta}\sum_{\gamma,\delta} \exp\left[-i\epsilon\left(e_\alpha^{(1)} - e_\beta^{(1)}\right)\left(e_\gamma^{(2)} - e_\delta^{(2)}\right)\right]. \tag{5.39}$$

This is a general result, applicable to any coupled strongly chaotic systems of the form $U_\epsilon(U_1 \otimes U_2)$. Moreover, this result is valid for long time.

For the coupled kicked tops $H_{12} = J_{z_1} \otimes J_{z_2}/j$. Therefore, for this particular system, the above formula would become,

$$\begin{aligned} S_R(n) &\simeq 1 - \frac{1}{N^4} p(\epsilon)^{4(n-1)} \sum_{m_1,n_1=-j}^{+j} \sum_{m_2,n_2=-j}^{+j} \exp\left[-i\frac{\epsilon}{j}(m_1 - n_1)(m_2 - n_2)\right] \\ \text{where} \quad p(\epsilon) &= \frac{1}{N^2} \sum_{m_1,m_2=-j}^{+j} \exp\left(-i\frac{\epsilon}{j} m_1 m_2\right) \quad \text{and} \quad N = 2j+1 \end{aligned} \tag{5.40}$$

In large j-limit, we can substitute above sums by approximate integrals and then performing those integrals we get (for details, see *Appendix B*),

$$\begin{aligned} S_R(n) &\simeq 1 - p(\epsilon)^{4(n-1)} \left[\frac{2}{N}\left\{1 + \frac{\mathrm{Si}\big(2N\epsilon\big)}{\epsilon}\right\} - \left(\frac{1}{N\epsilon}\right)^2 \big\{1 - \cos\big(2N\epsilon\big) \right. \\ &+ \left. \mathrm{Ci}\big(2N\epsilon\big) - \ln\big(2N\epsilon\big) - \gamma\big\}\right] \end{aligned} \tag{5.41a}$$

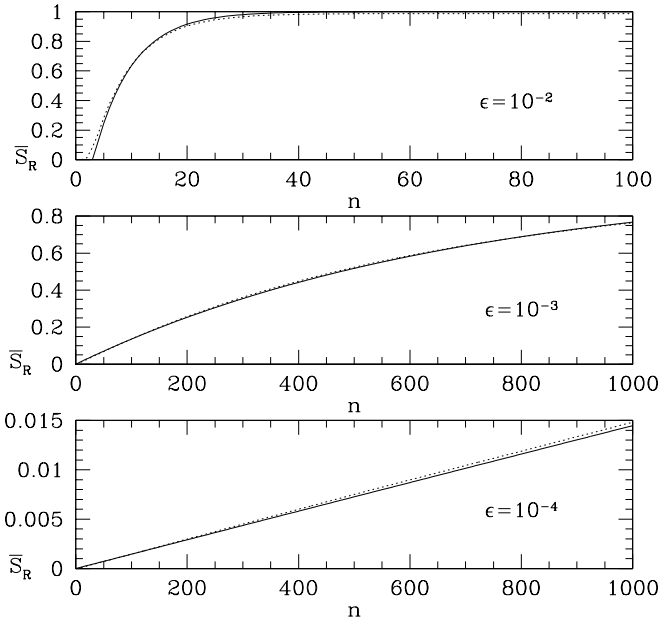

Figure 5.9: Evolution of the Linear entropy for the coupled strongly chaotic system is presented. The dotted line is the numerical results of the coupled kicked tops system. We choose $k = 6.0$ for the first top and $k = 6.1$ for the second top. The solid line is the theoretical estimation, given by Eq.(5.41).

where

$$p(\epsilon) \simeq \frac{2}{N}\left[1 + \frac{1}{\epsilon}\,\mathrm{Si}\left(\frac{N\epsilon}{2}\right)\right]. \tag{5.41b}$$

The functions Si and Ci are the standard *Sine-integral* and *Cos-integral* function, while $\gamma = 0.577216\ldots$ is the Euler constant. In the above derivation we have not assumed, unlike the perturbation theory [53], any particular order of magnitude of the coupling strength ϵ. Therefore, as we demonstrate below the above formula is applicable for non-perturbative coupling strengths as well.

In Fig.5.9, we show the numerical result of the Linear entropy (S_R) production in the coupled tops where the individual tops are strongly chaotic. Here we consider many initial coherent states at different parts of the phase space and present the Linear entropy production, averaged over all these initial states, with time. In all our previous calculations we only considered the entanglement production on coupling identical tops, therefore, permutation symmetry was present. As in the above derivation, we have not assumed any special symmetry property,

we break permutation symmetry by taking slightly non-identical tops with $k = 6.0$ for the first top and $k = 6.1$ for the second top.

Fig.5.9 demonstrates that our theoretical estimation, denoted by the solid curve, is not only valid for weak coupling case like $\epsilon = 10^{-4}$ but it also valid for sufficiently strong coupling cases like $\epsilon = 10^{-2}$. Moreover, this formula is applicable for very long times. If we consider weak coupling approximation, i.e., $j\epsilon \ll 1$, then the above formula will become approximately,

$$S_R(n) \simeq \frac{2\epsilon^2 j^2}{9}(n-1) + \mathcal{O}(\epsilon^3 j^3). \tag{5.42}$$

Therefore, at this weak coupling approximation, the entanglement production rate is $2\epsilon^2 j^2/9$, which has been calculated in a recent publication [53] by very different means.

Appendix A

Calculations of the integral present in Eq. (5.14) and Eq. (5.23) :

We know $\langle m|z\rangle = \langle m|\theta,\phi\rangle$ and using Eq.(4.4) from the previous chapter, the above mentioned integral becomes

$$\begin{aligned} & \frac{2j+1}{4\pi}\sqrt{\binom{2j}{j-i}\binom{2j}{j-k}\binom{2j}{j-l}\binom{2j}{j-m}} \\ \times \quad & \int_{\theta=0}^{\pi}\int_{\phi=-\pi}^{\pi}\left(1+\tan^2\frac{\theta}{2}\right)^{-4j}\left(\tan\frac{\theta}{2}\right)^{4j-i-k-l-m} \\ \times \quad & \exp\big[-i\phi\big\{(i+l)-(k+m)\big\}\big]\,\sin\theta d\theta d\phi. \end{aligned} \tag{5.43a}$$

After performing the ϕ-integral, we get

$$\begin{aligned} & (2j+1)\sqrt{\binom{2j}{j-i}\binom{2j}{j-k}\binom{2j}{j-l}\binom{2j}{j-m}}\;\delta_{i+l,k+m} \\ \times \quad & \int_{\theta=0}^{\pi}\left(\cos\frac{\theta}{2}\right)^{4j+2(i+l)+1}\left(\sin\frac{\theta}{2}\right)^{4j-2(i+l)+1}d\theta. \end{aligned} \tag{5.43b}$$

Substituting $\eta=\theta/2$, we get

$$\begin{aligned} & 2(2j+1)\sqrt{\binom{2j}{j-i}\binom{2j}{j-k}\binom{2j}{j-l}\binom{2j}{j-m}}\;\delta_{i+l,k+m} \\ \times \quad & \int_{\eta=0}^{\frac{\pi}{2}}(\sin\eta)^{4j-2(i+l)+1}(\cos\eta)^{4j+2(i+l)+1}d\eta. \end{aligned} \tag{5.43c}$$

The above integral is a β-integral, and therefore we get,

$$\begin{aligned} & (2j+1)\sqrt{\binom{2j}{j-i}\binom{2j}{j-k}\binom{2j}{j-l}\binom{2j}{j-m}} \\ \times \quad & \beta\big[\big\{(2j+1)-(i+l)\big\},\big\{(2j+1)+(i+l)\big\}\big]\,\delta_{i+l,k+m} \end{aligned} \tag{5.43d}$$

From the relation, $\beta(m,n)=\big[\Gamma(m)\Gamma(n)\big]/\Gamma(m+n)$, we get

$$\begin{aligned} & \frac{2j+1}{\Gamma(4j+2)}\sqrt{\binom{2j}{j-i}\binom{2j}{j-k}\binom{2j}{j-l}\binom{2j}{j-m}} \\ \times \quad & \Gamma\big\{(2j+1)-(i+l)\big\}\Gamma\big\{(2j+1)+(i+l)\big\}\,\delta_{i+l,k+m}. \end{aligned} \tag{5.43e}$$

We know that, for any integer m, $\Gamma(m+1) = m!$. Using this relation the above expression will be equal to Eq.(5.15) and Eq.(5.24).

Appendix B

Calculations of Eq. (5.41)

Let us first calculate the sum present in the expression of $p(\epsilon)$. That sum can be simplified in the following way.

$$\begin{aligned}
&\sum_{m_1,m_2=-j}^{+j} \exp\left(-i\frac{\epsilon}{j}m_1 m_2\right) \\
&= \frac{2N-1}{N^2} + \frac{1}{N^2}\left[\sum_{m_1=1}^{j}\sum_{m_2=1}^{j}\exp\left(-i\frac{\epsilon}{j}m_1 m_2\right) + \sum_{m_1=-j}^{-1}\sum_{m_2=1}^{j}\exp\left(-i\frac{\epsilon}{j}m_1\, m_2\right)\right. \\
&+ \left.\sum_{m_1=1}^{j}\sum_{m_2=-j}^{-1}\exp\left(-i\frac{\epsilon}{j}m_1 m_2\right) + \sum_{m_1=-j}^{-1}\sum_{m_2=-j}^{-1}\exp\left(-i\frac{\epsilon}{j}m_1\, m_2\right)\right] \\
&= \frac{2N-1}{N^2} + \frac{2}{N^2}\left[\sum_{m_1,m_2=1}^{j}\exp\left(i\frac{\epsilon}{j}m_1\, m_2\right) + \sum_{m_1,m_2=1}^{j}\exp\left(-i\frac{\epsilon}{j}m_1\, m_2\right)\right] \\
&= \frac{2N-1}{N^2} + \frac{4}{N^2}\,\mathbb{R}e\sum_{m_1,m_2=1}^{j}\exp\left(i\frac{\epsilon}{j}m_1\, m_2\right), \qquad \text{(5.44a)}
\end{aligned}$$

where 'Re' denoting the real part. Now we define $x \equiv m_1/j$, $y \equiv m_2/j$ and $\delta \equiv 1/j$, where $\delta \to 0$ in large j limit. We can convert the above sum into an integral in the large j-limit as,

$$\begin{aligned}
&j^2 \lim_{\delta\to 0}\int_{x=\delta}^{1}\int_{y=\delta}^{1} dx\, dy\, \cos\big(j\,\epsilon\, x\, y\big) \\
&= j^2 \lim_{\delta\to 0}\int_{x=\delta}^{1}\frac{\sin\big(j\,\epsilon\, x\big)}{j\,\epsilon\, x}\, dx \\
&= \frac{j}{\epsilon}\,\mathrm{Si}(j\,\epsilon) \qquad \text{(5.44b)}
\end{aligned}$$

In the large j-limit, $N = 2j+1 \simeq 2j$, therefore

$$p(\epsilon) \simeq \frac{2N-1}{N^2} + \frac{2}{N\epsilon}\,\mathrm{Si}\left(\frac{N\epsilon}{2}\right). \qquad \text{(5.44c)}$$

If we neglect N^{-2} term, then we get,

$$p(\epsilon) \simeq \frac{2}{N}\left[1+\frac{\mathrm{Si}\left(\frac{N\epsilon}{2}\right)}{\epsilon}\right]. \tag{5.44d}$$

Let us now calculate the bigger sum [see Eq. (5.40)]. If we define $l_1 \equiv m_1 - n_1$ and $l_2 \equiv m_2 - n_2$, then this sum will become,

$$\begin{aligned}
&\sum_{l_1,l_2=-M}^{+M}\left(N-|l_1|\right)\left(N-|l_2|\right)\exp\left(-i\frac{\epsilon}{j}l_1\,l_2\right)\;;\;\; M=2j=N-1\\
&= 2N\sum_{l_1=-M}^{+M}\left(N-|l_1|\right)+\sum_{\substack{l_1=-M\\ l_1\neq 0}}^{+M}\sum_{\substack{l_2=-M\\ l_2\neq 0}}^{+M}\left(N-|l_1|\right)\left(N-|l_2|\right)\exp\left(-i\frac{\epsilon}{j}l_1\,l_2\right)\\
&= 4N^2M+4\,\mathrm{Re}\sum_{l_1,l_2=1}^{M}\left(N-l_1\right)\left(N-l_2\right)\exp\left(i\frac{\epsilon}{j}l_1l_2\right)\\
&= 4N^2M+4\,N^2\,\mathrm{Re}\sum_{l_1,l_2=1}^{M}\exp\left(i\frac{\epsilon}{j}l_1l_2\right)-8\,N\,\mathrm{Re}\sum_{l_1,l_2=1}^{M}l_1\exp\left(i\frac{\epsilon}{j}l_1\,l_2\right)\\
&+ 4\,\mathrm{Re}\sum_{l_1,l_2=1}^{M}i\,l_1\,l_2\exp\left(i\frac{\epsilon}{j}l_1\,l_2\right)
\end{aligned} \tag{5.44e}$$

We can write the first sum of the above expression as,

$$\sum_{l_1,l_2=1}^{M}\exp\left(i\frac{\epsilon}{j}l_1\,l_2\right)=\sum_{l_1,l_2=1}^{M}\exp\left(i\frac{2\epsilon}{M}l_1\,l_2\right). \tag{5.44f}$$

This sum is similar to the sum which we have calculated to derive $p(\epsilon)$, see Eq. (5.44a). Therefore, using this previous result, we get the above sum as,

$$\sum_{l_1,l_2=1}^{M}\exp\left(i\frac{\epsilon}{j}l_1\,l_2\right)\simeq\frac{M}{2\epsilon}\,\mathrm{Si}\left(2\,M\,\epsilon\right). \tag{5.44g}$$

Now

$$\begin{aligned}
\text{Second sum} &= \mathrm{Re}\sum_{l_1,l_2=1}^{M}l_1\exp\left(i\frac{\epsilon}{j}\,l_1\,l_2\right)\\
&\simeq M^3\lim_{\delta\to 0}\int_{x=\delta}^{1}\int_{y=\delta}^{1}x\,\cos\left(2M\epsilon xy\right)dx\,dy\\
&\simeq \frac{M^2}{2\epsilon}\int_0^1\sin\left(2M\epsilon x\right)dx\\
&\simeq \frac{M}{4\epsilon^2}\left[1-\cos\left(2M\epsilon\right)\right]
\end{aligned} \tag{5.44h}$$

$$\begin{aligned}
\text{Third sum} &= \text{Re} \sum_{l_1,l_2=1}^{M} l_1\, l_2\, \exp\left(i\frac{\epsilon}{j} l_1\, l_2\right) \\
&\simeq M^4 \lim_{\delta\to 0} \int_{x=\delta}^{1} \int_{y=\delta}^{1} dx\, dy xy\, \cos\big(2M\epsilon xy\big) \\
&\simeq \frac{M^3}{2\epsilon} \lim_{\delta\to 0} \left[\int_{x=\delta}^{1} \sin\big(2M\epsilon x\big) dx \,+\, \int_{x=\delta}^{1} \frac{\cos\big(2M\epsilon x\big)-1}{2M\epsilon x}\, dx\right] \\
&\simeq \frac{M^2}{4\epsilon^2}\left[1-\cos(2M\epsilon) \,+\, \text{Ci}\big(2M\epsilon\big) \,-\, \ln\big(2M\epsilon\big) \,-\, \gamma\right]. \qquad \text{(5.44i)}
\end{aligned}$$

For large j-limit, $M \simeq N$ and therefore substituting above results in Eq.(5.44e), we will arrive at Eq.(5.41).

Chapter 6

Mixed state entanglement and Operator entanglement

In the previous two chapters we have extensively discussed the effect of underlying classical dynamics on the entanglement, where we only considered the entanglement production for the initially pure state. That means, we assumed that the initial state of the coupled quantum system is completely known. But this is not the general scenario, in realistic situation, most of the time it is not possible to know the state of a quantum system completely. In this situation, the state of a quantum system is a mixed state, which arises from some ensemble $\{ p_i, |\psi_i \rangle \}$ of pure states. A mixed state can only be expressed in terms of the density matrix like $\rho = \sum_i p_i |\psi_i \rangle \langle \psi_i|$, where $\sum_i p_i = 1$. The probability for the system being in the state $|\psi_i \rangle$ is p_i. These probabilities have no quantum mechanical origin, rather they come from our ignorance into the quantum state.

A natural consequence and also a generalization of the previous two chapters is to study the entanglement production for the initially mixed states. The von Neumann entropy and the linear entropy are the good measures of entanglement for the pure bipartite states. For a mixed state, the entanglement can be measured as the average entanglement of its pure state decomposition. But there exists an infinite number of such decompositions, and therefore we have to minimize over this huge set. This procedure is really a nontrivial task. However, *Hill and Wootters* have shown that a new quantity called *concurrence* can be a measure of the mixed state entanglement of two two-level (qubits) systems

[104]. But for any arbitrary dimensional case, there is no consensus about the measure of the entanglement. This is a major obstacle to study the mixed state entanglement. Recently *Werner and Vidal*, following Peres' criterion of separability [105], have proposed a computable measure of entanglement called *Log-negativity* [74]. This measure is valid for the large Hilbert space dimension, and therefore we can use this measure to investigate the influence of the underlying classical dynamics on the entanglement of the mixed states. However, there is a problem with this measure which directly comes from the Peres' criterion. It has been shown that Peres' criterion is not applicable for a special kind of entangled states, called bound entangled state [106]. Since the log-negativity measure is based on Peres' criterion, therefore this is not a bonafide measure for the bound entangled states. Except this drawback, the log-negativity measure is applicable for any other entangled states. In our numerical study of the mixed state entanglement, we consider the entanglement production for the two different types of initial mixed states. In one case, we consider a product of mixed and pure state, i.e. the initial state corresponding to the first subsystem is mixed type, whereas the initial state corresponding to the other subsystem is the pure state. In another case, we consider a product of two mixed states corresponding to each subsystem, like $\rho(0) = \rho_1(0) \otimes \rho_2(0)$, as the initial state. These two initial states are the simplest type of mixed states which one can think of. We choose these states because our previous knowledge of pure state entanglement may be useful to understand the mixed state entanglement production.

As we have mentioned above that the subsystems entropies like the von Neumann entropy or the linear entropy are *no more* the measures for the mixed state entanglement. However, they are still very important quantities, which require elaborate study. Therefore, we also study the von Neumann entropy as well as the linear entropy of the subsystems. We observe that the behaviors of the subsystems entropies are qualitatively similar to the Log-Negativity measure of the entanglement. Even both of them show a statistical upper bounds (saturation) for the strongly chaotic and strongly coupled cases. These results indicate that even though the subsystems entropies are not the measures of mixed state entanglement, but they may have some relations with the entanglement. Using random

matrix theory, we estimate the saturation value of the subsystems linear entropy. Here we mention that, unlike the pure state case, the saturation value of the subsystems entropies depends on the initial subsystem entropies.

We know that, entanglement implies a quantum action or a quantum process by which disentangled or product states are transformed into entangled ones. Any quantum transformation can always be described by operators. Therefore, one may consider entanglement produced by the different operators. Let us assume, a given operator acting on a product state, transform the product state into an entangled state. This given operator is referred as *entangling operator*. Of course, not each operator is entangling, or neither their entangling powers are same. One given operator, operating on a product state, can create more entanglement than the another given operator. As an example, a unitary operator corresponding to a classically chaotic system, in general, produces more entanglement than a unitary operator corresponding to a regular system.

In this chapter we also study the entangling power of a given unitary time evolution operator corresponding to the coupled kicked tops, for different underlying classical dynamics of the individual tops and for different coupling strengths between the two tops. Recently Nielsen et al [107] have proposed a measure, based on a method called *Operator Schmidt decomposition*, of the entangling power of a given unitary operator. However, following a technique called *matrix reshaping*, it can be shown that the operator Schmidt decomposition and the state Schmidt decomposition are basically equivalent. Our numerical studies show that qualitatively operator entanglement has similar properties as the pure state entanglement. Few common properties are (1) the operator entanglement, in general, support '*more chaos more entanglement*' view ; (2) there exists saturation of operator entanglement for strongly chaotic and strongly coupled cases, and these saturation values are again in the form of $\ln(\gamma d)$ where d is the dimension of the *operator Hilbert space* (Hilbert-Schmidt space) ; (3) in case of weakly coupled tops, the operator entanglement corresponding to the regular dynamics are more than the chaotic cases, at least within our observational time.

6.1 Mixed state entanglement

6.1.1 Measure of the mixed state entanglement

Peres' separability criterion for density matrices [105] :

A quantum system consisting of two subsystems is separable, if its density matrix ρ can be expressed as

$$\rho = \sum_i p_i \, \rho_i^{(A)} \otimes \rho_i^{(B)}, \tag{6.1}$$

where the positive weight factors p_i satisfy $\sum_i p_i = 1$, $\rho_i^{(A)}$ and $\rho_i^{(B)}$ being density matrices for the two subsystems. It will be easier to understand the derivation of the separability criterion by writing the density matrix elements explicitly with all the indices. Hence Eq.(6.1) becomes

$$\rho_{m\mu,n\nu} = \sum_i p_i \left(\rho_i^{(A)}\right)_{m\,n} \left(\rho_i^{(B)}\right)_{\mu\,\nu}, \tag{6.2}$$

where Latin indices refer to the first subsystem and Greek indices refer to the second one. In general, the dimensions of the subsystems are unequal.

Let us now construct a new matrix σ from the above density matrix ρ as

$$\sigma_{m\,\mu,n\,\nu} \equiv \rho_{m\nu,n\mu}. \tag{6.3}$$

This expression shows that the Greek indices of ρ have been transposed, but not the Latin ones. This operation is called *partial transpose*. This is definitely not a unitary transformation, however the σ matrix is still Hermitian. If the density matrix ρ is separable, then Eq.(6.1) is valid, and therefore we can write the σ matrix as

$$\sigma = \sum_i p_i \, \rho_i^{(A)} \otimes \left(\rho_i^{(B)}\right)^T. \tag{6.4}$$

The transposed matrices $\left(\rho_i^{(B)}\right)^T = \left(\rho_i^{(B)}\right)^*$ are nonnegative matrices with unit trace, and hence they are legitimate density matrices. It follows that none of the eigenvalues of σ (partially transposed ρ) is negative. This necessary condition for the separability of ρ is the Peres' separability criterion for the density matrices.

Log-Negativity. A computable measure of entanglement / A quantitative version of Peres' criterion [74] :

Before going into the detail discussion of this measure, let us first set our notations. If we perform partial transpose over first (second) subsystem, then the resultant matrix will be denoted by ρ^{T_A} $\left(\rho^{T_B}\right)$. More explicitly, if ρ satisfies Eq. (6.1), then

$$\rho^{T_A} \equiv \sum_i p_i \left(\rho_i^{(A)}\right)^T \otimes \rho_i^{(B)} \tag{6.5a}$$

$$\text{and } \rho^{T_B} \equiv \sum_i p_i \rho_i^{(A)} \otimes \left(\rho_i^{(B)}\right)^T. \tag{6.5b}$$

Vidal and Werner [74] have proposed a computable measure of the entanglement based on the trace norm of the partial transpose ρ^{T_A} (or ρ^{T_B}) of the bipartite mixed state ρ. It essentially measures the degree to which ρ^{T_A} fails to be positive, and therefore it can be considered as a quantitative version of Peres' criterion.

The trace norm of any operator A is $||A|| \equiv \text{Tr}\sqrt{AA^\dagger}$. If A is Hermitian, then $||A||$ is the sum of the absolute value of the eigenvalues of A. All the eigenvalues of the density matrix ρ are positive and therefore $||\rho|| = \text{Tr}\,\rho = 1$. ρ^{T_A} also satisfies $\text{Tr}\rho^{T_A} = 1$, but if ρ is an entangled state, then ρ^{T_A} may have negative eigenvalues. Vidal and Werner have actually proposed two interdependent measures. The first one is the *negativity* $N(\rho)$, which actually measures the sum of the absolute value of the negative eigenvalues of ρ^{T_A} and it vanishes for unentangled states. After some simple algebraic manipulations, we get

$$N(\rho) = \frac{||\rho^{T_A}|| - 1}{2}. \tag{6.6}$$

The second measure, Log-Negativity is defined as

$$E_N(\rho) = \ln ||\rho^{T_A}||. \tag{6.7}$$

In terms of eigenvalues of ρ

$$N(\rho) = \frac{1}{2}\left(\sum_{i=1}^{N} |\lambda_i| - 1\right) \tag{6.8a}$$

$$E_N(\rho) = \ln\left(\sum_{i=1}^{N} |\lambda_i|\right) \tag{6.8b}$$

where N is the dimension of ρ.

6.1.2 Numerical results

Initial mixed states :

We consider two different types of initial unentangled mixed states.
(1) A product of mixed and pure states, i.e., the initial state corresponding to the first subsystem is mixed and the same for the second subsystem is pure. Mathematically we express this state as $\rho(0) = \rho_1(0) \otimes |\psi_2(0)\rangle\langle\psi_2(0)|$, where $\rho_1(0)$ is the initial mixed state of the first subsystem and $|\psi_2(0)\rangle$ is the initial pure state of the second subsystem. We take $|\psi_2(0)\rangle$ as a generalized $SU(2)$ coherent state as presented earlier in Eq.(4.4). The mixed state $\rho_1(0)$ is a combination of two coherent states placed at two different points on the phase space, i.e.,

$$\rho_1(0) = p\,|\theta^a_{10},\,\phi^a_{10}\rangle\langle\theta^a_{10},\,\phi^a_{10}| + (1-p)\,|\theta^b_{10},\,\phi^b_{10}\rangle\langle\theta^b_{10},\,\phi^b_{10}|. \tag{6.9}$$

Here we take $(\theta^a_{10},\,\phi^a_{10}) = (0.89,\,0.63)$ and $(\theta^b_{10},\,\phi^b_{10}) = (2.25,\,-0.63)$, and $|\psi_2(0)\rangle = |\theta_{20} = 0.89,\,\phi_{20} = 0.63\rangle$. We only study $p = 1/2$ case, that means the contributions of both the coherent states are same on the formation of $\rho_1(0)$. Since the two coherent states are placed away from each other on the phase space, their overlapping is almost negligible (shown in Fig. 6.1), i.e., $\langle\theta^a_{10},\,\phi^a_{10}\,|\,\theta^b_{10},\,\phi^b_{10}\rangle \simeq 0$.

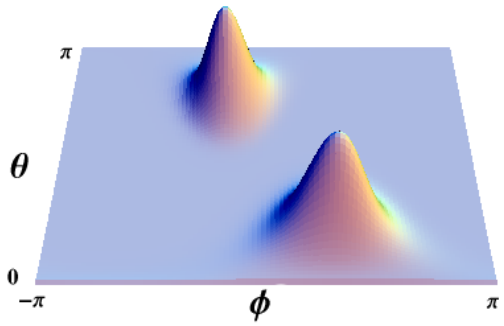

Figure 6.1: Husimi function of the initial mixed state $\rho_1(0)$. Center of the two peaks are at $(\phi,\,\theta) = \{(0.63,\,0.89)$ and $(-0.63,\,2.25)\}$.

(2) A product of mixed states, but of the very simple form $\rho(0) = \rho_1(0) \otimes \rho_2(0)$, where $\rho_1(0)$ is same as presented in Eq.(6.9). We also take the initial mixed state corresponding to the second subsystem $\rho_2(0)$ as same as $\rho_1(0)$.

The most general form of an unentangled mixed state is $\rho = \sum_i p_i\,\rho_1^{(i)} \otimes \rho_2^{(i)}$. However, our choice of these very simple initial mixed states will help us to under-

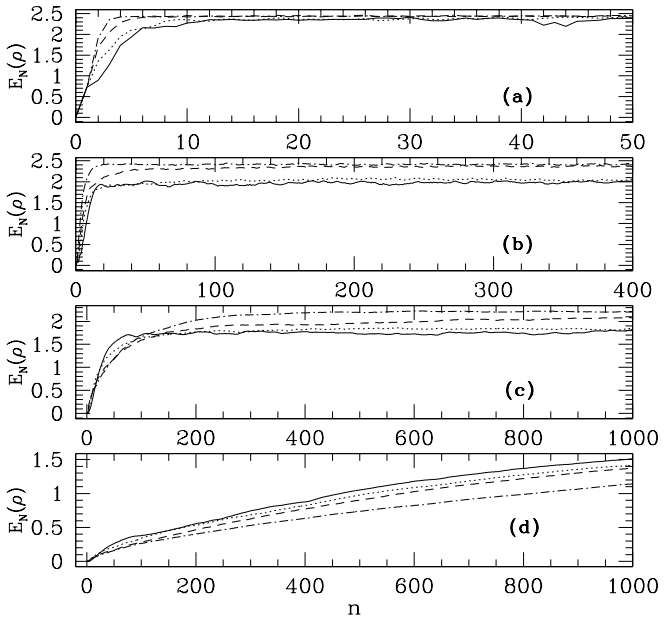

Figure 6.2: Evolution of the log-negativity measure (evolving under the coupled tops time-evolution operator U_T) corresponding to the case of the mixed-pure initial state is presented. Solid lines and dotted lines are representing the results corresponding to the non-chaotic cases ($k = 1.0$ and $k = 2.0$, respectively). Dashed lines are representing the mixed case ($k = 3.0$) and dash-dot lines are showing the results for the strongly chaotic case ($k = 6.0$). (a) Representing the results for the stronger coupling strength ($\epsilon = 1.0$). (b) This window is showing the results for $\epsilon = 0.1$. (c) This window is for $\epsilon = 0.01$ case. (d) This window is showing the results for the weak coupling case ($\epsilon = 0.001$).

stand better the mixed state entanglement. We now evolve the initial mixed states $\rho(0)$ by the time evolution operator corresponding to the coupled kicked top, i.e.

$$\rho(n) \; = \; U_T^n \, \rho(0) \, U_T^{-n}. \tag{6.10}$$

We now study the time-evolution of the log-negativity measure and the subsystem entropies (the von Neumann entropy and the linear entropy) of $\rho(n)$ corresponding to the above mentioned two initial mixed states.

Mixed-Pure case :

Let us start the discussion with the mixed-pure case, i.e., the initial unentangled mixed state corresponding to the coupled system is of type (1). In this case, first we discuss the time-evolution of the log-negativity measure of the entanglement

and then we discuss the time-evolution of the subsystem entropies.

(a) Log-Negativity measure : In Fig.6.2, we present the time-evolution of the log-negativity measure $E_N(\rho)$ for different individual top dynamics ($k = 1.0,\ 2.0,\ 3.0$ and 6.0) and for different coupling strengths. Let us discuss the case of a stronger coupling $\epsilon = 1.0$, whose results are presented in Fig.6.2(a). This coupling strength is very strong and therefore, irrespective of the individual top dynamics, the over all coupled system is chaotic. Therefore, the location of the initial states and the dynamics of the individual tops are irrelevant for the saturation of the $E_N(\rho)$. Hence we see almost same saturation values of $E_N(\rho)$ for all the different values of k.

The time-evolution of $E_N(\rho)$ corresponding to $\epsilon = 0.1$ is presented in Fig.6.2(b). We now observe that the saturation values of $E_N(\rho)$ corresponding to two non-chaotic cases ($k = 1.0$ and $k = 2.0$) are less than the saturation values corresponding to the other two cases. These lower saturation values of $E_N(\rho)$ corresponding to the non-chaotic cases are due to the influence of the regular orbits on the evolution of the mixed state. Consequently we notice that the saturation values of $E_N(\rho)$, corresponding to the non-chaotic cases, are less than the saturation values observed in the case of stronger coupling ($\epsilon = 1.0$). However, the saturation values of $E_N(\rho)$ corresponding to the other two cases, $k = 3.0$ and $k = 6.0$, are almost equal to the previous case ($\epsilon = 1.0$).

Now for the coupling strength $\epsilon = 0.01$, whose results are presented in Fig.6.2(c), the saturation values of $E_N(\rho)$ corresponding to the non-chaotic cases are again less than the other two cases. In addition, the saturation values of $E_N(\rho)$ corresponding to the non-chaotic cases are less than the corresponding saturation values observed in the previous two coupling strengths ($\epsilon = 1.0$, $\epsilon = 0.1$). But here we notice that, when $50 \lesssim n \lesssim 200$, the magnitude of $E_N(\rho)$ corresponding to the non-chaotic cases are larger than the other two cases. The saturation value corresponding to the mixed case ($k = 3.0$) is now less than the saturation value corresponding to the chaotic case ($k = 6.0$). This implies that, for this moderate coupling strength, the presence of small regular islands in $k = 3.0$ case effects the entanglement production.

Finally when coupling strength is weak, $\epsilon = 0.001$, we observe completely dif-

ferent behaviors of the time-evolution of $E_N(\rho)$ and these results are presented in Fig.6.2(d). For this coupling strength, $E_N(\rho)$ corresponding to the non-chaotic cases are higher than the chaotic cases within our time of observation. These results imply that, in case of weak coupling, the presence of chaos in the system actually suppresses the entanglement production. This suppression of the entanglement production by chaos, corresponding to the weak coupling case, was also observed for the pure state entanglement production, which we have already discussed in Chapter 5.

(b) Subsystem entropy : Here we study *two* different measures of the subsystem entropy. One is the linear entropy S_R and the other one is the von Neumann entropy S_V. In case of mixed state, the subsystem entropies are not the measure of the entanglement. However, the subsystem entropies are still very important quantities to investigate. In addition, we find that the qualitative behaviors of the subsystem entropies are similar to the log-negativity measure. This implies that the subsystem entropies may have some connection with the entanglement.

Two subsystem entropies are defined in the usual way. We have the total density matrix $\rho(n)$ at time n which is defined in Eq.(6.10). To determine the reduced density matrix (RDM) corresponding to the first (second) subsystem $\rho_1(n)$ $\left[\,\rho_2(n)\,\right]$, we have to trace over the second (first) subsystem. As usual, the subsystem von Neumann entropy is defined as $S_V^{(1)} = -\,\mathrm{Tr}_1\left[\,\rho_1(n)\,\ln\,\rho_1(n)\,\right]$ and $S_V^{(2)} = -\,\mathrm{Tr}_2\left[\,\rho_2(n)\,\ln\,\rho_2(n)\,\right]$. Corresponding linear entropies are $S_R^{(1)} = 1 - \mathrm{Tr}_1\,\rho_1(n)^2$ and $S_R^{(2)} = 1 - \mathrm{Tr}_2\,\rho_2(n)^2$. Since the initial state corresponding to the first subspace is mixed, so the corresponding subsystem entropies (S_V, S_R) are greater than *zero*. On the other hand, the initial state corresponding to the second subsystem is pure and therefore the corresponding subsystem entropies are zero. Consequently, the time-evolution of the subsystem entropies of the individual subsystems are different.

In Fig.6.3, we present the time-evolution of S_R for the individual subsystems. We have mentioned earlier that the overlapping between the two coherent states, which constructing $\rho_1(0)$, is almost *zero*. Therefore the initial value of S_R corre-

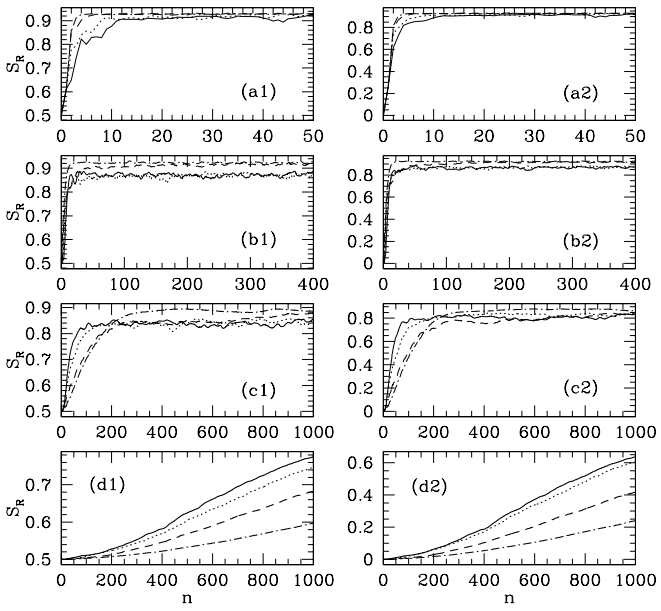

Figure 6.3: Evolution of the subsystem linear entropy (evolving under the coupled tops time-evolution operator U_T) corresponding to the case of mixed-pure initial state is presented. Left windows correspond to the first subsystem and the corresponding right windows are showing the results for the second subsystem. Solid lines and dotted lines are representing the results corresponding to the non-chaotic cases ($k = 1.0$ and $k = 2.0$, respectively). Dashed lines are representing the mixed case ($k = 3.0$) and dash-dot lines are showing the results corresponding to the strongly chaotic case ($k = 6.0$). (a1, a2) Representing the results for the stronger coupling strength ($\epsilon = 1.0$). (b1, b2) These windows are showing the results for $\epsilon = 0.1$. (c1, c2) These windows are for $\epsilon = 0.01$ case. (d1, d2) Representing the results for the weak coupling strength ($\epsilon = 0.001$).

sponding to the first subsystem can be obtained as follow.

$$\begin{aligned} S_R &= 1 - \mathrm{Tr}_1\, \rho_1(0)^2 \\ &= 1 - \mathrm{Tr}_1 \left[\frac{1}{4} \left(|\theta^a_{10},\, \phi^a_{10}\rangle \langle \theta^a_{10},\, \phi^a_{10}| + |\theta^b_{10},\, \phi^b_{10}\rangle \langle \theta^b_{10},\, \phi^b_{10}| \right) \right] \\ &= 1 - \frac{1}{4} \sum_{m_1} \left[\left| \langle m_1 | \theta^a_{10},\, \phi^a_{10} \rangle \right|^2 + \left| \langle m_1 | \theta^b_{10},\, \phi^b_{10} \rangle \right|^2 \right] \\ &= \frac{1}{2}. \end{aligned} \tag{6.11}$$

The second equality in the above expression is due to the above assumption of the non-overlapping coherent states and the last equality is due to the normalized coherent states. In Fig.6.3, we observe that the initial value of S_R corresponding to the first subsystem are indeed $1/2$. On the other hand, the initial state cor-

responding to the second subsystem is pure and hence the initial value of S_R is *zero*.

We now discuss the time-evolution of the linear entropy S_R, which is also referred as the production of S_R, corresponding to the different single top dynamics and the different coupling strengths which we have studied in case of the log-negativity measure. Let us start discussion with the stronger coupling strength $\epsilon = 1.0$, whose results are presented in Figs.6.3 (a1) and (a2). These figures show that, even though the initial values of S_R are different for the two subsystems, the saturation values of S_R are same for both the subsystems. Again, due to the strong coupling, the saturation values of S_R are *same* for all the different single top dynamics. Later we will show that the saturation value of S_R depends on the initial value of S_R and on the Hilbert space dimensions of the participating subsystems.

The time-evolution of S_R corresponding to $\epsilon = 0.1$ is presented in Figs.6.3(b1) and (b2). Now we observe that the saturation values of S_R corresponding to the non-chaotic cases ($k = 1.0$ and $k = 2.0$) are less than the other two cases. This observation is valid for both the subsystems. A similar behavior of the saturation was also observed in our study of the time-evolution of $E_N(\rho)$.

The production of S_R corresponding to the both subsystems, for the coupling strength $\epsilon = 0.01$, are presented in Figs.6.3(c1) and (c2). Here we observe that, for $n \lesssim 200$, production of S_R corresponding to the non-chaotic cases is larger than the production in other two cases. Another important observation is that, the saturation values of S_R are less than the previous two coupling strengths for all kind of single top dynamics.

Finally, we come to the weak coupling case, $\epsilon = 0.001$, whose results are presented in Figs.6.3(d1) and (d2). In this case, within our observational time, we find that the production of S_R corresponding to the non-chaotic cases is larger than the production in chaotic cases. More precisely, the production of S_R decreases with the increment of the parameter k and this is observed for both the subsystems. However, due to the different initial values of S_R, the production of S_R for all the different values of k is always larger for the first subsystem than the second subsystem.

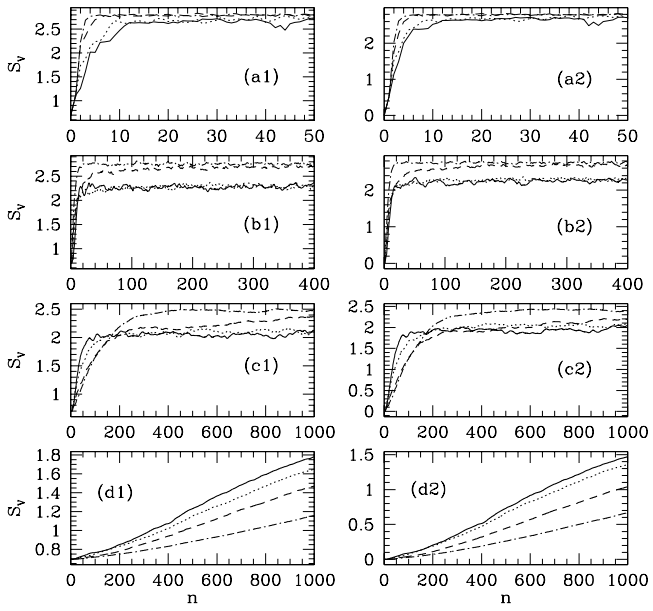

Figure 6.4: Evolution of the subsystem von Neumann entropy (evolving under the coupled tops time-evolution operator U_T) corresponding to the case of mixed-pure initial state is presented. Left windows correspond to the first subsystem and the corresponding right windows are showing the results for the second subsystem. Solid lines and dotted lines are representing the results corresponding to the non-chaotic cases ($k = 1.0$ and $k = 2.0$, respectively). Dashed lines are representing the mixed case ($k = 3.0$) and dash-dot lines are showing the results corresponding to the strongly chaotic case ($k = 6.0$). (a1, a2) Representing the results for the stronger coupling strength ($\epsilon = 1.0$). (b1, b2) These windows are showing the results for $\epsilon = 0.1$. (c1, c2) These windows are for $\epsilon = 0.01$ case. (d1, d2) Representing the results for the weak coupling strength ($\epsilon = 0.001$).

In Fig.6.4, we present the production of the von Neumann entropy S_V for different individual top dynamics and different coupling strengths. Because of the identical qualitative behaviors of S_R and S_V, we are not giving any elaborate discussion on the production of S_V. The above description of the production of S_R is well applicable for the production of S_V.

Mixed-Mixed case :

In this case, the initial unentangled state is a product of mixed states of the form $\rho(0) = \rho_1(0) \otimes \rho_2(0)$, where $\rho_2(0)$ is identical to $\rho_1(0)$, and $\rho_1(0)$ is defined in Eq.(6.9). Following earlier sequence, we first discuss the time-evolution of the log-negativity measure $E_N(\rho)$ and then we discuss the production of the subsystem

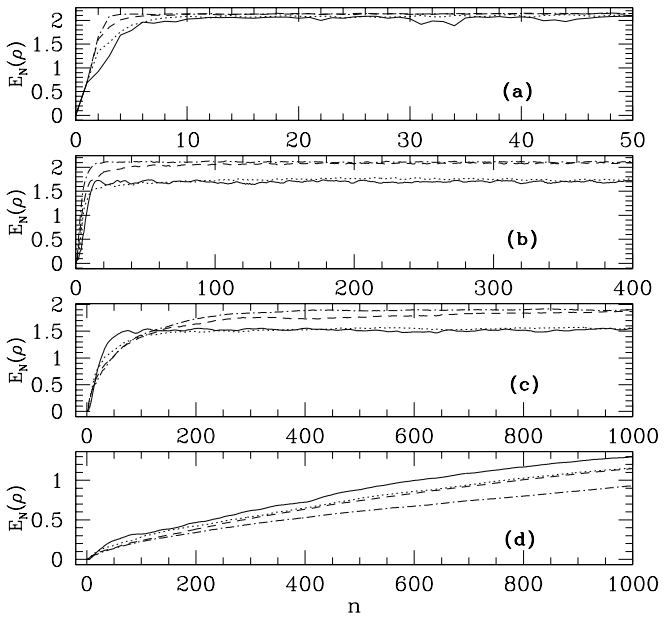

Figure 6.5: Evolution of the log-negativity measure (evolving under the coupled tops time-evolution operator U_T) corresponding to the case of the mixed-mixed initial state is presented. Solid lines and dotted lines are representing the results corresponding to the non-chaotic cases ($k = 1.0$ and $k = 2.0$, respectively). Dashed lines are representing the mixed case ($k = 3.0$) and dash-dot lines are showing the results for the strongly chaotic case ($k = 6.0$). (a) Representing the results for the stronger coupling strength ($\epsilon = 1.0$). (b) This window is showing the results for $\epsilon = 0.1$. (c) This window is for $\epsilon = 0.01$ case. (d) This window is showing the results for the weak coupling case ($\epsilon = 0.001$).

entropies.

(a) Log-Negativity measure : In Fig.6.5, we present the time-evolution of $E_N(\rho)$ for different individual top dynamics ($k = 1.0,\ 2.0,\ 3.0$ and 6.0) and for different coupling strengths. If we compare Figs.6.5 and 6.2, then we can clearly see that the qualitative behaviors of the time-evolution of $E_N(\rho)$ corresponding to the mixed-mixed case is same as the behaviors observed in the mixed-pure case. Therefore, for the present case, a detail qualitative description of the time-evolution of $E_N(\rho)$ is not required, and the description presented for the mixed-pure case is applicable for the present case. However, we identify a quantitative difference between these two cases. The time-evolution of $E_N(\rho)$ corresponding to the mixed-mixed case is always less than the mixed-pure case. This is true for all the *four* different single top parameter values and for all the coupling strengths. This result implies

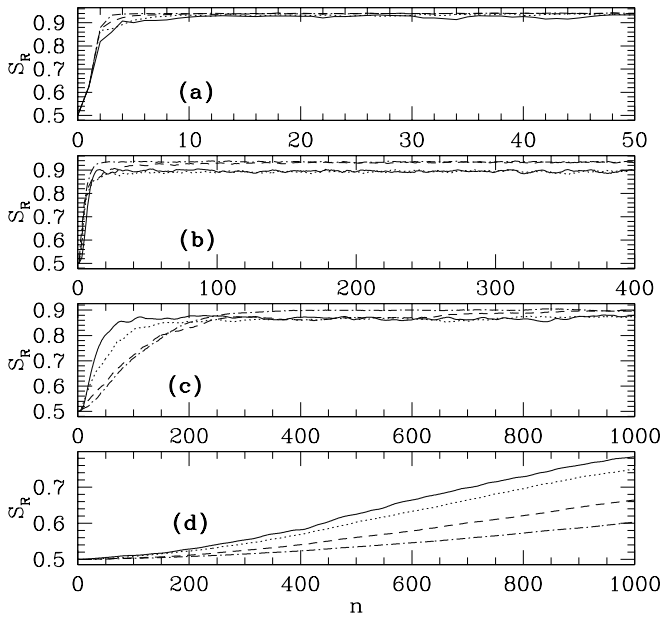

Figure 6.6: Evolution of the subsystem linear entropy (evolving under the coupled tops time-evolution operator U_T) corresponding to the case of mixed-mixed initial state is presented. Solid lines and dotted lines are representing the results corresponding to the non-chaotic cases ($k = 1.0$ and $k = 2.0$, respectively). Dashed lines are representing the mixed case ($k = 3.0$) and dash-dot lines are showing the results corresponding to the strongly chaotic case ($k = 6.0$). (a) Representing the results for the stronger coupling strength ($\epsilon = 1.0$). (b) This window is showing the results for $\epsilon = 0.1$. (c) This window is for $\epsilon = 0.01$ case. (d) Representing the results for the weak coupling strength ($\epsilon = 0.001$).

that the *mixedness* of the initial state corresponding to the second subsystem actually suppresses the entanglement production. This is an important observation which requires separate study.

(b) Subsystem entropy : In this case, the initial state corresponding to each subsystem is identical and therefore, the production of subsystem entropies (S_R and S_V) remains same for the each subsystem. Hence in Figs.6.6 and 6.7, we present the results of the production of subsystem entropies corresponding to the first subsystem only. A comparison between the present results and the results obtained in the mixed-pure case shows no qualitative differences between the two results. However, in contrast to the log-negativity measure, the production of the subsystem entropies are slightly higher for the present case than the previous case (mixed-pure), but these small differences are not distinctly visible

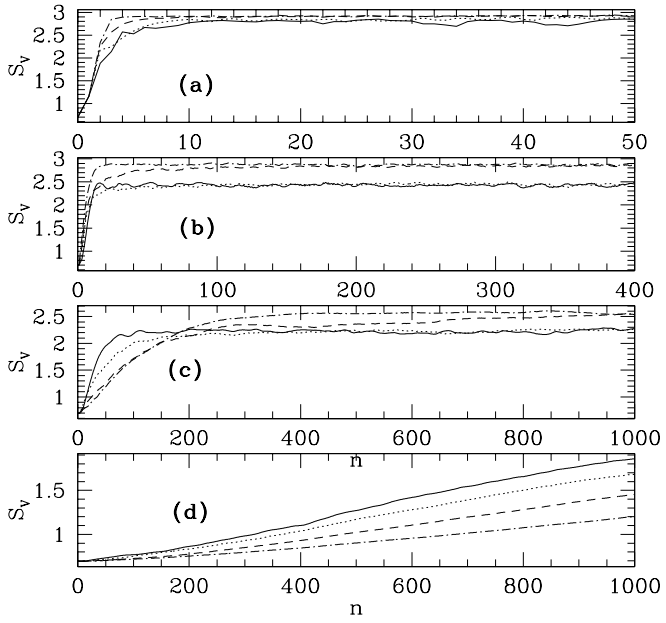

Figure 6.7: Evolution of the subsystem von Neumann (evolving under the coupled tops time-evolution operator U_T) corresponding to the case of mixed-mixed initial state is presented. Solid lines and dotted lines are representing the results corresponding to the non-chaotic cases ($k = 1.0$ and $k = 2.0$, respectively). Dashed lines are representing the mixed case ($k = 3.0$) and dash-dot lines are showing the results corresponding to the strongly chaotic case ($k = 6.0$). (a) Representing the results for the stronger coupling strength ($\epsilon = 1.0$). (b) This window is showing the results for $\epsilon = 0.1$. (c) This window is for $\epsilon = 0.01$ case. (d) Representing the results for the weak coupling strength ($\epsilon = 0.001$).

from the respective figures. In the next subsection, our random matrix estimation of the saturation of S_R, corresponding to the above two different type of initial states, will show the larger saturation value for the mixed-mixed case than the mixed-pure case.

6.1.3 Saturation of the subsystem linear entropy : A random matrix estimation

We now present the RMT estimation of the saturation value of the subsystem linear entropy. Here we consider the initial state as the mixed-mixed type, i.e., $\rho(0) = \rho_1(0) \otimes \rho_2(0)$. Since the pure state is just a special case of the mixed state, we can also estimate the saturation of the subsystem linear entropy corresponding to the mixed-pure case as a special case of the mixed-mixed case. Following

identical procedure, it is also possible to estimate the saturation value of the subsystem linear entropy corresponding to the most general initial unentangled mixed state of the form $\rho = \sum_i p_i \rho_1^{(i)} \otimes \rho_2^{(i)}$. However, here we only present the whole derivation corresponding to the case which we have mentioned above and we only highlight the results corresponding to the most general unentangled initial mixed state. At the very beginning, we set some notations. We denote the subsystem linear entropies by S_i where $i = 1, 2$ represent two subsystems. In addition, we denote the RMT average of any quantity by a bar on the top, like $\overline{\bullet\bullet}$.

Let us take the initial state corresponding to two subsystems, in their respective eigenbasis, as

$$\rho_1(0) = \sum_{i=1}^{N} a_i \, |i\rangle \langle i| \text{ and } \rho_1(0) = \sum_{\alpha=1}^{M} b_\alpha \, |\alpha\rangle \langle \alpha|,$$

where $\sum_{i=1}^{N} a_i = 1 = \sum_{\alpha=1}^{M} b_\alpha$ and the coefficients, a_i's and b_α's, are real *positive semidefinite*. N and M are the dimensions of the first and the second subsystem respectively. Without loosing any generality, we assume $N \leq M$. Therefore, the initial state of the composite system is,

$$\begin{aligned} \rho(0) &= \rho_1(0) \otimes \rho_2(0) \\ &= \sum_{i=1}^{N} \sum_{\alpha=1}^{M} a_i \, b_\alpha \left(|i\rangle \otimes |\alpha\rangle \right) \left(\langle i| \otimes \langle \alpha| \right) \\ &= \sum_{i=1}^{N} \sum_{\alpha=1}^{M} a_i \, b_\alpha \, \rho^{(i\alpha)}(0) \end{aligned} \tag{6.12}$$

where

$$\rho^{(i\alpha)}(0) = \left(|i\rangle \otimes |\alpha\rangle \right) \left(\langle i| \otimes \langle \alpha| \right) \equiv |i, \alpha\rangle \langle i, \alpha|. \tag{6.13}$$

From now onwards, we use $|\bullet\rangle \otimes |\bullet\rangle = |\bullet, \bullet\rangle$.

Now

$$\rho^{(i\alpha)}(0) \xrightarrow{U^n} \rho^{(i\alpha)}(n) = U^n \, |i, \alpha\rangle \langle i, \alpha| U^{-n}. \tag{6.14}$$

Let us assume, $\{ |j\rangle \}$ is orthonormal basis for the first subsystem and $\{ |\beta\rangle \}$ is orthonormal basis for the second subsystem. Therefore,

$$\rho^{(i\alpha)}(n) = \sum_{j,k=1}^{N} \sum_{\beta,\gamma=1}^{M} a_{j\beta}^{(i\alpha)} \, a_{k\gamma}^{(i\alpha)*} \, |j, \beta\rangle \langle k, \gamma| \tag{6.15}$$

and hence

$$\begin{aligned}\rho(n) &= U^n\,\rho(0)\,U^{-n} \\ &= \sum_{i=1}^{N}\sum_{\alpha=1}^{M} a_i\,b_\alpha \sum_{j,k=1}^{N}\sum_{\beta,\gamma=1}^{M} a_{j\beta}^{(i\alpha)}\,a_{k\gamma}^{(i\alpha)^*}\,|j,\,\beta\rangle\,\langle\,k,\,\gamma|. \end{aligned} \tag{6.16}$$

The RDM corresponding to the first subsystem is

$$\begin{aligned}\rho_1(n) &= \sum_{\beta=1}^{M}\langle\,\beta|\,\rho(n)\,|\beta\,\rangle \\ &= \sum_{i=1}^{N}\sum_{\alpha=1}^{M} a_i\,b_\alpha \sum_{j,k=1}^{N}\sum_{\beta=1}^{M} a_{j\beta}^{(i\alpha)}\,a_{k\beta}^{(i\alpha)^*}\,|j\,\rangle\,\langle\,k| \\ &= \sum_{i=1}^{N}\sum_{\alpha=1}^{M} a_i\,b_\alpha\,A^{(i\alpha)}\,A^{(i\alpha)^\dagger} \end{aligned} \tag{6.17}$$

where $A^{(i\alpha)}$ is a rectangular matrix of size $N \times M$ and whose elements are the coefficients $\left\{\,a_{j\beta}^{(i\alpha)}\right\}$. Similarly, the RDM corresponding to the second subsystem is

$$\begin{aligned}\rho_2(n) &= \sum_{j=1}^{N}\langle\,j|\,\rho(n)|j\,\rangle \\ &= \sum_{i=1}^{N}\sum_{\alpha=1}^{M} a_i\,b_\alpha\,A^{(i\alpha)^\dagger}\,A^{(i\alpha)} \end{aligned} \tag{6.18}$$

We now derive the RMT averages of the subsystem linear entropies, $\overline{S}_1$ and $\overline{S}_2$. For the unequal Hilbert space dimensions ($N \neq M$), $\overline{S}_1$ and $\overline{S}_2$ are different. Let us first calculate $\overline{S}_2$. From Eq.(6.18), we have

$$\begin{aligned}\mathrm{Tr}_2\,\rho_2^2 &= \sum_{\gamma=1}^{M}\langle\,\gamma|\,\rho_2^2\,|\gamma\,\rangle \;=\; \sum_{i=1}^{N}\sum_{\alpha=1}^{M} a_i^2\,b_\alpha^2 \sum_{\gamma=1}^{M}\langle\,\gamma|\left(A^{(i\alpha)^\dagger}\,A^{(i\alpha)}\right)^2|\gamma\,\rangle \\ &+ \sum_{i=1}^{N} a_i^2 \sum_{\substack{\alpha,\beta=1\\ \alpha\neq\beta}}^{M}\sum_{\gamma=1}^{M} b_\alpha\,b_\beta\,\langle\,\gamma|\left(A^{(i\alpha)^\dagger}\,A^{(i\alpha)}\,A^{(i\beta)^\dagger}\,A^{(i\beta)} + \mathrm{h.c}\right)|\gamma\,\rangle \\ &+ \sum_{\substack{i,j=1\\ i\neq j}}^{N} a_i\,a_j \sum_{\alpha=1}^{M}\sum_{\gamma=1}^{M} b_\alpha^2\,\langle\,\gamma|\left(A^{(i\alpha)^\dagger}\,A^{(i\alpha)}\,A^{(j\alpha)^\dagger}\,A^{(j\alpha)} + \mathrm{h.c}\right)|\gamma\,\rangle \\ &+ \sum_{\substack{i,j=1\\ i\neq j}}^{N}\sum_{\substack{\alpha,\beta=1\\ \alpha\neq\beta}}^{M}\sum_{\gamma=1}^{M} a_i\,a_j\,b_\alpha\,b_\beta\,\langle\,\gamma|\left(A^{(i\alpha)^\dagger}\,A^{(i\alpha)}\,A^{(j\beta)^\dagger}\,A^{(j\beta)} + \mathrm{h.c}\right)|\gamma\,\rangle \end{aligned} \tag{6.19}$$

According to Ref.[99], the RMT average of the first term of the above expansion

$$\overline{\sum_{\gamma=1}^{M} \langle\, \gamma |\, \left(A^{(i\alpha)\dagger}\, A^{(i\alpha)} \right)^2 |\, \gamma \,\rangle} \;=\; \frac{M \,+\, N}{MN \,+\, 1}. \tag{6.20}$$

We now derive the RMT averages of the other *three* terms. All these terms are of the following general form

$$\sum_{\gamma=1}^{M} \langle\, \gamma |\, A^{\dagger}\, A\, B^{\dagger}\, B \,+\, \mathrm{h.c} \,|\gamma\rangle. \tag{6.21}$$

Note that,

$$\overline{\sum_{\gamma=1}^{M} \langle\, \gamma |\, A^{\dagger}\, A\, B^{\dagger}\, B \,+\, \mathrm{h.c} \,|\gamma \,\rangle} \;=\; 2\; \overline{\sum_{\gamma=1}^{M} \langle\, \gamma |\, A^{\dagger}\, A\, B^{\dagger}\, B \,|\gamma\rangle}. \tag{6.22}$$

Now we have

$$\begin{aligned}
&\sum_{\gamma=1}^{M} \langle\, \gamma |\, A^{\dagger}\, A\, B^{\dagger}\, B \,|\gamma \,\rangle \\
=\;& \sum_{\gamma,\delta=1}^{M} \sum_{k,l=1}^{N} \langle\, \gamma | A^{\dagger} | k \,\rangle \,\langle\, k | A | \delta \,\rangle \,\langle\, \delta | B^{\dagger} | l \,\rangle \,\langle\, l | B | \gamma \,\rangle \\
=\;& \sum_{\gamma,\delta=1}^{M} \sum_{k,l=1}^{N} a^{*}_{k\gamma}\, a_{k\delta}\, b^{*}_{l\delta}\, b_{l\gamma} \\
=\;& \sum_{\gamma=1}^{M} \sum_{k,l=1}^{N} \left| a_{k\gamma} \right|^2 \left| b_{l\gamma} \right|^2 \,+\, \text{other terms.}
\end{aligned} \tag{6.23}$$

The terms which we referred as the 'other terms' in the above expression contain only one a (or b) with same indices, and therefore the RMT averages of all such terms are *zero*. Hence

$$\begin{aligned}
&\overline{\sum_{\gamma=1}^{M} \langle\, \gamma |\, A^{\dagger}\, A\, B^{\dagger}\, B \,|\gamma \,\rangle} \\
=\;& \overline{\sum_{\gamma=1}^{M} \sum_{k,l=1}^{N} \left| a_{k\gamma} \right|^2 \left| b_{l\gamma} \right|^2} \\
=\;& \overline{\sum_{\gamma=1}^{M} \sum_{k,l=1}^{N} \left(a^{R\,2}_{k\gamma} \,+\, a^{I\,2}_{k\gamma} \right) \left(b^{R\,2}_{l\gamma} \,+\, b^{I\,2}_{l\gamma} \right)} \\
=\;& \overline{\sum_{\gamma=1}^{M} \sum_{k,l=1}^{N} \left[a^{R\,2}_{k\gamma}\, b^{R\,2}_{l\gamma} \,+\, a^{R\,2}_{k\gamma}\, b^{I\,2}_{l\gamma} \,+\, a^{I\,2}_{k\gamma}\, b^{R\,2}_{l\gamma} \,+\, a^{I\,2}_{k\gamma}\, b^{I\,2}_{l\gamma} \right]},
\end{aligned} \tag{6.24}$$

where $\mathrm{Re}\,(a,\,b) \equiv \left(a^R,\,b^R\right)$ and $\mathrm{Im}\,(a,\,b) \equiv \left(a^R,\,b^R\right)$. From the normalization condition

$$\sum_{k=1}^{N}\sum_{\gamma=1}^{M}\left|a_{k\gamma}\right|^2 = \sum_{k=1}^{N}\sum_{\gamma=1}^{M}\left(a_{k\gamma}^{R\,2} + a_{k\gamma}^{I\,2}\right) = 1$$

we have

$$\overline{a_{k\gamma}^{R\,2}} = \overline{a_{k\gamma}^{I\,2}} = \frac{1}{2MN},$$

and similarly we can get

$$\overline{b_{l\gamma}^{R\,2}} = \overline{b_{l\gamma}^{I\,2}} = \frac{1}{2MN}.$$

Substituting the last two results in Eq.(6.24), we get

$$\overline{\sum_{\gamma=1}^{M}\langle\,\gamma|\,A^\dagger\,A\,B^\dagger\,B\,|\gamma\,\rangle} = 4\,MN^2\left(\frac{1}{2MN}\right)^2 = \frac{1}{M}. \tag{6.25}$$

Using the results of Eqs.(6.20) and (6.25), we get from Eq.(6.19)

$$\begin{aligned}\overline{\mathrm{Tr}_2\,\rho_2^2} &= \frac{M+N}{MN+1}\sum_{i=1}^{N}\sum_{\alpha=1}^{M}a_i^2\,b_\alpha^2 \\ &+ \frac{1}{M}\left[\sum_{i=1}^{N}\sum_{\substack{\alpha,\beta=1\\ \alpha\neq\beta}}^{M}a_i^2\,b_\alpha\,b_\beta + \sum_{\substack{i,j=1\\ i\neq j}}^{N}\sum_{\alpha=1}^{M}a_i\,a_j\,b_\alpha^2 + \sum_{\substack{i,j=1\\ i\neq j}}^{N}\sum_{\substack{\alpha,\beta=1\\ \alpha\neq\beta}}^{M}a_i\,a_j\,b_\alpha\,b_\beta\right].\end{aligned} \tag{6.26}$$

From another normalization condition $\sum_{i=1}^{N}\sum_{\alpha=1}^{M}a_i\,b_\alpha = 1$, the term inside the bracket $[\ldots]$ can also be written as

$$1 - \sum_{i=1}^{N}\sum_{\alpha=1}^{M}a_i^2\,b_\alpha^2.$$

Therefore,

$$\overline{\mathrm{Tr}_2\,\rho_2^2} = \frac{M+N}{MN+1}\sum_{i=1}^{N}\sum_{\alpha=1}^{M}a_i^2\,b_\alpha^2 + \frac{1}{M}\left(1 - \sum_{\alpha=1}^{M}a_i^2\,b_\alpha^2\right) \tag{6.27}$$

and consequently

$$\overline{S_2} = 1 - \overline{\mathrm{Tr}_2\,\rho_2^2} = 1 - \frac{M+N}{MN+1}\sum_{i=1}^{N}\sum_{\alpha=1}^{M}a_i^2\,b_\alpha^2 - \frac{1}{M}\left(1 - \sum_{\alpha=1}^{M}a_i^2\,b_\alpha^2\right). \tag{6.28}$$

Now the initial subsystem entropies are

$$S_1(0) \,=\, 1 \,-\, \sum_i^N a_i^2 \;\; \text{and} \;\; S_2(0) \,=\, 1 \,-\, \sum_{\alpha=1}^M b_\alpha^2. \tag{6.29}$$

Therefore, in terms of the initial entropies, we can write

$$\overline{S_2} \,=\, 1 \,-\, \frac{M \,+\, N}{MN \,+\, 1} \,+\, \frac{M^2 \,-\, 1}{M(MN \,+\, 1)} \big[\, S_1(0) \,+\, S_2(0) \,-\, S_1(0)\, S_2(0) \big]. \tag{6.30}$$

Following an identical procedure, we get

$$\overline{S_1} \,=\, 1 \,-\, \frac{M \,+\, N}{MN \,+\, 1} \,+\, \frac{N^2 \,-\, 1}{N(MN \,+\, 1)} \big[\, S_1(0) \,+\, S_2(0) \,-\, S_1(0)\, S_2(0) \big]. \tag{6.31}$$

For $N \,=\, M$ case,

$$\overline{S_1} \,=\, \overline{S_2} \,=\, 1 \,-\, \frac{2N}{N^2 \,+\, 1} \,+\, \frac{N^2 \,-\, 1}{N(N^2 \,+\, 1)} \big[\, S_1(0) \,+\, S_2(0) \,-\, S_1(0)\, S_2(0) \big]. \tag{6.32}$$

The above derivation of the RMT average of the subsystem linear entropies are valid for the mixed-mixed initial states. For the mixed-pure initial states $S_2(0) \,=\, 0$. Therefore, for the mixed-pure case

$$\overline{S_1} \;\;=\;\; 1 \,-\, \frac{M \,+\, N}{MN \,+\, 1} \,+\, \frac{N^2 \,-\, 1}{N(MN \,+\, 1)}\, S_1(0) \tag{6.33a}$$

$$\overline{S_2} \;\;=\;\; 1 \,-\, \frac{M \,+\, N}{MN \,+\, 1} \,+\, \frac{M^2 \,-\, 1}{M(MN \,+\, 1)}\, S_1(0) \tag{6.33b}$$

and when $N \,=\, M$

$$\overline{S_1} \,=\, \overline{S_2} \,=\, 1 \,-\, \frac{2N}{N^2 \,+\, 1} \,+\, \frac{N^2 \,-\, 1}{N(N^2 \,+\, 1)}\, S_1(0). \tag{6.34}$$

Finally, we just want to present the RMT average of the subsystem linear entropies for the most general form of the unentangled initial mixed state $\rho(0) \,=\, \sum_i \, p_i \, \rho_1^{(i)}(0) \,\otimes\, \rho_2^{(i)}(0)$ and these are

$$\overline{S_1} \;\;=\;\; 1 \,-\, \frac{M \,+\, N}{MN \,+\, 1} \,+\, \frac{N^2 \,-\, 1}{N(MN \,+\, 1)} \sum_i \, p_i^2 \, \big[\, S_1^{(i)}(0) \,+\, S_2^{(i)}(0) \,-\, S_1^{(i)}(0)\, S_2^{(i)}(0) \,\big], \tag{6.35a}$$

$$\overline{S_2} \;\;=\;\; 1 \,-\, \frac{M \,+\, N}{MN \,+\, 1} \,+\, \frac{M^2 \,-\, 1}{M(MN \,+\, 1)} \sum_i \, p_i^2 \, \big[\, S_1^{(i)}(0) \,+\, S_2^{(i)}(0) \,-\, S_1^{(i)}(0)\, S_2^{(i)}(0) \,\big], \tag{6.35b}$$

where $S_k^{(i)}(0) \,=\, 1 \,-\, \mathrm{Tr}_k \, \big[\, \rho_k^{(i)}(0) \,\big]^2$, $k \,=\, 1,\, 2$. Derivation of the above expression is straightforward but lengthy. Therefore, we are not presenting it here.

Some numerics :

We now check the above RMT estimation of the saturation of the subsystem linear entropy with the numerical results obtained from the coupled kicked tops. Here we consider strongly coupled tops whose individual subsystems are strongly chaotic ($\epsilon = 1.0, k = 10.0$). Here again we consider same two different types of initial mixed states, i.e.,
(1) mixed-pure :

$$\rho(0) = \rho_1(0) \otimes |\psi_2(0)\rangle\langle\psi_2(0)|, \tag{6.36}$$

where $\rho_1(0) = p\,|\theta_{10}^a, \phi_{10}^a\rangle\langle\theta_{10}^a, \phi_{10}^a| + (1-p)\,|\theta_{10}^b, \phi_{10}^b\rangle\langle\theta_{10}^b, \phi_{10}^b|$ and $|\psi_2(0)\rangle = |\theta_{20}, \phi_{20}\rangle$. The states $|\theta, \phi\rangle$'s are usual $SU(2)$ coherent state.
(2) mixed-mixed :

$$\rho(0) = \rho_1(0) \otimes \rho_2(0) \tag{6.37}$$

where $\rho_1(0)$ is same as above and $\rho_2(0)$ is also identical to $\rho_1(0)$. In our detail study of the mixed state entanglement production, we only consider $p = 1/2$ case. Now we determine the saturation of the subsystem linear entropy for different p, where p actually determines the initial subsystem entropy. When $p = 0$ and $p = 1$, the initial state is pure. As we increase p from *zero*, the mixedness of the initial state increases and it reaches maxima at $p = 1/2$; then a further increase in p actually decreases the mixedness of the initial state and it reaches zero again at $p = 1$.

In Fig.6.8, we present the saturation of the subsystem linear entropy as a function of p. Figs.6.8(a) and 6.8(b), showing respectively the results corresponding to the mixed-pure and the mixed-mixed cases. In both the cases, our RMT estimations (solid line) match well with the numerical results. The small fluctuations are due to the finite-dimensional effects.

6.2 Operator entanglement

6.2.1 Operator Schmidt decomposition

We start our discussion on operator entanglement with a brief introduction to the operator Schmidt decomposition, a method recently proposed in Ref.[107]. Let us

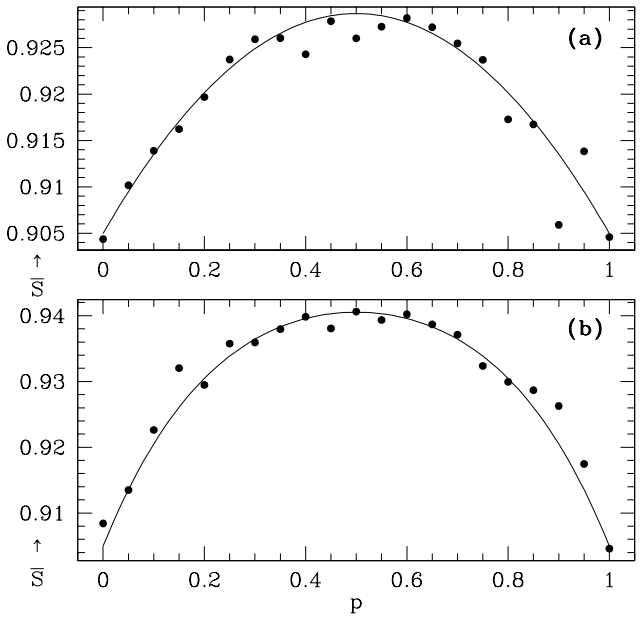

Figure 6.8: Saturation of the subsystem linear entropy corresponding to the coupled kicked tops is presented for different values of p. The magnitude of p determines the initial subsystem linear entropy. Solid curve is the RMT predicted estimation. (a) Representing the results corresponding to the initial mixed-pure case. (b) This window is showing the results corresponding to the initial mixed-mixed state. In both the cases, (a) and (b), RMT prediction match well with the numerical results.

first consider a Hilbert space of $N \times N$ operators whose inner product is defined as $(A, B) \equiv \mathrm{Tr}(A^\dagger B)$, where A and B are any two operators. Using this inner product, it is possible to define an orthonormal operator basis $\{A_i\}$ such that $(A_i, A_j) = \mathrm{Tr}(A_i^\dagger A_j) = \delta_{ij}$, where δ_{ij} is just the Krönecker delta. Note that the dimension of the operator Hilbert space of $N \times N$ operators is N^2. A very simple example of a complete orthonormal operator basis is $\{I_2, \sigma_i\}/\sqrt{2}$, where I_2 is the 2×2 unit matrix and σ_i's are the Pauli spin matrices. Here the dimension of the operator Hilbert space is $2^2 = 4$.

Suppose we have a unitary operator U acting on a space $\mathcal{H}_A \otimes \mathcal{H}_B$, where the dimension of $\mathcal{H}_A$ and $\mathcal{H}_B$ are N and M respectively. Without loss of any generality we can assume $N \leq M$. We expand U in orthonormal operator product bases

$\{A_i \otimes B_j\}$ as

$$U = \sum_{i=1}^{N^2} \sum_{j=1}^{M^2} u_{ij} A_i \otimes B_j, \tag{6.38}$$

where A_i and B_j are fixed orthonormal bases for $\mathcal{H}_A$ and $\mathcal{H}_B$ respectively, and u_{ij} are the coefficients. According to the singular value decomposition, the coefficient matrix u can be written as

$$u = \tilde{V} s V \tag{6.39}$$

where $\tilde{V}$ and V are the unitary matrices and s is a $N^2 \times M^2$ rectangular matrix of the form $[s] = s_i \delta_{ij}$ where s_i's are *nonnegative*. We thus obtain

$$\begin{aligned} U &= \sum_{i,k=1}^{N^2} \sum_{j,l=1}^{M^2} \tilde{V}_{ik} s_{kl} V_{lj} A_i \otimes B_j \\ &= \sum_{i=1}^{N^2} \sum_{j=1}^{M^2} \sum_{k=1}^{N^2} \tilde{V}_{ik} s_k V_{kj} A_i \otimes B_j. \end{aligned} \tag{6.40}$$

Let us now define

$$\tilde{A}_k \equiv \sum_{i=1}^{N^2} \tilde{V}_{ik} A_i \tag{6.41}$$

$$\tilde{B}_k \equiv \sum_{j=1}^{M^2} V_{kj} B_j. \tag{6.42}$$

It can be easily shown that $\tilde{A}_k$ and $\tilde{B}_k$ are also an orthonormal bases for $\mathcal{H}_A$ and $\mathcal{H}_B$. Hence we obtain the operator Schmidt decomposed form of U as,

$$U = \sum_{k=1}^{N^2} s_k \tilde{A}_k \otimes \tilde{B}_k. \tag{6.43}$$

6.2.2 Measure of operator entanglement

We can define the operator density matrix as,

$$\rho_U = U U^\dagger = \sum_{k,l=1}^{N^2} s_k s_l \left(\tilde{A}_k \tilde{A}_l^\dagger\right) \otimes \left(\tilde{B}_k \tilde{B}_l^\dagger\right). \tag{6.44}$$

But now $\mathrm{Tr}\,\rho_U = \mathrm{Tr}\,UU^\dagger = \sum_{k=1}^{N^2} s_k^2 = MN$. Therefore to normalize ρ_U, i.e., to make $\mathrm{Tr}\,\rho_U = 1$, we define

$$\tilde{s}_k = \frac{s_k}{\sqrt{NM}}. \tag{6.45}$$

The normalized form of the operator density matrix is

$$\rho_U = \sum_{k,l=1}^{N^2} \tilde{s}_k\,\tilde{s}_l\,\left(\tilde{A}_k\,\tilde{A}_l^\dagger\right) \otimes \left(\tilde{B}_k\,\tilde{B}_l^\dagger\right) \tag{6.46}$$

and then the operator RDM, say for the 1st subsystem, will be

$$\rho_U^{(1)} = \sum_{k=1}^{N^2} \tilde{s}_k^2\,\tilde{A}_k\,\tilde{A}_k^\dagger. \tag{6.47}$$

$\lambda_k \equiv \tilde{s}_k^2$ are the eigenvalues of the operator RDM. Now we can define the operator von Neumann entropy and the operator linear entropy respectively as

$$S_V(U) = -\mathrm{Tr}_1\,\rho_U^{(1)}\,\ln\,\rho_U^{(1)} = -\sum_{k=1}^{N^2} \tilde{s}_k^2\,\ln\,\tilde{s}_k^2 = -\sum_{k=1}^{N^2} \left(\frac{s_k^2}{NM}\right)\,\ln\left(\frac{s_k^2}{NM}\right) \tag{6.48}$$

$$\text{and} \qquad S_R(U) = 1 - \mathrm{Tr}_1\left(\rho_U^{(1)}\right)^2 = 1 - \frac{1}{N^2M^2}\sum_{k=1}^{N^2} s_k^4. \tag{6.49}$$

$S_V(U)$ and $S_R(U)$ are the measures of the operator entanglement.

6.2.3 Numerical results

The time evolution operator corresponding to the coupled kicked tops is

$$U_T = \left(U_1 \otimes U_2\right) U_\epsilon^{12}, \tag{6.50}$$

where U_1 and U_2 are the time evolution operators corresponding to the individual tops and U_ϵ^{12} is the coupling term. We have already discussed this particular system in the Chapter 3. Presently we are interested in studying the evolution of the operator entanglement of U_T, i.e. in studying the operator entanglement of U_T^n as a function of the time step n. In our numerical calculation, we choose the complete orthonormal operator bases corresponding to each subsystem as,

$$A_\alpha = |m_1\rangle\langle n_1| \tag{6.51}$$

$$\text{and} \quad B_\beta = |m_2\rangle\langle n_2| \tag{6.52}$$

where

$$\alpha \equiv N(m_1 + j_1) + (n_1 + j_1 + 1); (m_1, n_1) = -j_1, \ldots, j_1$$

$$\beta \equiv M(m_2 + j_2) + (n_2 + j_2 + 1); (m_2, n_2) = -j_2, \ldots, j_2$$

and $N = 2j_1 + 1,\ M = 2j_2 + 1$. In these orthonormal bases, U_T can be expressed as

$$U_T = \sum_{\alpha=1}^{N^2} \sum_{\beta=1}^{M^2} u_{\alpha\beta}\, A_\alpha \otimes B_\beta. \tag{6.53}$$

Since U_T^n is also a unitary operator, so we can write it in the above bases as,

$$U_T^n = \sum_{\alpha=1}^{N^2} \sum_{\beta=1}^{M^2} u_{\alpha\beta}(n)\, A_\alpha \otimes B_\beta. \tag{6.54}$$

Now applying the operator Schmidt decomposition and following the procedure given in the preceding subsection, we determine the operator von Neumann entropy $S_V(U_T^n)$ as a function of n. In Fig.6.9, we present our numerical results corresponding to the operator entanglement production for the coupled kicked tops of spin size $j_1 = j_2 = j$ (say) $= 10$. For this spin size, the operator Hilbert space dimension corresponding to each subsystem is $N^2 = (2j + 1)^2 = 441$. As we go from top to bottom window of Fig.6.9, coupling strength is increasing by a factor *ten*. Top window corresponds to $\epsilon = 10^{-3}$, next window is showing the results for $\epsilon = 10^{-2}$, the third window from the top corresponds to $\epsilon = 10^{-1}$ and the bottom window is showing the results for $\epsilon = 1.0$. For each coupling strength, we study the operator entanglement production for the same *four* different *single top* parameter values, which we studied in case of the *state* entanglement production (Chapter 5).

Let us first discuss the case of weaker coupling $\epsilon = 10^{-3}$, whose results are presented in the top most window of Fig.6.9. Here, within our time of observation $n = 1000$, we observe a larger operator entanglement production for the non-chaotic cases than the same for the chaotic one. In the preceding chapter, we observed similar behavior of the state entanglement production, but for the weaker coupling strength $\left(\epsilon = 10^{-4}\right)$. However, in case of the pure state entanglement

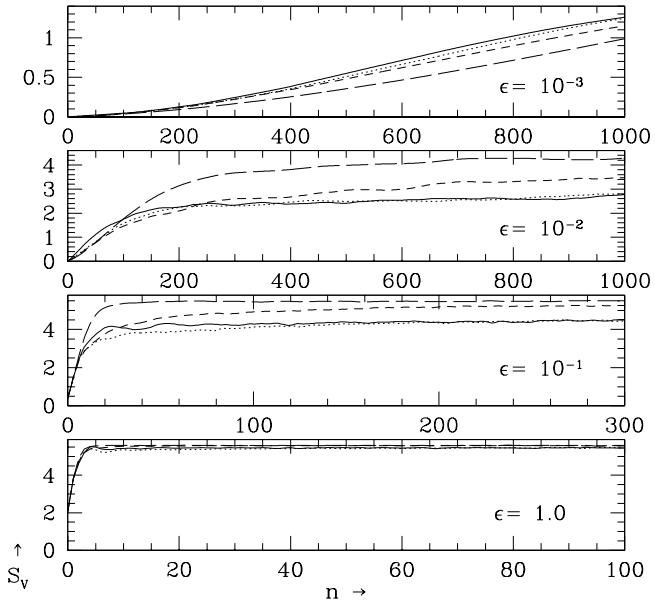

Figure 6.9: Time evolution of the operator von Neumann entropy corresponding to the coupled kicked tops is presented for different coupling strengths and for different underlying classical dynamics. Solid line represents $k = 1$, dotted line corresponds to $k = 2$, dashed line is for $k = 3$ and dash-dot line represents $k = 6$.

production, the initial state plays a crucial role. But the operator entanglement is a property of the operator itself and therefore it is completely independent of any kind of initial states. The conclusion is that, for the weakly coupled case, the presence of chaos actually suppresses the operator entanglement production.

The results corresponding to the case $\epsilon = 10^{-2}$ are presented in the second window from the top of Fig.6.9. For a non-chaotic case $k = 1.0$, the initial ($n \lesssim 95$) operator entanglement production is larger than all the other cases. Moreover, for $n \lesssim 240$, the operator entanglement production corresponding to both the non-chaotic cases is larger than the same corresponding to the mixed case ($k = 3.0$). However, the operator entanglement corresponding to both the non-chaotic cases eventually saturates at a value lower than the values corresponding to the mixed ($k = 3.0$) and the chaotic ($k = 6.0$) cases. We also observe that the operator entanglement production corresponding to the chaotic case is always larger than the mixed case.

Let us now come to a reasonably stronger coupling strength $\epsilon = 10^{-1}$, whose

results are presented in the third window from the top of Fig.6.9. For this coupling strength, we observe the saturation of the operator entanglement production corresponding to chaotic and non-chaotic cases. However, these saturation values are clearly different for non-chaotic, mixed and chaotic cases. For the chaotic case $k = 6.0$, the saturation value is very close to $\ln\left(0.6\,N^2\right) = \ln\left(0.6 \times 441\right) \simeq 5.578....$; whereas the saturation value corresponding to the mixed case $k = 3.0$ is slightly lower than this value. But the saturation values corresponding to *two* non-chaotic cases are distinctly lower than the other two cases.

Finally, the results corresponding to the case of very strong coupling ($\epsilon = 1.0$) are presented in the bottom window of Fig.6.9. Here, due to the strong coupling, the over all coupled system is chaotic, irrespective of the underlying classical dynamics of the individual subsystems. Therefore, the saturation values of the operator entanglement production are almost same for all the different values of k and these saturation values are very close to ~ 5.57. However, if we closely observe these saturation values, then we find minute differences between the non-chaotic (means, subsystems are non-chaotic) and the chaotic cases.

Saturation of the operator entanglement :

We have observed the saturation of the operator entanglement production corresponding to the cases when the individual top dynamics is chaotic and their coupling strength is also very strong. Most important observation is that the saturation value of the operator von Neumann entropy is equal to $\sim \ln(0.6d)$ where $d = N^2$ is the dimension of the operator Hilbert space. Therefore, from our previous knowledge of the saturation of the pure state entanglement, we expect the distribution of the eigenvalues of the operator RDM should follow the Laguerre ensemble. In Fig.6.10, we present the distribution of the eigenvalues of the operator RDM corresponding to the coupled kicked tops for the different Hilbert space dimensions M of the second top, while the dimension of the Hilbert space of the first top is fixed at $N = 2j_1 + 1 = 21$. The solid curve is representing the RMT

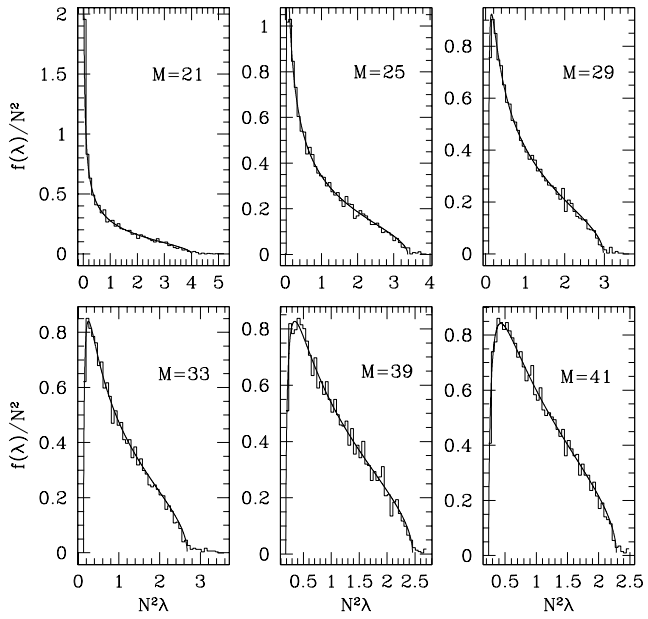

Figure 6.10: Distribution of the eigenvalues of the operator RDMs of coupled kicked tops. $N = 2j_1 + 1 = 21$. Solid curves correspond to the theoretical RMT predicted distribution function [Eq. (6.55)]

predicted Laguerre distribution

$$\begin{aligned} f(\lambda) &= \frac{d_1 Q}{2\pi} \frac{\sqrt{(\lambda_{max} - \lambda)(\lambda - \lambda_{min})}}{\lambda} \\ \lambda_{min}^{max} &= \frac{1}{d_1}\left(1 + \frac{1}{Q} \pm \frac{2}{\sqrt{Q}}\right) \end{aligned} \tag{6.55}$$

where $\lambda \in [\lambda_{min}, \lambda_{max}]$, $Q = d_2/d_1$, $d_1 = N^2$, $d_2 = M^2$; and the histograms are the numerical results corresponding to the coupled kicked tops. This figure clearly indicates the agreement between the RMT prediction and the numerical data. Using the above distribution and following the procedure of Chapter 4, we can estimate the saturation value of the operator entanglement production.

6.2.4 Operator entanglement and state entanglement : A relation

The measure of the operator entanglement is based on the operator Schmidt decomposition. Using a recently proposed *matrix reshaping* technique, it can be

shown that the operator Schmidt decomposition and the state Schmidt decomposition are basically equivalent [108]. Basic idea behind the matrix reshaping technique is very simple. Let us consider a rectangular matrix A of size $N \times M$. This matrix can be reshaped, by just putting its elements row after row in lexicographical order into a vector $|A\rangle$ of size NM. For example, let us consider a 2×2 matrix

$$A = \begin{pmatrix} a_{11} & a_{12} \\ a_{21} & a_{22} \end{pmatrix}. \tag{6.56}$$

After reshaping, we get

$$|A\rangle = \begin{pmatrix} a_{11} \\ a_{12} \\ a_{21} \\ a_{22} \end{pmatrix}. \tag{6.57}$$

Now the inner product of any two elements (A and B) of the operator Hilbert space is defined as $(A,\, B) = \mathrm{Tr}(A^\dagger B)$. If we take the matrix $B = \big((b_{11},\, b_{12}),\, (b_{21},\, b_{22})\big)$, then we have

$$\big(A,\, B\big) = \mathrm{Tr}\big(A^\dagger B\big) = a_{11}^*\, b_{11} + a_{12}^*\, b_{12} + a_{21}^*\, b_{21} + a_{22}^*\, b_{22}.$$

The above expression is the inner product of the vectors $|A\rangle$ and $|B\rangle$, i.e. $\langle A|B\rangle$, where $\langle A| = \big(a_{11}^*, a_{12}^*, a_{21}^*, a_{22}^*\big)$ is a row vector. Therefore, the matrix reshaping technique puts the operator inner product and the vector (state) inner product on a same footing.

Following the above technique, any unitary operator U can be reshaped into a vector $|U\rangle$ as,

$$|U\rangle = \sum_{\alpha=1}^{N^2} \sum_{\beta=1}^{M^2} u_{\alpha\beta}\, |A_\alpha,\, B_\beta\rangle \tag{6.58}$$

where $u_{\alpha\beta} = \langle A_\alpha,\, B_\beta |U\rangle$. Applying Schmidt decomposition to the above vector $|U\rangle$, we get

$$|U\rangle = \sum_{\alpha=1}^{N^2} s_\alpha\, |\tilde{A}_\alpha,\, \tilde{B}_\alpha\rangle. \tag{6.59}$$

Thus the matrix reshaping technique shows that the operator Schmidt decomposition is not a special technique, it is equivalent to the well known state Schmidt decomposition. Moreover, this also explains why the saturation value of the operator entanglement $\left[\ln\left(\gamma d\right)\right.$, where $d = N^2\left.\right]$ depends on the dimension of the operator Hilbert space in such a manner which is identical to the observed saturation values $\left[\ln\left(\gamma N\right)\right]$ of the state entanglement.

Summary and Future Outlook

Summary :

In classical physics, an important class of dynamical systems is the Hamiltonian systems. We can divide the dynamics of the Hamiltonian systems into *two* different types : the regular motion of the integrable systems and the chaotic motion of the nonintegrable systems. In this thesis we have studied both types of dynamical systems.

In Chapter 2, we have presented our work on the integrable systems. Here we have studied, both classically and quantum mechanically, a time dependent one dimensional nonlinear integrable system, namely, the time dependent harmonic oscillator with an inverse square potential. We have evaluated the exact invariant of this system by applying our Lie-algebraic interpretation of the Lewis-Riesenfeld invariant of the time dependent harmonic oscillator. This evaluation of the exact invariant has established the integrability of the above nonlinear system. One can apply our Lie-algebraic method to determine the invariant of any time-dependent Hamiltonian formed by the generators of any closed algebra. We have studied extensively the special and interesting case of a kicked-quadratic potential from which we have derived a new integrable, nonlinear, area preserving two dimensional map that may, for instance, be used in numerical algorithms that integrate Calogero-Sutherland-Moser Hamiltonian. Here we have derived that map from the Hamiltonian formed of the generators of the $\mathrm{su}(1,1)$ algebra. We expect that we can determine integrable two-dimensional mapping from the Hamiltonian formed by the generators of other closed algebra. We have constructed the classical time evolution operator, or the Perron-Frobenius operator for the nonlinear integrable system, taking advantage of a recent method of integrating the quantum Liouville-

Bloch equations. Our results have shown the exact one-to-one correspondence between the classical and the quantum dynamics.

Rest of the thesis is concentrated on the classical and the quantum mechanical study of the chaotic systems. However, we have studied the quantum mechanics of chaotic systems from slightly different point of view. Recently, entanglement has been discussed extensively due to its crucial role in quantum computation and quantum information theory. Entanglement is an unique property of a quantum mechanical system, which consists of at least two interacting subsystems. Since a quantum computer is a many particle system, entanglement is inevitable. The many particle nature of a quantum computer may be prone to problem of chaos. Some studies have inquired whether chaos will help or hinder in the operation of quantum computer. However, in this thesis, we have investigated at a more basic level the effect of the underlying classical dynamics on entanglement.

We have mentioned that entanglement can be observed in a quantum system which consists of at least two interacting subsystems. Therefore, to study the effect of classical chaotic dynamics on entanglement, we have to consider a coupled chaotic system which consists of at least two chaotic subsystems. Kicked top is a well-studied model of chaotic system. Moreover, coupled kicked tops has already been used in the study of entanglement. Therefore, we have also considered coupled kicked tops as our model. The classical limit of the coupled kicked tops presented in an earlier work was unfortunately incorrect, in fact it was not even canonical. In Chapter 3 we have derived the correct classical map and we have also described different classical dynamical properties of the kicked top.

Recent results indicate that chaos can lead to substantial entanglement production, but this still falls short of maximality. There exists a statistical upper bound on entanglement whose value depends on the Hilbert space dimension of the participating subsystems. Random matrix theory (RMT) has been successful in calculating many important universal statistical properties of quantum chaotic systems. We have also applied RMT to derive the above mentioned statistical bound on entanglement. More importantly, we have presented a universal distribution of the eigenvalues of the reduced density matrices which determines the saturation value of (statistical bound) the entanglement entropy, and have also

demonstrated that this distribution is realized in quantized chaotic systems by using the model of coupled kicked tops. Chapter 4 of this thesis is devoted to the discussion on the above mentioned statistical bound on entanglement.

The saturation of entanglement is the property of a strongly coupled highly chaotic system. In Chapter 5, we have studied entanglement production in coupled kicked tops corresponding to different underlying classical dynamics and different coupling strengths. We have found that, in general, the entanglement production is higher for stronger chaotic cases. Moreover, coupling strength between two tops is also an important parameter for the entanglement production. For example, when the coupling strength between two tops was very weak, we have found that the entanglement production is higher for sufficiently long time corresponding to nonchaotic cases. Here we have used the reduced Husimi function, the Husimi function of the reduced density matrix, to visualize the possible behaviors of a wavepacket. We have studied a phase-space based measure of complexity of the time evolving state and used RMT to model the strongly chaotic cases. In this chapter we have also derived an approximate formula, based on the ideas of RMT, for the entanglement production in coupled strongly chaotic system. This formula is applicable, unlike perturbation theory, to large coupling strengths and is valid for sufficiently long time.

Chapter 6 of this thesis is divided into two parts. In the first part, we have studied the entanglement production for the initially mixed unentangled state. Here we have used log-negativity measure to study the influence of the underlying classical dynamics on the mixed state entanglement production. We have found that the presence of chaos, in general, enhances the entanglement production. We have also observed that the mixedness of the initial state actually suppresses the entanglement production. This is an important observation, which requires further studies. In case of mixed state, the subsystem entropies are not the measures of the entanglement. But still they are very important quantities. Therefore, in this chapter, we have also studied the production of the subsystem von Neumann entropy as well as the linear entropy. We have found that the production of the subsystem entropies and the entanglement production have some similar qualitative properties. Existence of a statistical upper bound is one such property

which is common to both the above mentioned quantities. We have used RMT to estimate the statistical upper bounds (or the saturation value) of the subsystem linear entropy.

In the second part of the Chapter 6, we have studied the operator entanglement as a measure of the entangling power of a given operator. We have actually investigated the entangling power of a unitary time evolution operator corresponding to the coupled kicked tops, for different underlying classical dynamics of the individual top and for different coupling strengths between the tops. Our numerical studies have shown that the operator entanglement production and the pure state entanglement production share some common properties.

Future outlook :

Most of the studies on the effect of underlying classical dynamics on the entanglement production are restricted for the pure state case. There is almost nothing have been done in case of mixed state. In this thesis, we have taken some initiative in this direction. More elaborate study of the mixed state entanglement production can definitely be an extension of this thesis. We have also initiated the study of the operator entanglement production, a measure of the entangling power of a given operator. An extensive study of the operator entanglement production can also be regarded as a possible future direction of this thesis.

Until very recently, the topic of 'chaos and entanglement' has been a purely theoretical one. But now, due to some recent proposals, we believe that the results obtained in this thesis can be experimentally verified in the near future. Therefore, without going into details, it is worthwhile to mention some of those experimental proposals. In one proposal, multiple scattering of electrons in a quantum dot has been considered [109]. If the scattering is chaotic, a universal random matrix description (statistical description) of the entanglement production is possible. Therefore, this experimental setting can be used to verify the different universal statistical properties of the entanglement production observed theoretically in this thesis. In another proposal, an atom trapped in a magneto-optical lattice (AMOL) has been shown as a feasible experimental system to test the effect of classical dynamics on the entanglement production [110]. The AMOL

can exhibit generic features of entanglement dynamics, for example quasiperiodicity for a state initially localized in a regular regime and a rapid increase of entanglement in a chaotic regime. These results are very similar to the results obtained in Chapter 5 of this thesis.

References

[1] V. I. Arnold, *Mathematical Methods in Classical Mechanics* (Springer, New York, 1978).

[2] A. J. Lichtenberg and M. A. Lieberman, *Regular and Chaotic Dynamics* (Springer-Verlag, New York, 1992) ; M. Tabor, *Chaos and Integrability in Nonlinear Dynamics : An Introduction* (John-Willey, New York, 1989).

[3] R. L. Devaney, *An Introduction to Chaotic Dynamical systems* (Addison-Wesely, New york, 1987).

[4] J. Banks, J. Brooks, G. Cairns, G. Davis, and P. Stacey, Amer. Math. Monthly **99**, 332 (1992).

[5] D. Asaf, IV and S. Gadbois, Amer. Math. Monthly **99**, 865 (1992).

[6] M. Vellekoop and R. Bergland, Amer. Math. Monthly **101**, 353 (1994).

[7] B. Chirikov, e-print arxiv: chao-dyn/9705003.

[8] V. I. Arnold, Sov. Math. Dokl. **5**, 581 (1964).

[9] M. V. Berry, Proc. R. Soc. London A **413**, 183 (1987).

[10] J. E. Bayfield and P. M. Koch, Phys. Rev. Lett. **33**, 258 (1974).

[11] J. G. Leopold and I. C. Percival, J. Phys. B **12**, 709 (1979).

[12] R. V. Jensen, S. M. Susskind, and M. M. Sanders, Phys. Rep. **201**, 1 (1991).

[13] R. Blümel and U. Smilansky, Phys. Rev. Lett. **52**, 137 (1984).

[14] G. Casati, B. V. Chirikov, I. Guarneri, and D. L. Shepelyansky, Phys. Rev. Lett. **56**, 2437 (1986).

[15] G. Casati *et al* in *Stochastic Behaviour of Classical and Quantum Hamiltonian Systems*, G. Casati and J. Ford (eds.), Lecture Notes in Physics, Vol. **93**, Springer-Verlag Berlin, Heidelberg, New York, pp. 334.

[16] F. L. Moore, J. C. Robinson, C. F. Bharucha, B. Sundaram, and M. G. Raizen, Phys. Rev. Lett. **75**, 4598 (1995).

[17] S. Fishman, D. R. Grempel, and R. E. Prange, Phys. Rev. Lett. **49**, 509 (1982) ; D. R. Grempel, R. E. Prange, and S. Fishman, Phys. Rev. A **29** 1639 (1984).

[18] W. H. Zurek, Nature **412**, 712 (2001).

[19] M. Brack and R. K. Bhaduri, *Semiclassical Physics*, (Addison-Wesley, Reading, Mass. 1997).

[20] M. C. Gutzwiller, *Chaos in Classical and Quantum Mechanics* (Springer, New York, 1990)

[21] O. Bohigas, M. J. Giannoni, and C. Scmit, Phys. Rev. Lett. **52**, 1 (1984)

[22] M. V. Berry, Philos. Trans. R. Soc. London A **287**, 237 (1977).

[23] A. Voros in Ref. [15], pp. 326.

[24] D. W. Noid, M. L. Koszykowski, and R. A. Marcus, J. Chem. Phys. **71**, 2864 (1979).

[25] H. S. Hutchinson and R. E. Wyatt, Chem. Phys. Lett. **72**, 378 (1980).

[26] S. W. Mcdonald and A. N. Kaufman, Phys. Rev. Lett. **42**, 1189 (1979).

[27] E. Heller, Phys. Rev. Lett. **53**, 1515 (1984).

[28] L. Kaplan and E. J. Heller, Annals of Phys. **264**, 171 (1998).

[29] R. L. Waterland, J. M. Yuan, C. C. Martens, R. A. Gillilan, and W. P. Reinhardt, Phys. Rev. Lett. **61**, 2733 (1988) ; B. Eckhardt and G. Hose, Phys. Rev. A **39**, 3776 (1989).

[30] D. Wintgen and A. Hönig, Phys. Rev. Lett. **63**, 1467 (1989)

[31] S. Sridhar, Phys. Rev. Lett. **67**, 785 (1991)

[32] P. B. Wilkinson, T. M. Fromhold, L. Eaves, F. W. Sheard, N. Miura, and T. Takamasu, Nature **380**, 608 (1996).

[33] E. Schrödinger, Proc. Camb. Phil. Soc. **31**, 555 (1935).

[34] A. Einstein, B. Podolsky, and N. Rosen, Phys. Rev. **47**, 777 (1935).

[35] B. Georgeot and D. L. Shepelyansky, Phys. Rev. E **62**, 3504 (2000) ; **62**, 6366 (2000).

[36] J. S. Bell, Physics (N.Y.) **1**, 195 (1965).

[37] M. Lamehi-Rachti and W. Mittig, Phys. Rev. D **14**, 2543 (1976) ; A. Aspect, P. Grangier, and G. Roger, Phys. Rev. Lett. **47**, 460 (1981) ; *ibid* **49**, 91 (1982).

[38] C. H. Bennett, G. Brassard, C. Crépeau, R. Jozsa, A. Peres, and W. K. Wotters, Phys. Rev. Lett. **70**, 1895 (1993).

[39] C. H. Bennet and G. Brassard, *Proc. of IEEE Int. Conf. on Comp., Sys. and Sig. Proc., Bangalore, India*, 175 (1984) ; A. Ekert, Phys. Rev. Lett. **68**, 661 (1991).

[40] C. H. Bennett and S. J. Wiesner, Phys. Rev. Lett. **69**, 2881 (192).

[41] P. W. Shor, In *Proceedings of the 35th Annual Symposium on Foundations of Computer Science*, edited by S. Goldwasser (IEEE Computer Society, Los Alamitos, CA, 1994), p. 124.

[42] L. K. Grover, Phys. Rev. Lett. **79**, 325 (1997) ; **79**, 4709 (1997) ; **80**, 4329 (1998).

[43] A. Peres, Phys. Lett. A **202**, 16 (1995) ; A. V. Thapliyal, Phys. Rev. A **59**, 3336 (1999) ; A. K. Pati, e-print quant-ph/9911073v2.

[44] C. H. Bennett, H. J. Bernstein, S. Popescu, and B. Schumacher, Phys. Rev. A **53**, 2046 (1996)

[45] S. Popescu and D. Rohrlich, Phys. Rev. A **56**, R3319 (1997).

[46] K. Furuya, M. C. Nemes, and G. Q. Pellegrino, Phys. Rev. Lett. **80**, 5524 (1998).

[47] W. H. Zurek and J. P. Paz, Phys. Rev. Lett. **72**, 2508 (1994).

[48] R. M. Angelo, K. Furuya, M. C. Nemes, and G. Q. Pellegrino, Phys. Rev. E **60**, 5407 (1999).

[49] R. M. Angelo, K. Furuya, M. C. Nemes, and G. Q. Pellegrino, Phys. Rev. A **64**, 043801 (2001).

[50] P. A. Miller and S. Sarkar, Phys. Rev. E **60**, 1542 (1999).

[51] P. G. Silvestrov, H. Schomerus, and C. W. J. Beenakker, Phys. Rev. Lett. **86**, 5192 (2001).

[52] A. Lakshminarayan, Phys. Rev. E **64**, 036207 (2001).

[53] A. Tanaka, H. Fujisaki, and T. Miyadera, Phys. Rev. E **66**, 045201(R) (2002); H. Fujisaki, T. Miyadera, and A. Tanaka, Phys. Rev. E **67**, 066201 (2003).

[54] A. Lahiri and S. Nag, Phys. Lett. A **318**, 6 (2003).

[55] A. J. Scott and C. M. Caves, J. Phys. A **36**, 9553 (2003).

[56] K. M. O'Connor and W. K. Wootters, Phys. Rev. A **63**, 052302 (2001)

[57] D. Gunlycke, S. Bose, V. M. Kendon, and V. Vedral, Phys. Rev. A **64**, 042302 (2001)

[58] P. Zanardi, Phys. Rev. A **65**, 042101 (2002).

[59] A. Lakshminarayan and V. Subrahmanyam, Phys. Rev. A **67**, 052304 (2003).

[60] X. Wang, S. Ghose, B. C. Sanders, and B. Hu, e-print quant-ph/0312047.

[61] L. F. Santos, G. Rigolin, and C. O. Escober, Phys. Rev. A **69**, 042304 (2004).

[62] W. H. Zurek, Rev. Mod. Phys. **75**, 715 (2003).

[63] *Decoherence and the Appearance of a Classical World in Quantum Theory*, D. Giulini, E. Joos, C. Kiefer, J. Kupsch, I. -O. Stamatescu, and H. D. Zeh (eds.) (Springer-Verlag, Berlin Heidelberg, 1996).

[64] D. Monteoliva and J. P. Paz, Phys. Rev. Lett. **85**, 3373 (2000); Phys. Rev. E **64**, 056238 (2001).

[65] P. Bianucci, J. P. Paz, and M. Saraceno, Phys. Rev. E **65**, 046226 (2002).

[66] A. K. Pattanayak, Phys. Rev. Lett. **83**, 4526 (1999).

[67] P. A. Miller and S. Sarkar, Nonlinearity **12**, 419 (1999); S. Nag, A. Lahiri, and G. Ghosh, Phys. Lett. **292A**, 43 (2001).

[68] A. K. Pattanayak and P. Brumer, Phys. Rev. E **56**, 5174 (1997); Phys. Rev Lett. **79**, 4131 (1997).

[69] A. K. Pattanayak, B. Sundaram, and B. D. Greenbaum, Phys. Rev. Lett., **90**, 014103 (2003).

[70] H. Kubotani, T. Okamura, and M. Sakagami, Physica **214A**, 560 (1995).

[71] D. Cohen and T. Kottos, Phys. Rev. E **69**, 055201(R) (2004).

[72] W. G. Unruh, Phys. Rev. A **51**, 992 (1995).

[73] M. Steffen, L. M. K. Vandersypen, and I. L. Chuang, IEEE Micro **21**, 24 (March 2001).

[74] G. Vidal and R. F. Werner, Phys. Rev. A **65**, 032314 (2002).

[75] A. Einstein, Inst. Int. Phys. Solvay Con.Phys. [Rapp. Discuss] **1**, 450 (1911).

[76] H. R. Lewis, Jr., Phys. Rev. Lett. **18**, 510 (1967).

[77] H. R. Lewis, Jr., J. Math. Phys. **9**, 1976 (1968).

[78] H. R. Lewis, Jr. and W. B. Riesenfeld, J. Math. Phys. **10**, 1458 (1969).

[79] M. Kruskal, J. Math. Phys. **3**, 806 (1962).

[80] C. J. Eliezer and A. Gray, SIAM **30**, 463 (1976).

[81] N. J. Günther and P. G. L. Leach, J. Math. Phys. **18**, 572 (1977).

[82] H. R. Lewis and P. G. L. Leach, J. Math. Phys. **23**, 165 (1982).

[83] P. Camiz, A. Geradi, C. Machioro, E. Presutti, and E. Scacciatelli, J. Math. Phys. **12**, 2040 (1971) ; I. A. Pedrosa, G. P. Serra, and I. Guedes, Phys. Rev. A **56**, 4300 (1997).

[84] (a) F. Calogero, J. Math. Phys. **12**, 419 (1971). (b) B. Sutherland, J. Math. Phys. **12**, 246 (1971) ; **12**, 251 (1971). (c) J. Moser, Adv. Math. **16**, 197 (1975).

[85] A. R. P. Rau, Phys. Rev. Lett. **81**, 4785 (1998).

[86] S. J. Wang, W. Zuo, A. Weiguny, and F. L. Li, Phys. Lett. A **196**, 7 (1994).

[87] F. Haake, M. Kus, and R. Scharf, Z. Phys. B **65**, 381 (1987); F. Haake, *Quantum Signatures of Chaos*, 2nd ed. (Springer-Verlag, Berlin, 2000)

[88] G. M. D'Ariano, L. R. Evangelista, and M. Saraceno, Phys. Rev. A **45**, 3646 (1992).

[89] J. J. Sakurai, *Modern Quantum Mechanics* (Addison-Wesley, Reading, MA, 1994).

[90] A. Peres and D. Terno, Phys. Rev. E **53**, 284 (1996).

[91] D. A. Varshalovich, A. N. Moskalev, and V. K. Khersonskii, *Quantum Theory of Angular Momentum* (World Scientific, Singapore, 1988).

[92] L. Laloux, P. Cizeau, J-P. Bouchaud, and M. Potters, Phys. Rev. Lett. **83**, 1467 (1999); A. M. Sengupta and P. P. Mitra, Phys. Rev. E **60**, 3389 (1999).

[93] T. A. Brody *et. al.*, Rev. Mod. Phys. **53**, 385 (1981); F. J. Dyson, Rev. Mex. Fis. **20**, 231 (1971).

[94] M. S. Santhanam and P. K. Patra, Phys. Rev. E **64**, 016102 (2001).

[95] N. Ullah and C. E. Porter, Phys. Letts. **6**, 301 (1963).

[96] K. Życzkowski and H-J. Sommers, J. Phys. A **34**, 7111 (2001).

[97] D. N. Page, Phys. Rev. Lett. **71**, 1291-1294 (1993).

[98] S. K. Foong and S. Kanno, Phys. Rev. Lett. **72**, 1148 (1994) ; J. Sanchez-Ruiz, Phys. Rev. E **52**, 5653 (1995) ; S. Sen, Phys. Rev. Lett. **77**, 1 (1996).

[99] E. Lubkin, J. Math. Phys. **19**, 1028 (1978)

[100] A. Sugita and H. Aiba, Phys. Rev. E **65**, 036205 (2002).

[101] A. Wehrl, Rep. Math. Phys. **16**, 353 (1979) ; A. Wehrl, Rev. Mod. Phys. **50**, 221 (1978)

[102] E. J. Heller, Phys. Rev. A **35**, 1360 (1987).

[103] C. Manderfeld, J. Phys. A **36**, 6379 (2003).

[104] S. Hill and W. K. Wootters, Phys. Rev. Lett. **78**, 5022 (1997).

[105] A. Peres, Phys. Rev. Lett. **76**, 1413 (1996).

[106] M. Horodecki, P. Horodecki, and R. Horodecki, Phys. Lett. A **223**, 1 (1996).

[107] M. A. Nielsen, C. M. Dawson, J. L. Dodd, A. Gilchrist, D. Mortimer, T. J. Osborne, M. J. Bremner, A. W. Harrow, and A. Hines, Phys. Rev. A **67**, 052301 (2003).

[108] K. Życzkowski and I. Bengtsson, Open Syst. Inf. Dyn. **11**, 3 (2004) ; also available from : e-print quant-ph/0401119.

[109] C. W. J. Beenakker, M. Kindermann, C. M. Marcus, and A. Yacoby, e-print cond-mat/0310199.

[110] S. Ghose and B. C. Sanders, e-print quant-ph/0404171.

List of Publications

Paper published in Journals

1. *Algebraic approach in the study of time-dependent nonlinear integrable systems : Case of the singular oscillator*, J. N. Bandyopadhyay, A. Lakshminarayan and V. B. Sheorey, Phys. Rev. A **63**, 042109 (2001).

2. *Testing statistical bounds on entanglement using quantum chaos*, J. N. Bandyopadhyay and A. Lakshminarayan, Phys. Rev. Lett. **89**, 060402 (2002).

3. *Entanglement production in coupled chaotic systems : Case of the Kicked Tops*, J. N. Bandyopadhyay and A. Lakshminarayan, Phys. Rev. E **69**, 016201 (2004).

Paper/Abstract published in Conference Proceeding

1. *Quantum Chaos and Entanglemant*, V. B. Sheorey, J. N. Bandyopadhyay, and A. Lakshminarayan, in *Proceedings of XVIII International Conferenece on Atomic Physics 2002*, in Massachusetts Institute of Technology, Cambridge, MA, July 27-August 2, 2002 (World Scientific, Singapore).

2. *Entanglement measures in quantum and classical chaos*, A. Lakshminrayan, J. N. Bandyopadhyay, M. S. Santhanam, and V. B. Sheorey, in *Proceedings of First National Conference on Nonlinear Systems and Dynamics* in Indian Institute of Technology, Kharagpur, India, 28-30 Dec, 2003.